

A MULTIDISCIPLINARY INVESTIGATION OF THE
HEMOCYTOGENIC NATURE OF THE WHITE BODIES OF
THE OMMASTREPHID ILLEX ILLECEBROSUS
(LESUEUR, 1821) (CEPHALOPODA: COLEOIDEA)

CENTRE FOR NEWFOUNDLAND STUDIES

**TOTAL OF 10 PAGES ONLY
MAY BE XEROXED**

(Without Author's Permission)

FLORENCE ELIZABETH (WAY) JOHNSON



C07002

This thesis damaged in shipment from Bindsay



A MULTIDISCIPLINARY INVESTIGATION OF THE HEMOCYTOGENIC
NATURE OF THE WHITE BODIES OF THE OMMASTREPHID
ILLEX ILLECEBROSUS (LESUEUR, 1821)
(CEPHALOPODA: COLEOIDEA)

by

© Florence Elizabeth (Way) Johnson, B.Sc., B.Ed., M.Sc.

A thesis submitted to the School of Graduate
Studies in partial fulfillment of the
requirements for the degree of
Doctor of Philosophy

Faculty of Medicine
Memorial University of Newfoundland
March 1984

St. John's

Newfoundland

A MULTIDISCIPLINARY INVESTIGATION OF THE EPIDEMIOLOGY

OF THE DISEASE IN THE DISTRICT OF

THE DISTRICT OF

(GENERALIST, 1981)

BY

THOMAS WILSON (M.D., M.Sc., M.H., M.B.)

WILSON

A Thesis submitted to the School of Medicine

in partial fulfillment of the

requirements for the degree of

Doctor of Philosophy

Faculty of Medicine

Memorial University of Newfoundland

St. John's 1981

Several aspects of the multidisciplinary study were intended for either duplication or expansion in 1983-1984. The complete failure of the squid (Illex illecebrosus) to appear in Newfoundland waters during the summer and autumn of 1983 precluded any such opportunities however. It is fully realized by the author that some of the immunological studies and those involving the use of tritiated thymidine need further elaboration.

". . . fearfully and wonderfully made."

David

Psalm 139:13-14

ABSTRACT

The present study extends previous descriptions of the white body of cephalopods by providing new information with regard to (1) morphometry, (2) gross anatomy, (3) microscopic anatomy, (4) vasculature, and (5) immunology of the white bodies within Illex illecebrosus.

The white bodies of I. illecebrosus are paired multilobular organs; one attached to the medial surface of each eye. The multilobate configuration of each white body is related to the compartmentalized nature of the optic sinus that envelops the white body.

Presumably, each white body is located upon the medial surface of a squid's eye to affect access of its products to the optic sinus and, hence, the general circulation. Hemooscula provide the means whereby this may be accomplished. These portals, the hemooscula, are herein described for the first time.

In a squid of a given size, the white body (or particular parts of same) is smaller in the male than it is in the female. The length of the subganglionic process is probably one of the first morphometric characteristics of a white body to be established.

Microscopic structure of white bodies of I. illecebrosus is similar to that of other species of cephalopod molluscs. The internal fibrous network of a white

body together with the outer capsule form a framework for the internal tissue and vasculature. The tissue of the white body is arranged into repetitious, morphological units or groupings of cells. The individual components of the latter can be identified on the basis of their nuclear appearance.

Four variations of white body cells are presented as comprising a developmental series that produces the circulating hemocytes. These perceived variations (1 through 4) can best be defined on the basis of differences in nuclear morphology. Earlier workers have attempted to define developmental stages for circulating cells of other cephalopods and a range of invertebrates based on measurements of the nucleus or the presence of cytoplasmic inclusions and have failed to achieve clarity or consistency. The fourth variation in the series, here presented for the first time, is presumably the final developmental stage prior to the circulating hemocytes, although Variation 3 may also be liberated successfully into the circulating blood.

Cells comprising the internal tissue of a white body are characterized as a renewing population of cells. Failure to demonstrate the incorporation of tritiated thymidine into the nuclei of such cells may have resulted from extrinsic factors, as herein discussed.

The white bodies of I. illecebrosus are well vascularized. Blood flows to a white body by way of the

anterior and posterior ophthalmic arteries; passes through its tissue via small vessels, sinuli and hemal spaces; and eventually leaves the tissue to enter the enveloping optic sinus by way of the hemooscula; from the optical sinus, entering the venous circulation via the anterior vena cava.

Based upon immunological characteristics ascertained during studies of unabsorbed and absorbed rabbit antiserum, the possibility of hemocytes being derived from the white body is very high.

The information compiled within this thesis provides strong evidence in favor of the hypothesis that the white bodies are the site of hemocytogenesis, as has been earlier suggested on less valid grounds.

ACKNOWLEDGEMENTS

Appreciation is expressed to my supervisor, Dr. R.G. Huntsman, and the members of my supervisory committee, Dr. F.A. Aldrich, Dr. J.A. Barrowman, and Dr. B. Larsen, for their constant support and encouragement.

The awarding of a Provincial Government Fellowship, 1979-1982, and a financial supplement from the Faculty of Medicine at Memorial University of Newfoundland, 1982, are also gratefully acknowledged at this time.

Mr. M.J. Mercer and others of the staff at the Marine Sciences Research Laboratory supplied the teuthoid specimens required during this investigation.

Blood smears from Ommastrephes pteropus Steenstrup, 1855, were collected during a federal fisheries research cruise aboard the GADUS ATLANTICA, February 20-March 11, 1981. The author expresses appreciation to the Fisheries and Oceans, St. John's, for this invaluable experience.

The interest and cooperation of Dr. R.S. Harris and his research assistant, Mr. D. Jones, enabled the author to pursue angiography studies of the Newfoundland bait squid.

The opportunity to investigate the immunological relationships of selected tissues of squid was made possible by Dr. B. Larsen. She graciously provided instruction, lab facilities, and materials during such experiments.

Dr. F.A. Aldrich and Dr. D.R. Idler are acknowledged for their help in acquiring tritium-labeled thymidine.

Special thanks are also extended to those individuals who assisted the author during the employment of various research procedures.

Mr. Greg Bennett is recognized for his instructional assistance during the running of graphic and statistical computer programs. Furthermore, Computing Services, Henrietta Harvey Building, M.U.N., provided the hardware and computer time necessary to complete this work.

Black and white photographs were prepared by Mr. P. Hyam of the Faculty of Medicine, and E.T.V., M.U.N. Color prints were processed by either Northlight Photographic, St. John's, or in a few instances, Mr. W. White of M.U.N.'s E.T.V.

Librarians of the Memorial University Library are recognized for their help in retrieving relevant journal articles.

Special mention is also given to Mrs. P. Moore for her aid in translating scientific papers from the original French and Italian of their authors. Dr. R.J. Clark, M.U.N. Department of Classics, is acknowledged for his expert advice regarding the usage, derivation, and correctness of Latin assigned by this author to newly described structures.

Lastly, the author wishes to acknowledge Miss L.M. Sullivan and Mrs. D. Strange who typed the final manuscript of this thesis.

TABLE OF CONTENTS

| | Page |
|---|------|
| Abstract | ii |
| Acknowledgements | vi |
| List of Tables | xi |
| List of Figures | xiii |
| INTRODUCTION | 1 |
| 1. Statement of Research Proposal | 1 |
| 2. Classification and General Anatomy of the Experimental Animal, <u>Illex illecebrosus</u> | 1 |
| 3. Historical Review of the Literature | 8 |
| A. The White Bodies as the Site of Hemocytogenesis | 8 |
| B. Alternate Sites of Hemocytogenesis | 15 |
| 4. The Hemocytes of <u>Illex illecebrosus</u> | 19 |
| MATERIALS AND METHODS | 26 |
| 1. Squid Collection and Maintenance | 26 |
| 2. Anesthetization Procedure | 26 |
| 3. Anatomical Investigations | 28 |
| A. Gross Anatomical Studies | 28 |
| i. Descriptive Analysis of the White Bodies | 28 |
| ii. Morphometric Analysis of the White Bodies | 28 |
| B. Scanning Electron Microscopy Studies | 31 |

| | Page |
|--|------|
| C. Light Microscopy Studies | 32 |
| i. Basic Histological Techniques | 32 |
| ii. Frozen Tissue Techniques | 32 |
| D. Transmission Electron Microscopy Studies | 33 |
| E. Numeric and Morphometric Studies of the White Body Cells | 35 |
| F. Vascular Studies | 36 |
| i. Latex Injection Techniques | 36 |
| ii. Drawing Ink Injection Techniques | 37 |
| iii. Angiography Techniques | 38 |
| 4. Immunological Studies | 38 |
| A. Antisera Preparation | 39 |
| B. Agglutination | 41 |
| C. Smear and Tissue Section Preparation | 41 |
| D. Tissue Homogenates | 42 |
| E. Absorbed Antisera | 43 |
| F. Immunofluorescence | 43 |
| 5. Mitotic Index Study | 44 |
| 6. Radioisotope Labeling Studies | 47 |
| A. Employment of Radioisotope | 47 |
| B. Histological Techniques | 50 |
| C. Autoradiography Techniques | 53 |
| RESULTS | 55 |
| 1. Morphological Studies of the White Bodies | 55 |
| A. Gross Anatomy | 55 |
| i. Descriptive Analysis | 55 |
| ii. Morphometric Analysis | 73 |

| | Page |
|---|------|
| B. Microscopic Anatomy | 155 |
| i. The Capsule | 155 |
| ii. Internal Features | 172 |
| C. Vascular Studies | 225 |
| i. Arterial Blood Supply to the White Bodies | 226 |
| ii. White Body Tissue Circulation | 248 |
| iii. Venous Drainage | 249 |
| 2. Immunological Studies of the White Bodies. | 253 |
| A. Unabsorbed Rabbit Antiserum | 254 |
| B. Absorbed Rabbit Antiserum | 259 |
| 3. Mitotic Index Study of the White Bodies. | 259 |
| 4. Radioisotope Labeling Studies of the White Bodies | 267 |
| GENERAL DISCUSSION AND CONCLUSIONS | 271 |
| REFERENCES CITED | 326 |

APPENDICES

| | |
|---|---------|
| APPENDIX 1: Descriptive statistics pertaining to the morphological Variables ascertained in the course of the morphometric study of the white bodies of the squid <u>Illex</u> <u>illecebrosus</u> | 332-334 |
| APPENDIX 2: Raw data from morphometric study of the white bodies of the squid <u>Illex illecebrosus</u> | 335-343 |
| APPENDIX 3: Morphometric analysis of the four recognizable Variables observed in cells of the several components of the white body of the squid <u>Illex</u> <u>illecebrosus</u> | 344-348 |
| APPENDIX 4: The frequency of occurrence of the four recognizable Variations of cells in each of the components of the white body of the squid <u>Illex illecebrosus</u> | 349 |

LIST OF TABLES

| TABLE | Page/Pages |
|--|------------|
| 1. An historical review of studies relating to the production site of blood cells within cephalopod molluscs | 9-12 |
| 2. Ultrastructural characteristics of developing and mature hemocytes within <u>Octopus briareus</u> , as described by Cowden and Curtis (1974, 1981) | 16-17 |
| 3. The morphological characteristics of hemocytes of the squid, <u>Illex illecebrosus</u> (from Way, 1975) | 23-24 |
| 4. Immunization schedule for the production of antisera to <u>Illex illecebrosus</u> white body cells | 40 |
| 5. <u>I. illecebrosus</u> specimens employed during the mitotic index study | 46 |
| 6. Schedule of exposure to tritiated thymidine and morphometric and other data on specimens of <u>Illex illecebrosus</u> sacrificed in the study | 48-49 |
| 7. The results of t-tests in which the morphometric statistics (recorded in centimeters) of each white body were compared with the sex of the squid from which the white body was collected | 142-143 |
| 8. The results of t-tests in which the morphometric statistics (recorded in centimeters) of each component of the right white body were compared with corresponding values for the left white body | 144-145 |
| 9. Comparison of nuclear and cytoplasmic features of cell variants in the white body of <u>Illex illecebrosus</u> | 198 |

10. A table indicating arterial routes from the systemic heart to the various parts of the white bodies 247
11. Indirect immunofluorescent reactions of antiserum prepared against I. illecebrosus white body cells. Antiserum tested against various squid tissues with subsequent addition of fluorescent sheep antiserum to rabbit immunoglobulin . . . 260
12. Indirect immunofluorescent reactions of antiserum prepared against I. illecebrosus white body cells. Unabsorbed antiserum and antiserum absorbed with various tissues from I. illecebrosus tested against various squid tissues with subsequent addition of fluorescent sheep antiserum to rabbit immunoglobulin . . . 263
13. Data collected during the mitotic index study of white body tissue from I. illecebrosus 265-266
14. The incidence of tritiated thymidine within the blood and selected tissues of I. illecebrosus subsequent to varying intervals of (1) exposure time to the radioisotope and (2) incubation time to reveal the latter's presence 268-269

LIST OF FIGURES

| FIGURE | Pages |
|---|-------|
| 1. A photograph illustrating the dorsal external anatomy of <u>Illex illecebrosus</u> (female; 240 mm DML). 0.3x | 4-5 |
| 2. A photograph illustrating the dominant internal organs and structures of <u>I. illecebrosus</u> (female; 204 mm DML). 0.5 x | 6-7 |
| 3. Photographs indicating the various nuclear configurations exhibited by circulating hemocytes of <u>I. illecebrosus</u> (after Way, 1975, pp. 49-50). Villanueva 1210 x | 20-21 |
| 4. A photograph to illustrate the dorsal, cephalic, T-shaped incision required to view the white body tissue and facilitate its subsequent removal (female <u>I. illecebrosus</u> ; 240 mm DML). 0.7 x | 29-30 |
| 5. Diagram illustrating the method of injecting tritiated thymidine (right lateral view). 2.4 x | 51-52 |
| 6. A dorsal, cephalic dissection of <u>I. illecebrosus</u> (female; 240 mm DML) revealing the postganglionic lobes of the two white bodies. 1.7 x | 56-57 |
| 7. An external, medial view of the right eye (female <u>I. illecebrosus</u> ; 240 mm DML) showing the discontinuous ring configuration of the white body | 58-59 |
| 8. A photograph showing the alignment between the dorsal tip of the postganglionic lobe (→) and the vertical stripe on the eye's lateral surface (female <u>I. illecebrosus</u> ; 240 mm DML; freshly dissected right eye). 2.3 x | 61-62 |

| | | |
|-----|--|-------|
| 9. | A photograph illustrating the position of the subganglionic process in relation to the remaining white body structures (female <u>I. illecebrosus</u> ; 240 mm DML; right eye). 4 x | 63-64 |
| 10. | Photographs illustrating the serpentine configuration of the subganglionic process and the latter's association with the ventral portion of the postganglionic lobe (female <u>I. illecebrosus</u> ; 240 mm DML) | 65-66 |
| 11. | A photograph illustrating the gross anatomy of the inferior preganglionic lobe and the latter's relationship to the subganglionic process (female <u>I. illecebrosus</u> ; 240 mm DML; right eye). 5 x | 68-69 |
| 12. | Photographs showing the surface irregularities exhibited by the postganglionic lobe (female <u>I. illecebrosus</u> ; 240 mm DML). | 71-72 |
| 13. | A composite drawing illustrating the gross anatomy of a white body from <u>I. illecebrosus</u> . 10 x | 74-75 |
| 14. | A scattergram in which values for the width of the right postganglionic lobe are plotted against values for the dorsal mantle length | 77-78 |
| 15. | A scattergram in which values for the width of the left postganglionic lobe are plotted against values for the dorsal mantle length | 79-80 |
| 16. | A scattergram in which values for the length of the right postganglionic lobe are plotted against values for the dorsal mantle length | 81-82 |
| 17. | A scattergram in which values for the length of the left postganglionic lobe are plotted against values for the dorsal mantle length | 83-84 |
| 18. | A scattergram in which values for the width of the right subganglionic process are plotted against values for the dorsal mantle length | 85-86 |

| FIGURE | Pages |
|---|---------|
| 19. A scattergram in which values for the width of the left subganglionic process are plotted against values for the dorsal mantle length | 87-88 |
| 20. A scattergram in which values for the length of the right subganglionic process are plotted against values for the dorsal mantle length | 89-90 |
| 21. A scattergram in which values for the length of the left subganglionic process are plotted against values for the dorsal mantle length | 91-92 |
| 22. A scattergram in which values for the width of the right inferior preganglionic lobe are plotted against values for the dorsal mantle length | 93-94 |
| 23. A scattergram in which values for the width of the left inferior preganglionic lobe are plotted against values for the dorsal mantle length | 95-96 |
| 24. A scattergram in which values for the length of the right inferior preganglionic lobe are plotted against values for the dorsal mantle length | 97-98 |
| 25. A scattergram in which values for the length of the left inferior preganglionic lobe are plotted against values for the dorsal mantle length | 99-100 |
| 26. A scattergram in which values for the width of the right superior preganglionic lobe are plotted against values for the dorsal mantle length | 101-102 |
| 27. A scattergram in which values for the width of the left superior preganglionic lobe are plotted against values for the dorsal mantle length | 103-104 |
| 28. A scattergram in which values for the length of the right superior preganglionic lobe are plotted against values for the dorsal mantle length | 105-106 |

29. A scattergram in which values for the length of the left superior preganglionic lobe are plotted against values for the dorsal mantle length 107-108
30. A scattergram in which values for the width of the right postganglionic lobe are plotted against values for the weight of the squid 110-111
31. A scattergram in which values for the width of the left postganglionic lobe are plotted against values for the weight of the squid 112-113
32. A scattergram in which values for the length of the right postganglionic lobe are plotted against values for the weight of the squid 114-115
33. A scattergram in which values for the length of the left postganglionic lobe are plotted against values for the weight of the squid 116-117
34. A scattergram in which values for the width of the right subganglionic process are plotted against values for the weight of the squid 118-119
35. A scattergram in which values for the width of the left subganglionic process are plotted against values for the weight of the squid 120-121
36. A scattergram in which values for the length of the right subganglionic process are plotted against values for the weight of the squid 122-123
37. A scattergram in which values for the length of the left subganglionic process are plotted against values for the weight of the squid 124-125
38. A scattergram in which values for the width of the right inferior preganglionic lobe are plotted against values for the weight of the squid 126-127

| FIGURE | Pages |
|--|---------|
| 39. A scattergram in which values for the width of the left inferior preganglionic lobe are plotted against values for the weight of the squid | 128-129 |
| 40. A scattergram in which values for the length of the right inferior preganglionic lobe are plotted against values for the weight of the squid | 130-131 |
| 41. A scattergram in which values for the length of the left inferior preganglionic lobe are plotted against values for the weight of the squid | 132-133 |
| 42. A scattergram in which values for the width of the right superior preganglionic lobe are plotted against values for the weight of the squid | 134-135 |
| 43. A scattergram in which values for the width of the left superior preganglionic lobe are plotted against values for the weight of the squid | 136-137 |
| 44. A scattergram in which values for the length of the right superior preganglionic lobe are plotted against values for the weight of the squid | 138-139 |
| 45. A scattergram in which values for the length of the left superior preganglionic lobe are plotted against values for the weight of the squid | 140-141 |
| 46. A scattergram in which values for the total length of the right white body are plotted against values for the dorsal mantle length | 147-148 |
| 47. A scattergram in which values for the total length of the right white body are plotted against values for the weight of the squid | 149-150 |
| 48. A scattergram in which values for the total length of the left white body are plotted against values for the dorsal mantle length | 151-152 |

49. A scattergram in which values for the total length of the left white body are plotted against values for the weight of the squid 153-154
50. Light micrographs illustrating the fibrous capsule that envelops the white body of I. illecebrosus 156-157
51. Scanning electron micrographs of the white body capsule (female I. illecebrosus; 252 mm DML) 158-159
52. An electron micrograph illustrating the fibrous structure of the capsule of the white body (cross section of the right postganglionic lobe; female I. illecebrosus; 252 mm DML). 29,948 x 161-162
53. A light micrograph showing a longitudinal section of trabeculae within the right subganglionic process of a female I. illecebrosus (252 mm DML). Toluidine Blue; 588 x 163-164
54. An electron micrograph to illustrate the relationship between a trabecula and the internal fibrous network of the white body (longitudinal section of the right postganglionic lobe; female I. illecebrosus; 252 mm DML). 28,728 x 165-166
55. Scanning electron micrographs of the external surface of the white body (female I. illecebrosus; 252 mm DML) 168-169
56. Scanning electron micrographs illustrating the structure of the capsular hemoacula (female I. illecebrosus; 252 DML) 170-171
57. A light micrograph illustrating aspects of the fibrous supportive network of the white body (cross section of the right postganglionic lobe; female I. illecebrosus; 252 mm DML). Toluidine blue; 820 x 173-174
58. Scanning electron micrographs of the white body interior (female I. illecebrosus; 252 mm DML) 175-176

59. An electron micrograph illustrating the periodicity displayed by fibers of the supportive network (cross section of the left postganglionic lobe; female I. illecebrosus; 252 mm DML). 12,130 x . . . 178-179
60. A light micrograph illustrating fibroblastoid cells of the white body interior (cross section of the right postganglionic lobe; female I. illecebrosus; 252 mm DML). Toluidine blue; 820 x 180-181
61. An electron micrograph illustrating the close relationship between a fibroblastoid cell and the internal fibrous network of the white body lobe (cross section of the right postganglionic lobe; female I. illecebrosus; 252 mm DML). 8,938 x 182-183
62. An electron micrograph illustrating the fine structure of fibroblastoid cells from the interior of a white body lobe (cross section of the right postganglionic lobe; female I. illecebrosus; 252 mm DML). 1,810 x 184-185
63. Micrographs illustrating the internal organization of the white body with regard to the density and arrangement of the cells 187-188
64. An electron micrograph of white body tissue from a female specimen of I. illecebrosus (252 mm DML; a cross section of the right postganglionic lobe). 8,928 x 190-191
65. An electron micrograph illustrating an intercellular junction between two Variation 1 white body cells (cross section of the right postganglionic lobe; female I. illecebrosus; 252 mm DML). 12,130 x 194-195
66. Electron micrographs illustrating the structural details of an intercellular junction (cross section of the left postganglionic lobe; female I. illecebrosus; 252 mm DML) 196-197

67. A light micrograph illustrating the presence and distribution of mitotic cells within white body tissue (cross section of the right inferior preganglionic lobe from a female I. illecebrosus; 232 mm DML; Villanueva). 470 x 198-200
68. An electron micrograph illustrating white body cells during mitosis (cross section of the left postganglionic lobe; female I. illecebrosus; 252 mm DML). 8,938 x 201-202
69. Electron micrographs illustrating the structural details of white body cells during mitosis (cross section of the left postganglionic lobe; female I. illecebrosus; 252 mm DML) 204-205
70. An electron micrograph illustrating one of the small blood vessels within the white body tissue of I. illecebrosus (cross section of the right postganglionic lobe; female specimen; 252 mm DML). 8,618 x 206-207
71. Scanning electron micrographs showing the vascular channels that penetrate the white body tissue (female I. illecebrosus; 252 mm DML) 209-210
72. Light micrographs illustrating sinuli within white body tissue 211-212
73. An electron micrograph illustrating the ultrastructure of a sinus within white body tissue (longitudinal section of the right postganglionic lobe; female I. illecebrosus; 252 mm DML). 6,065 x 213-214
74. A light micrograph illustrating a subcapsular sinus that was disrupted during processing of the white body tissue (cross section of the right subganglionic process; female I. illecebrosus; 252 mm DML). 950 x 216-217
75. An electron micrograph illustrating the hemal spaces within white body tissue from I. illecebrosus (cross section of the left postganglionic lobe; female specimen; 252 mm DML). 11,172 x, insert; 17,556 x 218-219

| FIGURE | Pages |
|---|---------|
| 76. Diagrammatic representation of cellular features as observed in the white body of <u>I. illecebrosus</u> | 221-222 |
| 77. Light micrographs to demonstrate that each lobe and subganglionic process of a white body are histologically similar | 223-224 |
| 78. Photographs of <u>I. illecebrosus</u> (male specimen; 214 mm DML) illustrating the systemic heart and anterior aorta following arterial injection of red Latex | 227-228 |
| 79. Illustrations to elucidate the relationship between the intracranial arteries, buccal artery, and the brachial trunk artery (female <u>I. illecebrosus</u> ; 227 mm DML: arterial injection of red Latex). 2.5 x . . . | 230-231 |
| 80. Diagram illustrating the general route of oxygenated blood from the gills to the arteries that vascularize the white bodies (modified from Bradbury, 1970, p. 197) . . . | 232-233 |
| 81. Photographs illustrating the right and left superior postganglionic arteries and their branches that vascularize the upper region of the postganglionic lobes (female <u>I. illecebrosus</u> ; 227 mm DML) | 234-235 |
| 82. A photograph showing arteries to the right subganglionic process and the lower region of the right postganglionic lobe (female <u>I. illecebrosus</u> ; 227 mm DML; anesthetized, Latex injected specimen). 4.5 x | 237-238 |
| 83. Photographs illustrating the right anterior ophthalmic artery following arterial injection of red Latex (male <u>I. illecebrosus</u> ; 214 mm DML) | 239-240 |
| 84. Photographs illustrating the right anterior white body artery and its branches as indicated by Latex injection . . | 241-242 |
| 85. Composite diagram illustrating the pathway of the right and left posterior ophthalmic arteries and their branches. 3.5 x | 243-244 |

| FIGURE | Pages |
|---|---------|
| 76. Diagrammatic representation of cellular features as observed in the white body of <u>I. illecebrosus</u> | 221-222 |
| 77. Light micrographs to demonstrate that each lobe and subganglionic process of a white body are histologically similar | 223-224 |
| 78. Photographs of <u>I. illecebrosus</u> (male specimen; 214 mm DML) illustrating the systemic heart and anterior aorta following arterial injection of red Latex | 227-228 |
| 79. Illustrations to elucidate the relationship between the intracranial arteries, buccal artery, and the brachial trunk artery (female <u>I. illecebrosus</u> ; 227 mm DML: arterial injection of red Latex). 2.5 x . . . | 230-231 |
| 80. Diagram illustrating the general route of oxygenated blood from the gills to the arteries that vascularize the white bodies (modified from Bradbury, 1970, p. 197) . . . | 232-233 |
| 81. Photographs illustrating the right and left superior postganglionic arteries and their branches that vascularize the upper region of the postganglionic lobes (female <u>I. illecebrosus</u> ; 227 mm DML) | 234-235 |
| 82. A photograph showing arteries to the right subganglionic process and the lower region of the right postganglionic lobe (female <u>I. illecebrosus</u> ; 227 mm DML; anesthetized, Latex injected specimen). 4.5 x | 237-238 |
| 83. Photographs illustrating the right anterior ophthalmic artery following arterial injection of red Latex (male <u>I. illecebrosus</u> ; 214 mm DML) | 239-240 |
| 84. Photographs illustrating the right anterior white body artery and its branches as indicated by Latex injection . . | 241-242 |
| 85. Composite diagram illustrating the pathway of the right and left posterior ophthalmic arteries and their branches. 3.5 x | 243-244 |

| FIGURE | Pages |
|---|---------|
| 86. Composite diagram illustrating the pathway of the right and left anterior ophthalmic arteries and their branches. 3.5 x | 245-246 |
| 87. A photographic sequence illustrating the position and configuration of the left and right optic sinuses as demonstrated by the injection of the radiopaque contrast agent, RENOGrafin-60 (female <u>I. illecebrosus</u> ; 265 mm DML). 0.75 x | 250-251 |
| 88. Photographs demonstrating the reactions that result upon exposure of squid tissues to antiserum and normal rabbit serum with subsequent addition of fluorescent sheep antiserum to rabbit immunoglobulin | 255-256 |
| 89. Photographs demonstrating the reactions that result upon exposure of squid hemocytes to antiserum and normal rabbit serum with subsequent addition of fluorescent sheep antiserum to rabbit immunoglobulin | 257-258 |
| 90. Photographs demonstrating the reactions that result upon exposure of hemocytes from <u>I. illecebrosus</u> to antiserum, absorbed antiserum, and normal rabbit serum with subsequent addition of fluorescent sheep antiserum to rabbit immunoglobulin | 261-262 |
| 91. Diagrammatic representation of the hemocytogenic series recognized within the white body of <u>I. illecebrosus</u> . 2,500 x. | 287-288 |
| 92. Diagrammatic representations of the relationship between a white body and the compartmentalized optic sinus in <u>Illex illecebrosus</u> 2.1 x | 301-302 |

INTRODUCTION

1. Statement of Research Proposal

As a Master's candidate, the author investigated the functional morphology of circulating blood cells within the Newfoundland bait squid, Illex illecebrosus (LeSueur, 1821). While that study raised several questions suitable for future pursuit, one of particular interest concerned the site at which such hemocytes were formed. Of interest is the fact that no conclusive evidence has ever been offered regarding the location of hemocyte production. The white bodies, organs within the cephalic region of cephalopods, are generally thought to be the formative sites; however, until the present study, this assumption has been based entirely upon histological data.

It has become this author's proposal, then, to undertake a comprehensive study of the white bodies of I. illecebrosus and, with the aid of various experimental methods, illuminate their functioning.

2. Classification and General Anatomy of the Experimental Animal, Illex illecebrosus

It would seem appropriate at this time to review the classification of the species under examination. The following outline is modified from that proposed by Bradbury (1970) and will familiarize the reader with upcoming morphological considerations and terminology.

- Phylum Mollusca.
- Class Cephalopoda (Cuvier, 1797).
- Subclass Coleoidea (Bather, 1888). Characterized by a single pair of gills and an internal shell considerably reduced (absent in some species of the subclass).
- Order Teuthoidea.[Teuthidida] (Naef, 1916). Internal shell.
- Suborder Oegopsida (d'Orbigny, 1839). Open eye (that is, without a cornea) directly bathed by sea water. The eye is closed by an eyelid, however.
- Family Ommastrephidae (Gill, 1871).
- (a) Presence of an inverted T-shaped hyponomal locking cartilage which is strongly developed.
- (b) Suckers of the sessile arms are biserial in arrangement whereas those of the tentacular manus and dactylus are tetraserial, with the exception of those of the dactylus of the genus Illex which are octaserial.
- (c) Buccal membrane connectives of the arms attached to the arms in the formula D:D:V:D (D = dorsal, V = ventral). The formula expresses the pattern characteristic of the attachment to the dorsal and ventral aspects of the buccal area, as first described by Verrill in 1880.
- (d) Anterior to the hyponomal locking cartilage, a muscular bridge passes from the hyponome to the ventrum of the head.

(e) the caudal fin is less than 60% of the mantle length (Roper et al., 1969).

Subfamily Illicinae (Posselt, 1890).

- (a) The hyponomal groove is smooth (Steenstrup, 1880), that is, it lacks both central and lateral foveolae, or pockets.
 (b) Photophores are lacking (Roper et al., 1969).

Genus Illex (Steenstrup, 1880). There are four rows of suckers on the manus and eight rows of suckers on the dactylus of the tentacular arm (Ferussac & d'Orbigny, 1835-1848).

Species I. illecebrosus (LeSueur, 1821).

- (a) The hectocotylus is distinct, but less well developed than in the other three species of the genus (I. coindeti, Vérany, 1837; I. argentinus, de Castellanos, 1960; and I. oxygenius, Roper et al., 1969) (Aldrich & Lu, 1968; Roper et al., 1969; Mangold et al., 1969).
 (b) No tentacular locking or fixing apparatus present (Steenstrup, 1880).

The general anatomy of I. illecebrosus is illustrated within the two figures that follow. The external anatomy is shown in Figure 1. Dominant internal organs and structures are identified in Figure 2.

Finally, the reader will note the phrase "dorsal mantle length" (DML) throughout this thesis. It (Figure 1) refers to the length of a squid when measured from the

Figure 1. A photograph illustrating the dorsal external anatomy of Illex illecebrosus (female; 240 mm DML). 0.3x.

| | |
|-----|----------------------|
| A | Sessile Arm |
| C | Chromatophores |
| CF | Caudal Fin |
| D | Distal Protuberance |
| DML | Dorsal Mantle Length |
| E | Eye |
| M | Mantle |
| T | Tentacle |

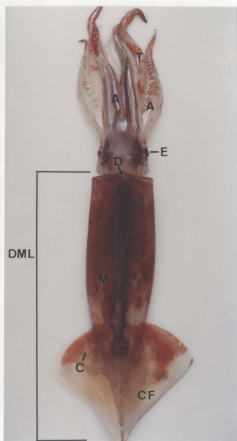
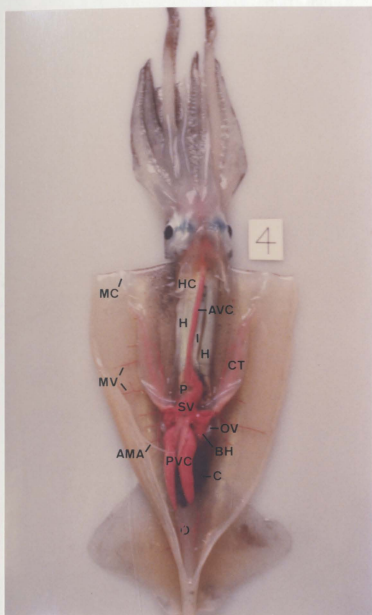


Figure 2. A photograph illustrating the dominant internal organs and structures of I. illecebrosus (female; 206 mm DML). 0.5x.

| | |
|-----|---|
| AMA | Anterior Mantle Artery |
| AVC | Anterior Vena Cava |
| BH | Branchial Heart |
| C | Caecum |
| CT | Ctenidium |
| H | Hepatic Portion of the Hepato-pancreas |
| HC | Hyponomal Cartilage |
| I | Ink Sac |
| MC | Mantle Cartilage |
| MV | Mantle Veins |
| O | Ovary |
| OV | Oviduct |
| P | Pancreatic Portion of the Hepato-pancreas |
| PVC | Posterior Venae Cavae |
| SV | Sinus Venosus |

Specimen shown with dorsal mantle surface cut open to reveal underlying internal organs and structures.



posterior point of the fin anteriorly to the distal protuberance on the mantle and is a standard measurement recorded in millimeters.

3. Historical Review of the Literature

A. The White Bodies as the Site of Hemocytogenesis

In 1950, Bolognari reviewed the subject of hemocyte production within cephalopods. He credited Cuvier (1817) with the first description of the two organs generally considered the site of blood cell production. Bolognari (1950) further stated that Hensen (1865) named each of these structures a white body (Hensen's weissen Körper) and that Faussek (1893) was the first to hypothesize their function in blood cell production. To date, the majority of researchers have corroborated Faussek's findings through histological evidence (Table 1).

Most notable in this regard are the works of Bolognari (1949, 1950, 1951), Cowden (1972), and Cowden and Curtis (1974, 1981). Bolognari (1949-1951) studied the teuthoids Heteroteuthis dispar (Ruppell, 1845), Illex coindetii (Vérany, 1837), Loligo vulgaris Lamarck, 1799, and Ommastrephes sagittatus (Lamarck, 1799); the sepioids Sepia officinalis Linnaeus, 1758, and Sepiola rondeletii Leach, 1817; and the octopods Eledone cirrosa (Lamarck, 1799), Octopus macropus Risso, 1826, and Octopus vulgaris Lamarck, 1798. White body tissue from each of the above species was examined by standard light microscopy techniques. Bolognari noted

Table 1. An historical review of studies relating to the production site of blood cells within cephalopod molluscs.

| | |
|-----|--------------------------------------|
| BHT | Basic Histological Techniques |
| DIM | Differential Interference Microscopy |
| FM | Fluorescence Microscopy |
| IVS | <u>in vitro</u> Studies |
| LM | <u>Light</u> Microscopy |
| PM | Phase Microscopy |
| TC | Tissue Culture |
| TEM | Transmission Electron Microscopy |

| Researcher(s) | Species | Proposed Site of Hemocyte Production | Method(s) of Investigation |
|----------------------|--|---|----------------------------|
| Joubin (1885) | <u>Argonauta argo</u> Linnaeus, 1758 <u>Eledone</u> sp. <u>Octopus</u> sp. <u>Ommastrephes sagittatus</u> (Lamarck, 1799) <u>Sepia officinalis</u> Linnaeus, 1758 | Branchial Gland | BHT/LM |
| Vogt and Yung (1888) | <u>S. officinalis</u> | (white body described as cushion of fatty tissue) | BHT/LM |
| Cuénot (1891) | <u>Eledone aldrovandi</u> Rafinesque, 1814 <u>Eledone moschata</u> (Lamarck, 1799) <u>Octopus vulgaris</u> Lamarck, 1798 <u>Sepia elegans</u> d'Orbigny, 1839 <u>S. officinalis</u> <u>Sepiola rondeletii</u> Leach, 1817 | Branchial Heart Appendage | BHT/IVS/LM |
| Faussek (1893) | <u>Loligo</u> sp. <u>Octopus</u> sp. <u>Sepia</u> sp. | White Body | BHT/IVS/LM |
| Cuénot (1897) | <u>E. aldrovandi</u> <u>S. officinalis</u> | White Body | IVS/LM |
| Carazzi (1901) | <u>Octopus defilippi</u> Verany, 1851 <u>O. vulgaris</u> <u>S. elegans</u> <u>S. officinalis</u> <u>S. rondeletii</u> | White Body | BHT/LM |

Table 1 (cont'd.)

| Researcher(s) | Species | Proposed Site of Hemocyte Production | Method(s) of Investigation |
|------------------------------|---|--------------------------------------|----------------------------|
| Kollmann (1908, 1924) | <u>E. aldrovandi</u> <u>E. moschata</u> <u>O. vulgaris</u> <u>S. elegans</u> <u>S. officinalis</u> | White Body | BHT/LM |
| Noel and Jullien (1933) | <u>E. moschata</u> <u>Loligo vulgaris</u> Lamarck, 1799 <u>O. vulgaris</u> <u>S. officinalis</u> | White Body | BHT/LM |
| Thore (1936) | <u>O. vulgaris</u> | White Body | BHT/LM |
| Cazal and Bogorage (1943) | <u>O. vulgaris</u> | White Body | BHT/LM |
| Bolognari (1949, 1950, 1951) | <u>Eledone cirrosa</u> (Lamarck, 1799) <u>Heteroteuthis dispar</u> (Ruppell, 1845) <u>Illex coindeti</u> (Verany, 1837) <u>L. vulgaris</u> <u>Octopus macropus</u> Risso, 1826 <u>O. vulgaris</u> <u>O. sagittatus</u> <u>S. officinalis</u> <u>S. rondeletii</u> | White Body | BHT/LM |
| Necco and Martin (1963) | <u>O. vulgaris</u> | White Body | TC/LM |

Table 1 (cont'd.)

| Researcher(s) | Species | Proposed Site of Hemocyte Production | Method(s) of Investigation |
|--------------------------------|---|--------------------------------------|----------------------------|
| Baginski (1965) | <u>E. cirrosa</u> <u>E. moschata</u> <u>Octopus</u> sp. | Branchial Gland | BHT/LM |
| Cowden (1972) | <u>O. vulgaris</u> | White Body | BHT/LM |
| Cowden and Curtis (1973) | <u>Octopus briareus</u> (Robson, 1932) | White Body | IVS/PM/DIM/FM |
| Cowden and Curtis (1974, 1981) | <u>O. briareus</u> | White Body | BHT/LM/TEM |
| Bolognari et al. (1981) | <u>Todarodes sagittatus</u> (Lamarck, 1799) | White Body | BHT/LM/TEM |

that all species possessed white bodies composed of what he called "cordoni globuligeni" (leucopoietic cords). These cords, extending from the organ's periphery toward its center, met along their length to form a network with sinuses occupying the intermediate spaces.

In cross section, these cords appeared circular or polyhedral in shape. Each cord he saw to be surrounded by "fibre reticolari" (reticular fibers) which interconnected with fibers he described as surrounding blood vessels and with the "tessuto connettivo fibrillare collagene" (collagenous fibrous connective tissue) that formed the external capsule of the white body. Associated with these reticular fibers, he described "fibrociti" (fibrocytes) with long, thin nuclei which may appear triangular in shape.

Bolognari (1949-1951) distinguished two types of elements within the "leucopoietic cords" of the white body: the "leucoblasti" (leucoblasts) and the "proleucociti" (proleucocytes). He described the former as being large cells with a highly basophilic cytoplasm. The oval nucleus of each such leucoblast measured 8-12 μm in diameter and exhibited a loose network of "bulky" chromatin and a basophilic nucleolus. Mitotic figures were described for this population of cells. The resulting daughter cells of "leucoblast" division which he called "proleucocytes", were categorized into three progressive stages of development. "First stage proleucocytes" possessed very basophilic cytoplasm and an ovoid or spherical nucleus which measured 8-10 μm in diameter. The nuclear

envelope may exhibit deep hollows which foreshadowed the lobate nucleus of the mature "leucocyte." The nuclear chromatin still appeared as a coarse network and a nucleolus was visible. The "second stage proleucocytes" possessed a less basophilic cytoplasm and a smaller (6-8 μm in diameter) nucleus of more varied shape. The nuclear chromatin was similar to that of the first stage cell, however, the nucleolus was generally absent. In the last stage, the basophilic nature of the cytoplasm was considerably reduced. The nucleus was even smaller (5-7 μm in diameter) and fine eosinophilic granules could be observed within the cytoplasm. Bolognari (1949-1951) contended that cells of this last stage mature in the sinuses of the white body. The result was a "leucocyte" that possessed a smaller, more polymorphic nucleus and larger, more numerous, and more uniformly distributed eosinophilic granules. According to Bolognari, the passage from "leucopoietic cord" to sinus was via the means of diapedesis. This observation supported the earlier statements of Noel and Jullien (1933) and Cazal and Bogoraze (1943); the forementioned researchers all utilized light microscopy techniques.

Cowden (1972) also studied the white bodies of Octopus vulgaris, however, he proposed a different classification scheme for the "leucopoietic cells". Cowden's (1972) scheme varies from that of Bolognari (1949-1951) in the following ways:

- (1) The first distinguishable cell type is recognized as a "hemocytoblast" or "reticulum cell" rather than a "leucoblast".
- (2) Two initial, developmental stages are recognized ("primary" and "secondary leucoblasts") rather than the three described by Bolognari.
- (3) An additional developmental stage is recognized by Cowden. The "proleucocyte" is considered to be a transitional form between the "secondary leucoblasts" and the mature hemocytes. Cowden's "proleucocyte" differs from Bolognari's third developmental stage in size (the former cell is larger) and nuclear organization (the nucleus of the former cell is more indented and its chromatin more concentrated).

Cowden and Curtis (1974, 1981) continued this examination of the developmental hemocyte types with a transmission electron microscopy study of white body tissue from the octopod Octopus briareus. They found that the "hemocytoblasts" could be readily distinguished from the surrounding "leucoblasts". The details concerning the ultrastructure of these cells, as described by Cowden and Curtis (1974, 1981), are listed in Table 2.

B. Alternate Sites of Hemocytogenesis

Although most workers supported the views of Faussek, Bolognari, and Cowden and Curtis, there were a few who did not. Joubin (1885) and Baginski (1965) suggested that the

Table 2. Ultrastructural characteristics of developing and mature hemocytes within Octopus briareus, as described by Cowden and Curtis (1974, 1981).

| | | | |
|-----|----------------------------------|----|-------------------------|
| A | Abundant | L | Large |
| CFM | Contains Fibrillar Matter | LA | Less Abundant |
| D | Diffuse | NP | Not Present |
| EG | Extremely Granular | O | Ovoid |
| FI | Further Increase | P | Present |
| FIA | Further increase in Abundance | PC | Prominent Concentration |
| FR | Further Reduction | R | Reniform |
| G | Granular | S | Spherical |
| GR | Greatly Reduced | SC | Slight Concentration |
| I | Irregular | SI | Slight Increase |
| IA | Increased Abundance | SR | Slight Reduction |
| IC | Increased Concentration | U | U-shaped |

| Cell Type | Ultrastructural Characteristics | | | | | | | | | | | | |
|----------------------|---------------------------------|--------------|---------------|---------|--------------------|------------------|---------------------|-------------------------|--------------------------|-----------------|-----------------------|--------------|-----------------------------|
| | Chromatin Pattern | Nuclear Area | Nuclear Shape | Nucleus | Cytoplasmic Appar. | Cytoplasmic Area | Electron Dense Rods | Electron Dense Vesicles | Electron Lucent Vesicles | Golgi Apparatus | Intercellular Bridges | Mitochondria | Rough Endoplasmic Reticulum |
| Hemocytoblast | D | L | O/S | P | EG | L | NP | P | CFM | P | P | P | A |
| Primary Leucoblast | SC | SR | O/S | P | EG | GR | NP | P | P | P | P | P | IA |
| Secondary Leucoblast | IC | FR | O/S | P | EG | FR | NP | IA | P | P | P | P | IA |
| Proleucocyte | PC | SI | R/U | NP | G | SI | NP | A | P | P | NP | P | FIA |
| Mature Leucocyte | PC | FI | I/U | NP | G | FI | P | P | P | P | NP | P | LA |

branchial gland was the site of blood cell production within cephalopods. Suspended from the dorsal mantle wall, this glandular complex is closely associated with each gill along the latter's entire dorsal surface. However, Dilly and Messenger (1972, O. vulgaris; S. officinalis), Messenger et al. (1974, Octopus sp. and an unidentified species of teuthoid) and Muzii (1981, Eledone moschata) have provided strong evidence indicating that the branchial gland is the site of hemocyanin synthesis.

In 1891, Cuénot proposed that cephalopod blood cells were produced within the branchial heart appendage. However, six years later he changed his view and supported Faussek's theory. More recently, Harrison and Martin (1965), Potts (1965, 1968), and Witmer and Martin (1973), all working with Octopus dofleini martini Pickford, have offered evidence indicating that the branchial heart appendage is the formation site of pericardial fluid rather than hemocytes.

While Vogt and Yung (1888, S. officinalis) did not propose an alternate site for hemocytogenesis, they did suggest that the white bodies were not the site. Vogt and Yung thought the white bodies were composed of fatty tissue. They envisioned each white body as a cushion on which the adjacent eye rested. However, fatty tissue has never been reported within the histological preparations of white body material collected from cephalopods.

4. The Hemocytes of *Illex illecebrosus*

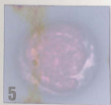
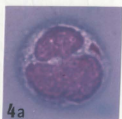
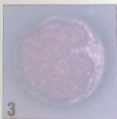
An investigation of hemocytogenesis can never be entirely complete without some mention of the end product; the circulating hemocytes, themselves. Consequently, the following description of the morphology and function of hemocytes within the blood of *I. illecebrosus* has been included. The description is from Way (1975).

Defined as eosinophilic granulocytes, these hemocytes were round or ovoid in shape and had an average diameter of 20-22 μm in stained preparations. The nucleus was a most conspicuous feature due to its size and vivid staining properties. High resolution micrographs revealed a double membrane, interrupted by nuclear pores, with the outermost unit supporting attached ribosomes. Peripheral concentrations of chromatin were visible. A highly polymorphic condition existed whereby the nucleus may assume six different configurations (Figure 3). These ranged from compacted forms through a series of seemingly graded indentations to, eventually, the appearance of three or four lobes.

The nucleus, in addition to other organelles, were suspended within a homogeneous, cytoplasmic matrix. Electron micrographs revealed the presence of dispersed ribosomes which confirmed the basophilic nature of this substance as indicated from stained preparations. Granular endoplasmic reticulum also contributed to the cytoplasm's affinity for basic dyes.

Figure 3. Photographs indicating the various nuclear configurations exhibited by circulating hemocytes of I. illecebrosus (after Way, 1975, pp. 49-50). Villanueva 1210x

1. Spherical or Ovoid Nucleus
2. Slightly Indented Nucleus
3. Progressively Indented Nucleus
4. Bilobate Nuclei
5. Trilobate Nuclei
6. Multilobate Nucleus



10 μ m

Large (5 μ m x 6 μ m), refractile vacuoles, prominent at the level of light microscopy, were identified from electron micrographs as multivesicular bodies.

Conventionally stained blood smears revealed two types of cytoplasmic granules: eosinophilic granulations and basophilic rods and spheres. The former indicated the specific nature of this cell type--"eosinophilic granulocytes". At the ultrastructural level, such granules were uniformly electron-dense.

The general structure and arrangement of the basophilic rods and spheres suggested mitochondria, especially when compared to results obtained from hemocytes stained with Janus green. However, mitochondria are reportedly not detectable under light microscopy using Romanowski stains (Bessis, 1973). Electron micrographs, however, clearly demonstrated mitochondria in these loci.

Cellular translocation (by pseudopodial amoeboid movement), phagocytosis, and agglutination, studied by means of time-lapse photography (Way, 1975), were shown to be integral characteristics of the hemocytes.

It was reported by Way (1975, p. 100) that the hemocytes of I. illecebrosus "possess functional and morphological characteristics similar to those described for leucocytes of related cephalopods". The previous description of I. illecebrosus hemocytes is condensed within Table 3.

Table 3. The morphological characteristics of hemocytes of the squid, Illex illecebrosus (from Way, 1975).

| | |
|-----|-------------------------------------|
| C | Concentrated along Nuclear Membrane |
| E | Eccentric |
| Eo | Eosinophilic |
| MVB | Multivesicular Bodies |
| NP | Not Present |
| O | Ovoid |
| P | Present |
| PM | Polymorphic |
| S | Spherical |

| Cell Type | Morphological Characteristics |
|--------------------------|---|
| Eosinophilic Granulocyte | Cell Diameter* 20-22 μm Cell Shape S/O C Nuclear Diameter* 18 μm E PM NP P Nuclear Position Nuclear Shape Nucleolus Free Ribosomes P Golgi Apparatus P Eo P Granules P Mitochondria P MVB Refractile Bodies P Rough Endoplasmic Reticulum P Vacuoles P Pseudopodia P |

*Cell and nuclear diameters were recorded for hemocytes observed in conventionally prepared blood smears.

This, therefore, has been a statement of much of the existing general knowledge concerning the white body, hemocytogenesis, and the hemocytes with respect to cephalopods, in general, and squid, in particular. As noted in the Statement of Research Proposal on page 1, it is the intention of this study to elucidate morphological, histological and morphometric characteristics of the white bodies of Illex illecebrosus and of its several lobes. It shall be attempted to demonstrate correlations between the several parts of the white body and the size of Ommastrephid squid and to demonstrate the transmission from premature hemocyte stages to the mature circulating hemocytes. There will also be speculation upon the means whereby these hemocytes once produced and released in premature stages gain entry to the general circulating vascular fluid of I. illecebrosus.

MATERIALS AND METHODS

1. Squid Collection and Maintenance

Specimens of Illex illecebrosus were collected between the months of July and October, 1979, 1980 and 1982 at Portugal Cove, Conception Bay, Newfoundland. The traditional Neyle's patent hand-line jigger and the mechanized Japanese model were employed during capture or the animals were retrieved by dip net from a squid trap (2.2 cm mesh; 73.2 M perimeter, 45.7 M leader). Once secured, the squid were placed in a 150-liter tank of aerated sea water until the boat docked. At that time the squid were transferred to a 980-liter circular tank and quickly transported by truck to the Marine Sciences Research Laboratory at Logy Bay. These teuthoids were maintained at the Marine Lab in 5,000-liter circular holding tanks supplied with a continuous flow of sea water (temperature approximately 14°C). During their captivity the squid received daily feedings of caplin (Mallotus villosus Müller, 1776).

2. Anesthetization Procedure

Squid were anesthetized before dissection or experimental work commenced. The animals were either exposed to a 2% solution of ethanol in sea water for 10 minutes, or packed in ice for 20 minutes. Flaccidity and chromatophore contraction denoted anesthetization.

Two exceptions to these procedures are noted. The first occurred during a federal fisheries research cruise aboard the GADUS ATLANTICA (February 20 through March 11, 1981). A male specimen of another species of ommastrephid squid, Ommastrephes pteropus Steenstrup, measuring 201 mm in dorsal mantle length, was caught in an Engle mid-water trawl. The trawl had been lowered to a depth of 300 meters at Station 30; latitude $40^{\circ}37.4$, longitude $56^{\circ}02.8$.

Within 30 minutes of this squid's capture, the author had been notified and her own examination of the teuthoid initiated. The peristaltic action of the branchial veins and anterior vena cava could still be observed through the ventral mantle length incision previously made by the federal biologist. The freshness of the animal's condition prompted the making of standard blood smears which were subsequently stored at -20°C for future immunological work.

The second exception occurred during the injection of tritiated thymidine (discussed in detail later herein). Although the I. illecebrosus used here were positioned over ice throughout the procedure, anesthetization was not complete due to the short interval of time involved. However, prior to the collection of blood and tissue samples, all other squid were anesthetized by standard methods as outlined above.

3. Anatomical Investigations

A. Gross Anatomical Studies

i. Descriptive Analysis of the White Bodies

The gross anatomy of the white bodies is here described from that tissue of a female specimen of I. illecebrosus; dorsal mantle length (DML), 240 mm.

Figure 4 illustrates the dorsal cephalic, T-shaped incision required to view the white bodies and facilitate their subsequent removal.

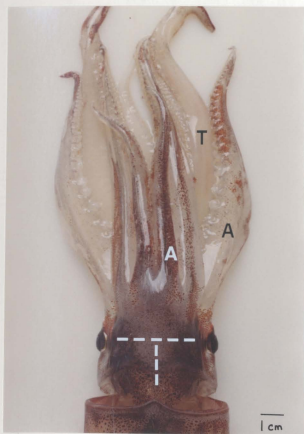
The white bodies from the above animal (representative of the species under study) were observed both immediately and following overnight fixation in formalin and sea water (1:8). This preserved material was then exposed to Giemsa hematologic stain so as to aid visualization of the white body surfaces. Photographs illustrating the gross anatomy of the white bodies were taken by the author with a Canon AE-1, 35 mm camera and Canon 50 mm macro lens. Slides and prints developed from Kodacolor fast color negative film (ASA 400) were processed commercially.

ii. Morphometric Analysis of the White Bodies

The right and left white bodies from 179 specimens of I. illecebrosus were measured during the course of this study. Dimensions of each postganglionic lobe, subganglionic process, inferior preganglionic lobe, and superior preganglionic lobe were recorded as greatest

Figure 4. A photograph to illustrate the dorsal, cephalic, T-shaped incision required to view the white body tissue and facilitate its subsequent removal (female I. illecebrosus; 240 mm DML). 0.7X

A Sessile Arm
T Tentacle
---- Line of Incision



width (cm) and greatest length (cm). These measurements were made using a standard centimeter rule. Subsequently, computer analyses provided the descriptive statistics for each measurement and plots (in the form of scattergrams) indicating the association between each measurement and the dorsal mantle length, weight, and/or sex of the squid from which a white body was collected. The computer programs, SPSS (Statistical Package for the Social Sciences) and SPSS Graphics, were employed throughout the above procedures (Nie et al., 1975).

B. Scanning Electron Microscopy Studies

White bodies from a female specimen of I. illecebrosus (dorsal mantle length, 252 mm) were fixed with acrolein followed by osmium tetroxide (Hawkes & Stehr, 1980). Acrolein was chosen due to its good preservation of marine tissues (Hawkes & Stehr, 1980) while post fixing in osmium tetroxide is commonly employed to reduce problems with charging during SEM viewing. Immediately following a fixation period of six hours, the specimens were dehydrated through a graded ethanol series. These specimens were then transferred from 100% ethanol through a graded series of Freon 113. Following infiltration with Freon 113, the specimens were critical-point dried from Freon 13 in a Bomar SPC-900/EX critical-point drying apparatus. Next, the dried specimens were mounted on aluminum stubs with silver conducting paint and gold coated in an Edwards Vacuum Coating Unit, Model E12E, with continual rotation using a planetary rotation stage. A

Cambridge Scientific Instruments "Stereoscan" Mark 2A microscope, operated at an accelerating voltage of 10 kv, was used to view the white body material.

Photographs of the white body tissue prepared for scanning electron microscopy were taken (through the viewing screen of the microscope) by the author with a Polaroid camera using Polaroid positive negative film, type 665.

C. Light Microscopy Studies

i. Basic Histological Techniques

White bodies from seven specimens of I. illecebrosus (three males: dorsal mantle lengths of 190 mm, 195mm, and 220 mm; four females: dorsal mantle lengths of 205 mm, 215 mm, 232 mm, and 242 mm) were placed in one of the four routine fixatives for general micro-anatomy (Humason, 1972). These included Bouin, formalin in sea water (1:8 as suggested by Bradbury, 1970), Helly, and Zenker fixatives. Standard histological techniques were followed during the fixation, subsequent processing and embedding of these white body samples. Paraplast (Scientific Products) sections, 7 μ m in thickness were cut on a Spencer "820" microtome and stained with Wright, Giemsa, and Villanueva hematologic stains.

ii. Frozen Tissue Techniques

Conventional freezing techniques (Humason, 1972) were also undertaken. Illex illecebrosus white bodies from two females (dorsal mantle lengths, 217 mm and 224 mm) were placed in OCT compound (a tissue embedding medium; Canlab) and frozen with an isopentane and liquid nitrogen

mixture. Frozen sections, 7 μm in thickness, were cut on a Bright Cryostat and stained with hematoxylin and eosin.

Both the standard fixation technique and the frozen tissue technique were employed so that a means for comparing the quality of white body preservation would be obtained. Photographs of white body tissue processed for light microscopy were taken by the author with an Orthomat-W microscope camera (automatic exposure; natural filter) and Kodak Ektachrome 50 tungsten film. Slides and color prints were developed commercially.

D. Transmission Electron Microscopy Studies

Karnovsky fixative is one of the standard fixatives employed in electron microscopy. During the present study (procedure by Hyam, 1981) five variations of this fixative were utilized to ensure good preservation of white body tissue. Three of these five Karnovsky variations had pH and osmolarity values adjusted to those of the squid's blood.

A pH meter (Corning) was used to analyze I. illecebrosus blood collected with a 5 cc disposable syringe from the systemic heart, branchial hearts, branchial veins, cephalic aorta, and posterior venae cavae of an anesthetized female (dorsal mantle length 278 mm).

To ascertain the osmolarity of the circulating fluid within I. illecebrosus, the author collected blood with 1 ml disposable syringes from the systemic heart,

branchial hearts, branchial veins, cephalic aorta, and posterior venae cavae of two anesthetized females (dorsal mantle lengths 255 mm and 257 mm). The blood samples (one from each animal) were then analyzed separately with the aid of a Digimatic Osmometer (Advanced Instruments, Inc.).

The white body tissue examined throughout this EM study was obtained from six I. illecebrosus specimens; two males (dorsal mantle lengths of 230 mm and 242 mm) and four females (dorsal mantle lengths of 250 mm, 252 mm, 257 mm, and 260 mm).

Tissue samples from the right postganglionic lobe of each male and three of the four females were removed and placed in one of five variations of Karnovsky fixative, while tissue samples from the entire right white body of the 252 mm DML female specimen were removed and placed solely within the variation 5 Karnovsky fixative. The variations of fixative included: (1) the standard Karnovsky fixative made with sodium cacodylate buffer; (2) Karnovsky fixative made with sea water; (3) standard Karnovsky fixative with sodium cacodylate buffer, pH adjusted to that of squid's blood; (4) Karnovsky fixative with sea water, pH adjusted to that of squid's blood; and (5) Karnovsky fixative with sodium cacodylate buffer, pH and osmolarity adjusted to that of squid's blood.

Immediately following a fixation period of 20 minutes (Hyam, 1981), all the white body samples were washed in sodium cacodylate buffer and then post-fixed in

osmium tetroxide. A second wash in sodium cacodylate buffer preceded block staining with saturated aqueous uranyl acetate. All samples were then dehydrated through a graded ethanol series and embedded in Epon 812. Both thick (0.5 μm) and thin (600-900 \AA) sections of white body tissue were cut on a Reichert OMU-3 ultramicrotome. Thick section preparations were stained with toluidine blue and viewed by means of light microscopy. Photographs of these thick sections were taken by the author with an Orthomat-W microscope camera (automatic exposure; natural filter) and Kodak Ektachrome 50 tungsten film. Slides and color prints were developed commercially. Thin section preparations were stained with lead citrate and viewed with a Phillips 300 electron microscope. Micrographs of these thin sections were developed and printed following standard darkroom techniques.

E. Numeric and Morphometric Studies of the White Body Cells

The frequency at which each variation of white body cell occurs within a given white body component was investigated. One hundred white body cells, within a randomly chosen field of view, were examined using a Nikon microscope and an AO Spencer eyepiece micrometer (100 squares; each 1 square mm). The number of cells representing each variation was recorded. This procedure was repeated for each component of the right white body collected from a female specimen of I. illecebrosus; dorsal mantle length,

257 mm. The forementioned tissue was processed by means of transmission electron microscopy techniques. Although corresponding samples from additional specimens were not available, individual samples (the right postganglionic lobe, only) collected from two males, dorsal mantle lengths of 230 mm and 242 mm, and three females, dorsal mantle lengths of 250 mm, 252 mm, and 260 mm, were available for comparative purposes.

A morphometric analysis of the white body cells was undertaken to determine if differences in cellular diameter exist among the four variations. Twenty-five examples of each of the four variations of white body cells were randomly chosen within each white body component and their diameters recorded. For comparison, like measurements were made of circulating hemocytes. Tissues examined during this analysis were collected from a female specimen of I. illecebrosus, dorsal mantle length of 257 mm, and processed by transmission electron microscopy methods.

F. Vascular Studies

i. Latex Injection Techniques

Latex injections were employed to elucidate the blood supply of the white bodies. Five I. illecebrosus specimens were studied using this approach: two males (dorsal mantle lengths of 212 mm and 214 mm) and three females (dorsal mantle lengths of 206 mm, 211 mm, and 227 mm).

A 1:1 mixture of red Latex (Ward's Natural Science) and distilled water was used to outline the vascular system

of the white bodies. This Latex mixture was injected into the circulation with a 5 ml sterilized, disposable syringe fitted with a 21 G sterile needle. To ensure that an adequate supply of the mixture reached the white body tissue, a ventral mantle length incision was made and the hepatic mesentery perforated. By displacing the hepatic portion of the hepatopancreas laterally, the cephalic aorta was exposed in a region anterior to this gland. The injection was made via the cephalic aorta at that point. Such a procedure is necessary because the hepatic portion of the hepatopancreas receives a copious supply of blood from the cephalic aorta, posterior to that point (Bradbury, 1970, p. 16). Within 20 minutes the dorsal cephalic region of the squid can be carefully dissected and the vascular system of the white bodies visualized.

ii. Drawing Ink Injection Techniques

The vascular system of the white bodies was also studied following injections of full strength Staedtler red drawing ink. Two female specimens of I. illecebrosus (dorsal mantle lengths of 204 mm and 208 mm) were involved. The methods employed during this study were identical to those described for the Latex investigation, with the exception of the agent injected. This technique should reveal the smaller vessels which would otherwise remain undefined by the Latex method.

iii. Angiography Techniques

Further understanding of the white body vasculature required the employment of angiography techniques. Three female specimens of I. illecebrosus (dorsal mantle lengths 230 mm, 245 mm, and 265 mm) were involved in this study.

Anesthetized squid were individually placed on plastic covered x-ray plates. A ventral, mantle length incision was made and the postvisceral mesentery perforated so as to expose the cephalic aorta. Surgical suture (black, braided type B non-absorbable 5-10 silk) was passed beneath the aorta and the two free ends secured with mosquito clamps. This procedure not only elevated the vessel but also helped to maintain it in a stationary position. Ten ml of RENOgrafin-60 (a radiopaque contrast agent; Squibb) were injected via the cephalic aorta at a point immediately anterior to the systemic heart using a Butterfly 21 (0.8 mm) infusion set. X-ray plates were exposed at 55 kilovolts at 16 milliamps per second. Standard processing methods were followed during the development of these x-ray plates. In addition, a dynamic record of the blood supply to the white bodies was preserved on video cassette tape. Each squid was kept moist with sea water between exposures.

4. Immunological Studies

The following studies were undertaken to investigate immunological relationships existing between

I. illecebrosus white body tissue cells and the hemocytes of the blood.

A. Antisera Preparation

Frozen white body tissue from a male specimen of I. illecebrosus (dorsal mantle length, 215 mm) was thawed, rinsed in sea water, and then gently squeezed with forceps in order to produce a cell suspension. This suspension was diluted with sea water before being filtered through a Pasteur pipette, one-quarter filled with glass wool. To ensure complete separation of cells from particulate matter, the suspension was layered over Ficoll-Paque density gradient medium (Pharmacia, density 1.077) and centrifuged at 6°C for 15 minutes at 450 g. The supernatant was then removed and the resultant pellet of cells resuspended in phosphate-buffered saline (PBS). This material was then centrifuged at 6°C for a further 15 minutes at 350 g. An additional wash with PBS was performed to ensure the removal of any remaining Ficoll-Paque. A cell count was then made on the above cell suspension using a Spencer Bright-Line Hemacytometer. Finally, 1 ml of the filtered and washed white body cell suspension of known cellular density was administered intravenously into the experimental rabbit (a male New Zealand White weighing 3 kgm). The schedule established for subsequent injections is outlined in Table 4.

Five ml syringes with 21 G needles were used to collect 4 ml blood samples from the rabbit, while a

Table 4

Immunization Schedule for the Production of
Antisera to Illex illecebrosus
White Body Cells

| Squid Sampled | | | | |
|---------------|-----|-------------------------------------|--------------------------|---|
| Time | Sex | Dorsal Mantle Length (DML) | No. of Cells Injected | Aliquot of Rabbit Blood Collected |
| 0 | M | 215 mm | 7.5×10^6 | - |
| 7 days | M | 210 mm | 15.0×10^6 | - |
| 21 days | F | 217 mm | 9.8×10^6 | 4 ml |
| 28 days | M | 206 mm | 138.0×10^6 | 4 ml |
| 35 days | - | - | - | 45 ml |

Butterfly-23 G infusion set was employed to collect the final sample (per schedule in Table 4). Once obtained, the rabbit's blood was allowed to clot for 30 minutes, then centrifuged at room temperature for 20 minutes at 1000 g. The serum collected was stored at -20°C in 2 ml aliquots.

B. Agglutination

The slide agglutination technique was employed in the initial testing of the antisera samples. Several drops of white body cell suspension were placed on either end of a glass slide. One pool received an equal amount of anti-serum; the other, an equal amount of saline. A positive test was denoted by visible agglutination.

C. Smear and Tissue Section Preparation

The following squid tissues were employed to test antiserum by means of the indirect immunofluorescent technique:

- (1) white body, liver, and muscle sections from each of three specimens of I. illecebrosus (one male: DML, 198 mm; two females, DML: 217 mm and 224 mm, respectively);
- (2) prepared white body cell suspension smears from each of four I. illecebrosus specimens (three males, dorsal mantle lengths of 194 mm, 206 mm and 209 mm; one female, dorsal mantle length of 217 mm);

- (3) venous blood (branchial veins) smears from two specimens of I. illecebrosus (one male, dorsal mantle length, 198 mm; one female, dorsal mantle length, 224 mm), and a male specimen of Ommastrephes pteropus (dorsal mantle length, 201 mm);
- (4) serum absorbed with various I. illecebrosus tissues (refer to the Tissue Homogenates section which follows).

All tissue sections were prepared by conventional freezing methods as outlined previously, with the exception that they were not stained. Prepared white body cell suspension smears and blood smears were made by standard methods, allowed to air dry, and stored at -20°C if not used immediately.

D. Tissue Homogenates

Ink sac, liver, mantle (muscle), optic ganglion, ovary, and stomach tissue samples collected from three specimens of I. illecebrosus (dorsal mantle lengths not recorded) were individually, by tissue, placed in a Waring blender with sea water and homogenized. Each of the tissue samples was centrifuged at 6°C for 10 minutes at 850 g. The supernatant was then removed and the material re-suspended in phosphate-buffered saline. Two additional washes in PBS were performed.

E. Absorbed Antisera

A volume of 0.1 ml of the rabbit antiserum, diluted to 0.5 ml with PBS, was absorbed with 0.5 ml of tissue homogenate or white body cells (pooled from two male specimens of I. illecebrosus; 194 mm and 209 mm DML) at room temperature for one hour. The absorbed antiserum was collected after centrifugation at 6°C for 10 minutes at 850 g and stored at -20°C.

F. Immunofluorescence

Having completed the necessary processing of samples, the author employed indirect immunofluorescence* to test the rabbit antiserum. Prepared slides with the various tissue sections were placed in PBS for 5 minutes to remove the embedding medium. These slides were then air dried and transferred to an incubation chamber. Smears made from the prepared white body cell suspension or venous blood were also placed in the chamber at that time. Blood for the latter was obtained from the branchial veins of I. illecebrosus and O. pteropus using 1 ml sterile disposable tuberculin syringes and 26 G needles. Half of the O. pteropus blood smears were fixed in 95% ethanol for 10 minutes before their introduction to the chamber. Next, each section or smear was covered with 2-3 drops of the appropriate fluid (PBS or normal rabbit serum for controls; rabbit antiserum or rabbit antiserum absorbed with one of the six tissue homogenates for experimental tests).

*

JOHNSON, G.D. and E.J. HOLBOROW, 1973 "Immunofluorescence" in Handbook of Experimental Immunology, D.M. Weir (Ed.), Blackwell Scientific Publication, pp 18.1-18.20

Incubation proceeded at room temperature for 30 minutes. After a rinse with PBS, each slide was immersed in the same for 10 minutes to remove any unbound antibodies. Upon removal from the PBS, these slides were air dried and returned to the incubation chamber. All slides were then exposed to fluorescent sheep antibody to rabbit immunoglobulin (Wellcome Reagents), diluted 1:10 with PBS, for 30 minutes under dark conditions. A final wash in PBS preceded the addition of glycerine and a coverslip.

All slides were prepared in duplicate and read by a person who was unaware of their identification or nature. Photographs illustrating immunofluorescence were taken with a Nikon fluorescent microscope camera (automatic exposure; barrier 50 filter) and Kodak Ektachrome 400 film. Slides and color prints were developed commercially.

5. Mitotic Index Study

To evaluate a given tissue's capacity for cellular renewal, as in the case of suspected hemocyte producing tissues, one may ascertain the percentage of cells undergoing division at any given time. This percentage, known as the mitotic index, is calculated using the formula (Kruse & Patterson, 1973; Sheeler & Bianchi, 1980) in which

$$I_m = \frac{N_m}{N} \times 100$$

I_m refers to the mitotic index; N_m , the number of cells with nuclei observed within the mitotic process; and N , the

total number of cells observed.

The mitotic index of white body tissue from I. illecebrosus was computed by this method. Samples of white body tissue from six specimens of I. illecebrosus (Table 5) were observed. The white body tissue collected included the right postganglionic lobe from each squid and, in the case of the December 5, 1979 specimen, additional samples from each remaining portion of the right white body. Tissue samples were collected over a four month interval (September-December, 1979) and processed by the transmission electron microscopy methods outlined previously. Thick (0.5 μm) sections stained with toluidine blue were employed during the actual calculation of the mitotic index. The procedure involved the random counting of 1,000 white body cells per sample, using a Nikon microscope and an AO Spencer eyepiece micrometer (100 squares; each 1 square mm). The ratio of mitotic figures (cells undergoing mitosis) to the total number of cells counted was observed for each sample and recorded. Mitotic figures were recognized as follows:

| | |
|------------------|--|
| <u>Prophase</u> | The presence of chromosomes. |
| <u>Metaphase</u> | A centrally arranged pattern of chromosomes. |
| <u>Anaphase</u> | Separation of the chromosomes to opposite regions of the cell. |

Telophases were not counted in this index for reasons that will be discussed later (DISCUSSION).

Table 5

Descriptive Data on Specimens of I. illecebrosus
Employed in Determination of Mitotic
Index in White Bodies

| Squid No. | Sex of Squid | Dorsal Mantle Length (DML) of Squid | Date on Which White Body Tissue Was Sampled |
|-----------|--------------|-------------------------------------|---|
| 1 | M | 230 mm | September 19, 1979 |
| 2 | M | 242 mm | September 19, 1979 |
| 3 | F | 252 mm | October 1, 1979 |
| 4 | F | 260 mm | October 25, 1979 |
| 5 | F | 250 mm | November 5, 1979 |
| 6 | F | 257 mm | December 5, 1979 |

6. Radioisotope Labeling Studies

In an effort to ascertain if an isotope labeled compound could be used to trace circulating cells of the squid from white body tissue cells, part of this study involved the use of tritiated thymidine injected in I. illecebrosus.

A. Employment of Radioisotope

A 1% solution of saline was added to a concentration of 0.75 μ Ci of tritiated thymidine (6.7 Ci/mmol. specific activity; New England Nuclear) per gram weight of squid to make a final volume of 1 ml (technique modified from Feinendegen, 1967). This radioactive material was injected via the cephalic aorta of each of 16 specimens of I. illecebrosus using a 1 ml disposable syringe. In Table 6 is detailed information regarding the squid employed in this phase of the study and experimental procedures.

The squid used in these tritiated thymidine studies were individually netted from the MSRL 5,000-liter holding tank and immediately placed in a container filled with 20 liters of sea water. Each squid was then weighed using a Mettler PL 300 balance and promptly transferred to a 20-liter tank supplied with circulating sea water. In preparation for the radioisotope injections, each squid was placed on its dorsum on paper towelling previously saturated with sea water; the entire

Table 6. Schedule of exposure to tritiated thymidine and morphometric and other data on specimens of Illex illecebrosus sacrificed in the study.

| Squid No. | Sex of Squid | Dorsal Mantle Length (DML) of Squid | Weight of Squid | Duration of Exposure to Tritiated Thymidine before Sacrifice of Experimental Squid |
|-----------|--------------|-------------------------------------|-----------------|--|
| 1 | F | 178 mm | 119.4 gm | 30 minutes |
| 2 | M | 198 mm | 132.6 gm | |
| 3 | M | 172 mm | 93.6 gm | 1 hour |
| 4 | M | 195 mm | 128.8 gm | |
| 5 | F | 176 mm | 124.5 gm | 3 hours |
| 6 | F | 180 mm | 122.7 gm | |
| 7 | F | 200 mm | 156.7 gm | 5 hours |
| 8 | F | 195 mm | 119.5 gm | |
| 9 | M | 180 mm | 99.6 gm | 10 hours |
| *10 | F | 215 mm | 228.0 gm | |
| 11 | M | 186 mm | 136.8 gm | 24 hours |
| 12 | M | 187 mm | 127.2 gm | |
| 13 | M | 180 mm | 122.9 gm | 48 hours |
| *14 | M | 193 mm | 142.5 gm | |
| 15 | F | 200 mm | 139.8 gm | 72 hours |
| 16 | F | 186 mm | 109.4 gm | |

*Experimental animal expired during course of exposure to tritiated thymidine.

assemblage of squid and towelling overlying crushed ice. The tapered end of plastic, sea water conducting tubing (6 mm in diameter) was introduced into the mantle cavity thereby supplying a continuous flow of sea water over the ctenidia. During an inhalatory phase, with mantle expansion, a 2.25 cm ventral mantle incision was made over the site of the systemic heart and adjacent organs. The sea water supply to the mantle cavity was then discontinued and the aperture of the incision widened with the aid of tissue retractors. Perforation of the post-visceral mesentery exposed the cephalic aorta into which the tritiated thymidine/saline solution was injected at a point immediately anterior to the systemic heart (Figure 5). Following the injections, tissue retractors were removed and sea water re-introduced to the mantle cavity. With the return of strong and regular mantle contractions, the squid were placed in a container filled with sea water and quickly transported to a 980-liter tank supplied with circulating sea water. Each squid remained within the tank for the duration of the experiment. Subsequently, each squid was anesthetized with a 2% solution of ethanol in sea water prior to the removal of white body tissue and blood samples.

B. Histological Techniques

On the appointed day (see Table 6), the postganglionic lobe of a white body was excised and fixed in Carnoy's Fluid (Bogoroch, 1972) for 2 hours. The tissues were routinely processed for light microscopy. Histological

Figure 5. Diagram illustrating the method of injecting tritiated thymidine into specimens of I. illecebrosus (right lateral view). 2.4 x

| | |
|----|-------------------------|
| CA | Cephalic Aorta |
| MC | Mantle Cavity |
| PA | Posterior Aorta |
| PM | Post-visceral Mesentery |
| SH | Systemic Heart |
| TR | Tissue Retractors |
| VM | Ventral Mantle |

sections of this material, 4 μm in thickness, were cut and placed on microscope slides previously dipped in an aqueous solution of 0.5% gelatin and 0.05% chrome alum in preparation for autoradiography (Bogoroch, 1972).

In addition, blood smears were made utilizing microscope slides previously dipped in the gelatin solution mentioned above. Arterial and venous samples of blood were collected using 1 ml disposable syringes. The arterial blood was collected from the cephalic aorta and/or systemic heart while venous blood was collected from the anterior vena cava. This procedure immediately succeeded the placing of white body tissue into Carnoy's Fluid. After air drying, blood smears were fixed with 100% ethanol for 10 minutes and stored at room temperature.

C. Autoradiography Techniques

The following darkroom methods employed during the standard preparation and subsequent processing of each autoradiograph are those cited by Bogoroch (1972). All blood smears, prepared slides of white body tissue, and blank control slides were coated with Eastman Kodak NTB 2 photographic emulsion (by hand dipping) and allowed to air dry. Labeled and control dry slides were then arranged in a plastic slide box, one end of which contained a packet of the drying agent, Drierite (Fisher Scientific). Prior to the storage of these slides at 4°C, the slide box lid was replaced and the entire container securely wrapped in aluminum foil. Multiple slides were made from each sample

so that autoradiographs could be processed periodically to determine the results following varying periods of incubation. Standard techniques followed during the processing of the autoradiographs employed the Eastman Kodak developer D-19 and F-5 fixative. Processed slides were air dried, stained with toluidine blue, and mounted with coverslips. Each autoradiograph was examined by means of light microscopy (Nikon photomicroscope).

RESULTS

1. Morphological Studies of the White Bodies

A. Gross Anatomy

i. Descriptive Analysis

The white bodies within Illex illecebrosus comprise two incomplete rings of soft tissue that are either translucent or opaque white in color. Each partial ring, predominated by three lobes, is securely attached by connective tissue to the external medial surface of the adjacent eye and encircles the optic ganglion within that orbital cavity. The white body is attached, as described, to the eye; said connection via the media of connective tissue along the outer rim of the several lobes of which the organ is composed. The discontinuous white body ring of the right eye is a mirror image to that of the left. The largest lobe of each white body can be viewed following cephalic dissection (Figure 6). An entire white body lobe series is visible only following excision of an eye (Figure 7).

The largest of the lobes, here named the post-ganglionic lobe, is lacrimiform in shape and measures approximately 1.4 cm in greatest length and approximately 0.8 cm in greatest width (refer to Appendix 1).

Figure 6. A dorsal, cephalic dissection of I. illecebrosus (female; 240 mm DML) revealing the postganglionic lobes of the two white bodies. 1.7 x

| | |
|-----|---|
| BC | Brachial Cone; Displaced Anteriorly |
| CC | Cranial Cartilage |
| CG | Cephalic Ganglion |
| E | Esophagus |
| LEy | Left Eye |
| LOG | Left Optic Ganglion |
| LP | Postganglionic Lobe of the Sinistral White Body |
| M | Mantle; Anterior Margin Showing the Distal Protuberance |
| REy | Right Eye |
| ROG | Right Optic Ganglion |
| RP | Postganglionic Lobe of the Dextral White Body |

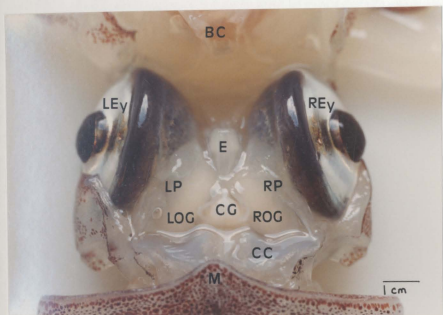


Figure 7. An external, medial view of the right eye (female I. illecebrosus; 240 mm DML) showing the discontinuous ring configuration of the white body.

A. Photograph illustrating the location, orientation, and general appearance of freshly dissected white body tissue. 4 x

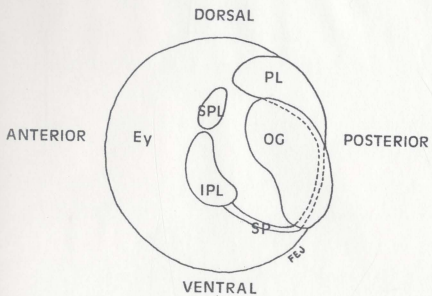
B. Diagrammatic representation of above.

| | |
|-----|-----------------------------|
| Ey | Eye |
| IPL | Inferior Preganglionic Lobe |
| OG | Optic Ganglion |
| PL | Postganglionic Lobe |
| SP | Subganglionic Process |
| SPL | Superior Preganglionic Lobe |

A



B



Each postganglionic lobe exhibits a free terminus of dorsal orientation, while the remaining portion curves around the optic ganglion to face posteriorly. The dorsal terminus aligns with the vertical stripe of the eye's lateral surface (Figure 8). This observation is noted for future reference should a visual external marker become necessary in the location of the postganglionic lobe. From the ventral portion of each postganglionic lobe there originates a narrow band of tissue that proceeds around the optic ganglion to contact the inferior preganglionic lobe of the white body (Figures 9 and 10). This connecting band of tissue is here named the subganglionic process. Measuring approximately 2.0 cm in length, it appears to be composed of two portions; that which extends from the postganglionic lobe and that which contacts the inferior preganglionic lobe. The former (Figure 10) constitutes approximately half of the total process length and measures 0.25 cm in width. Its wavy, serpentine configuration ends within the angulation of the Y-shaped structure that identifies the remaining portion of the subganglionic process. The base of this "Y" progresses dorsoanteriorly as a single band of tissue which subsequently passes beneath, and is hidden by, the inferior preganglionic lobe. Here, this portion of the subganglionic process increases to a width of approximately 0.4 cm before its impending termination. The forenamed inferior preganglionic lobe appears reniform (approximately 1.0 cm long, 0.5 cm wide)

Figure 8. A photograph showing the alignment between the dorsal tip of the postganglionic lobe (→) and the vertical stripe on the eye's lateral surface (female I. illecebrosus; 240 mm DML; freshly dissected right eye). 2.3 x

| | |
|-----|---------------------|
| L | Lens |
| OG | Optic Ganglion |
| PL | Postganglionic Lobe |
| REy | Right Eye |
| VS | Vertical Stripe |



Figure 9. A photograph illustrating the position of the subganglionic process in relation to the remaining white body structures (female I. illecebrosus; 240 mm DML; right eye). 4 x

| | |
|-----|--------------------------------|
| IPL | Inferior Preganglionic Lobe |
| PL | Postganglionic Lobe |
| REy | Right Eye |
| RN | Retinal Nerves |
| SP | Subganglionic Process |
| SPL | Superior Preganglionic Process |

The entire right eye was fixed in formalin and sea water (1:8) overnight and then stained with Giemsa hematologic stain.

Removal of the optic ganglion afforded an unobstructed view of the entire white body. The free lateral margin of the postganglionic lobe has been reflected posteriorly to reveal this lobe's surface normally applied against the eye ball; the ocular surface.

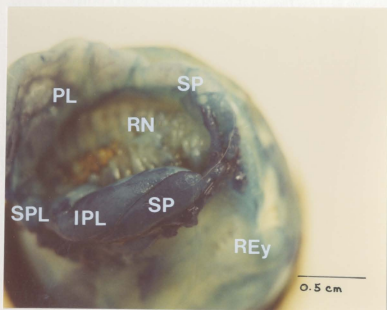


Figure 10. Photographs illustrating the serpentine configuration of the subganglionic process and the latter's association with the ventral portion of the postganglionic lobe (female I. illecebrosus; 240 mm DML).

A. Medial view of the right eye. 2.5 x

B. Lateral view of the right eye. 4.2 x

IPL Inferior Preganglionic Lobe
PL Postganglionic Lobe
REy Right Eye
RN Retinal Nerves
SP Subganglionic Process
SPL Superior Preganglionic Lobe

The entire right eye was fixed in formalin and sea water (1:8) overnight and then stained with Giemsa hematologic stain.

The optic ganglion has been removed.

A



B



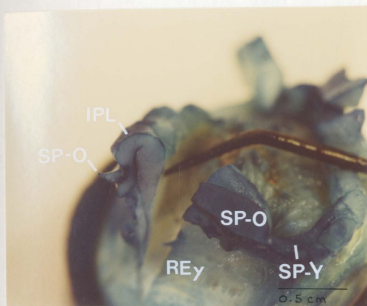
in shape when viewed in its customary position (Figure 7). However, when this lobe is displaced vertically (its posterior surface applied to the back of the squid's eye) and sectioned, the lobe's anterior rim is shown to extend beneath the reniform portion (Figure 11). It is this underlying segment of the inferior preganglionic lobe that contacts the subganglionic process (Figure 11). Closely associated with each inferior preganglionic lobe is the third and final lobe of the white body series (Figure 7). This is the smallest of the three lobes; measuring approximately 0.6 cm in length and 0.3 cm in width. In recognition of this lobe's location, it is here named the superior preganglionic lobe. Each superior preganglionic lobe displays an ovate shape. The ventral edge of the superior preganglionic lobe either contacts the dorsal edge of the adjacent inferior preganglionic lobe or occurs within 0.2 cm of the latter. At no time has the superior preganglionic lobe been observed in contact with the subganglionic process. The dorsal edge of the superior preganglionic lobe lies within 0.3 cm of the postganglionic lobe's free terminus.

These various white body components possess a similar external appearance, with the exception of the postganglionic lobe. Whereas the subganglionic process, the inferior preganglionic lobe, and the superior preganglionic lobe display exteriorly smooth surfaces, the postganglionic lobe exhibits irregularities. These irregularities

Figure 11. A photograph illustrating the gross anatomy of the inferior preganglionic lobe and the latter's relationship to the subganglionic process (female I. illecebrosus; 240 mm DML; right eye). 5 x

IPL Inferior Preganglionic Lobe
REy Right Eye
SP-0 Subganglionic Process; Obscured
by the IPL
SP-Y Subganglionic Process; the Y-shaped
Structure that Identifies This Portion
of the Process

The entire right eye was fixed in formalin and sea water (1:8) overnight and then stained with Giemsa hematologic stain.



assume three forms: a network of surface blood vessels, shallow notches, or deep furrows (Figure 12). The network of surface blood vessels creates a distinctive pattern across the postganglionic lobe's orbital surface while the shallow notches occur at intervals along the free margin of the lateral surface (that edge nearest the optic ganglion). On the left eye, the left free lateral surface is so involved, in the case of the right eye, the right. Deep furrows, which have not been observed in all instances, appear only where the postganglionic lobe is attached to the medial surface of the eye.

Therefore, the white bodies are presented as two discontinuous rings of soft tissue; each encircling an optic ganglion within an orbital cavity. Both white bodies are composed of three lobes and a connecting process. The components of each white body are labeled in accordance to their position relative to the adjacent optic ganglion. The postganglionic lobe is not only the largest lobe but also the most irregular in surface appearance. The subganglionic process appears to be made of two portions; a sinuous portion that extends from the ventral surface of the postganglionic lobe and a Y-shaped portion. The base of this latter portion proceeds dorsoanteriorly to a position beneath the inferior preganglionic lobe. The reniform-shaped inferior preganglionic lobe actually folds back on itself and it is this underlying portion which contacts the terminus of the subganglionic process. The white body "ring"

Figure 12. Photographs showing the surface irregularities exhibited by the postganglionic lobe (female I. illecebrosus; 240 mm DML).

- A. Medial view of the right eye. 2.7 x
- B. Enlargement of above; optic ganglion has been removed. 5.1 x
- C. Longitudinal section through a portion of the right postganglionic lobe. 5.3 x

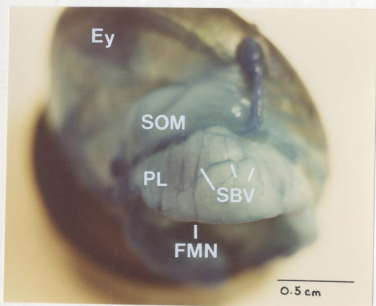
| | |
|-----|---|
| DF | Deep Furrow |
| Ey | Eye; Right |
| FMN | Free-Marginal Notch |
| IPL | Inferior Preganglionic Lobe of the White Body |
| OG | Optic Ganglion |
| PL | Postganglionic Lobe of the White Body |
| SBV | Surface Blood Vessels |
| SOM | Superior Oculomotor Muscle |
| SP | Subganglionic Process of the White Body |
| SPL | Superior Preganglionic Lobe of the White Body |

The entire eye was fixed in formalin and sea water (1:8) overnight and then stained with Giemsa hematologic stain.

A



B



C



is completed (Figure 13) with the superior preganglionic lobe which is situated between the inferior preganglionic lobe and the free terminus of the postganglionic lobe.

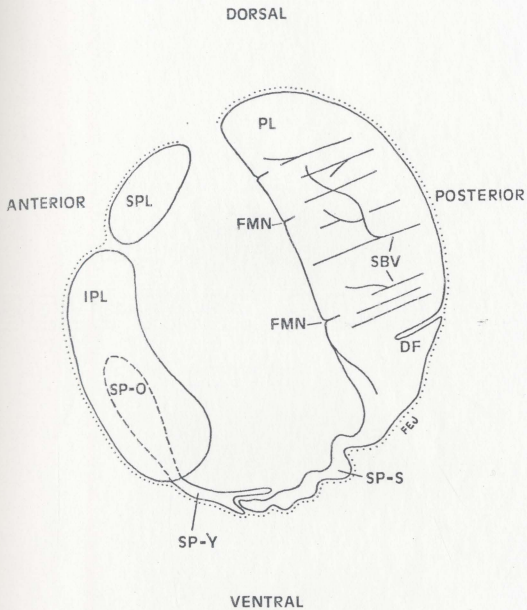
ii. Morphometric Analysis

Values representing the width or length of each component of the right and left white bodies from 179 specimens of I. illecebrosus were plotted against (1) values for the dorsal mantle length of the squid from which the white bodies were collected (Figures 14 through 29); (2) values for the weight of the squid from which the white bodies were collected (Figures 30 through 45); and (3) the sex of the squid from which the white bodies were collected (Table 7). Furthermore, values representing the width or length of each component of each right white body were compared with corresponding values for each left white body (Table 8). Finally, values representing the length of each component of each right white body were summed to give the total length of each right white body. These latter values were then plotted against values for the dorsal mantle length (Figure 46) or weight (Figure 47) of the squid from which the white bodies were collected. Similar computations provided information regarding the total length of each left white body and dorsal mantle length (Figure 48) or teuthoid weight (Figure 49). The data were sorted by sex.

In several instances, "missing values" were recorded. Such cases occurred when the squid's eye had collapsed,

Figure 13. A composite drawing illustrating the gross anatomy of a white body from I. illecebrosus. 10 x

| | |
|-------|---|
| DF | Deep Furrow |
| FMN | Free-Marginal Notch |
| IPL | Inferior Preganglionic Lobe |
| PL | Postganglionic Lobe |
| SBV | Surface Blood Vessels |
| SPL | Superior Preganglionic Lobe |
| SP-O | Subganglionic Process; Obscured Portion |
| SP-S | Subganglionic Process; Serpentine Portion |
| SP-Y | Subganglionic Process; Y-shaped Portion |
| | Area of Attachment |



Figures 14-29

The following statements summarize the information presented within Figures 14 through 29 (values representing the width or length of each component of a white body plotted against values for the DML of the squid from which a white body was obtained). Results of the morphometric study indicate a positive correlation at the 0.01 level of significance between (1) the width of each component of a white body and DML (2) the length of each component (except the subganglionic process) and DML. The evidence indicates that the correlation between the length of the subganglionic process and DML is not significantly different from zero at the 0.01 level.

When the above values are plotted with respect to the sex of the squid, the results of the morphometric study indicate a positive correlation at the 0.01 level of significance between (1) the width of each component of a white body and DML for females (2) the width of each component (except the right superior preganglionic lobe) and DML for males (3) the length of each component (except the subganglionic process) and DML for females (4) the length of each component (except the subganglionic process and superior preganglionic lobes) and DML for males. A positive correlation is obtained between the length of the superior preganglionic lobes and DML (for males) at the 0.05 level of significance. The evidence indicates that the correlation between the width of the right superior preganglionic lobe and DML (males) and the length of the subganglionic process and DML (males or females) is not significantly different from zero at the 0.01 or 0.05 level.

Figure 14. A scattergram in which values for the width of the right postganglionic lobe are plotted against values for the dorsal mantle length.

Statistics:

| | |
|----------------|---------|
| Correlation | 0.77357 |
| Significance | 0.00000 |
| Plotted Values | 178.0 |
| Missing Values | 1.0 |

The evidence indicates a positive correlation at the 0.01 level of significance.

Raw data are presented within Appendix 2.

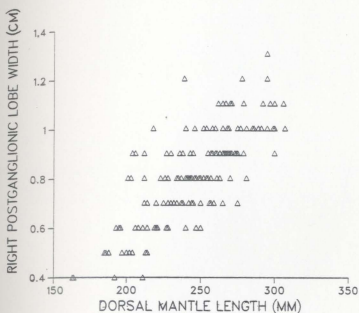
Figure 14A. The same as above, save that values obtained are sorted with respect to sex of the squid.

Statistics:

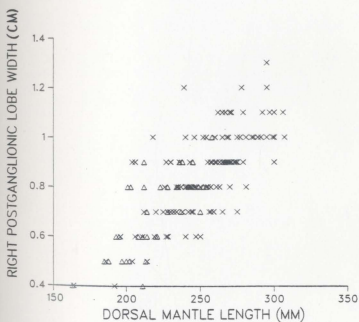
| | Males | Females |
|----------------|---------|---------|
| Correlation | 0.76662 | 0.71844 |
| Significance | 0.00000 | 0.00000 |
| Plotted Values | 41.0 | 137.0 |
| Missing Values | 0.0 | 1.0 |

In both sexes, the evidence indicates a positive correlation at the 0.01 level of significance.

14



14A



Legend

△ MALE,

× FEMALE

Figure 15. A scattergram in which values for the width of the left postganglionic lobe are plotted against values for the dorsal mantle length.

Statistics:

| | |
|----------------|---------|
| Correlation | 0.77022 |
| Significance | 0.00000 |
| Plotted Values | 175.0 |
| Missing Values | 4.0 |

The evidence indicates a positive correlation at the 0.01 level of significance.

Raw data are presented within Appendix 2.

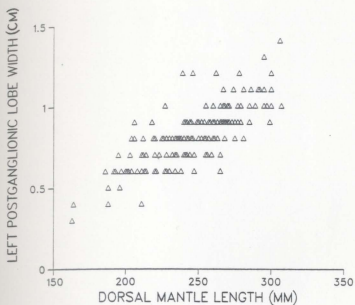
Figure 15A. The same as above, save that values obtained are sorted with respect to sex of the squid.

Statistics:

| | Males | Females |
|----------------|---------|---------|
| Correlation | 0.82688 | 0.68997 |
| Significance | 0.00000 | 0.00000 |
| Plotted Values | 40.0 | 135.0 |
| Missing Values | 1.0 | 3.0 |

In both sexes, the evidence indicates a positive correlation at the 0.01 level of significance.

15



15A

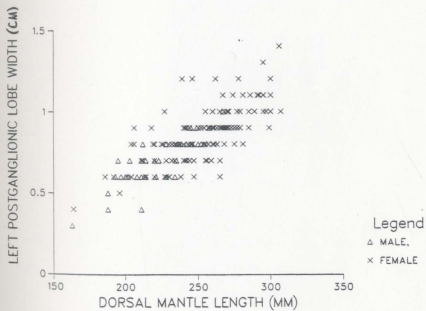


Figure 16. A scattergram in which values for the length of the right postganglionic lobe are plotted against values for the dorsal mantle length.

Statistics:

| | |
|----------------|---------|
| Correlation | 0.73992 |
| Significance | 0.00000 |
| Plotted Values | 178.0 |
| Missing Values | 1.0 |

The evidence indicates a positive correlation at the 0.01 level of significance.

Raw data are presented within Appendix 2.

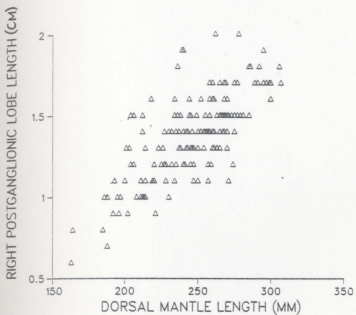
Figure 16A. The same as above, save that values obtained are sorted with respect to sex of the squid.

Statistics:

| | Males | Females |
|----------------|---------|---------|
| Correlation | 0.78354 | 0.66129 |
| Significance | 0.00000 | 0.00000 |
| Plotted Values | 41.0 | 137.0 |
| Missing Values | 0.0 | 1.0 |

In both sexes, the evidence indicates a positive correlation at the 0.01 level of significance.

16



16A

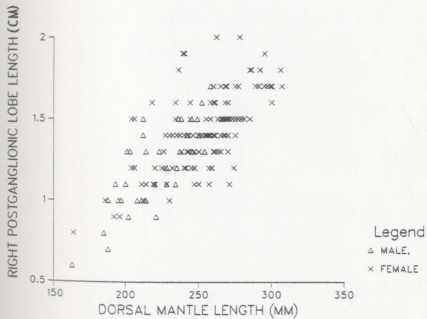


Figure 17. A scattergram in which values for the length of the left postganglionic lobe are plotted against values for the dorsal mantle length.

Statistics:

| | |
|----------------|---------|
| Correlation | 0.74509 |
| Significance | 0.00000 |
| Plotted Values | 175.0 |
| Missing Values | 4.0 |

The evidence indicates a positive correlation at the 0.01 level of significance.

Raw data are presented within Appendix 2.

Figure 17A. The same as above, save that values obtained are sorted with respect to sex of the squid.

Statistics:

| | Males | Females |
|----------------|---------|---------|
| Correlation | 0.77933 | 0.67900 |
| Significance | 0.00000 | 0.00000 |
| Plotted Values | 40.0 | 135.0 |
| Missing Values | 1.0 | 3.0 |

In both sexes, the evidence indicates a positive correlation at the 0.01 level of significance.

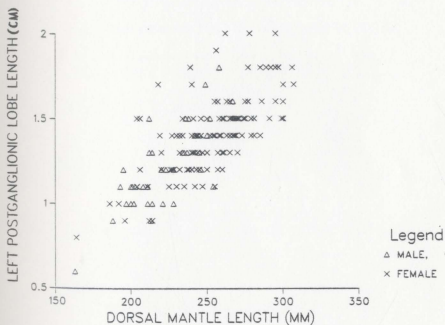
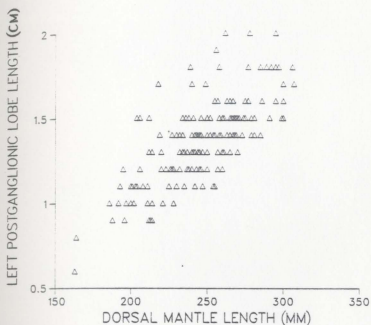


Figure 18. A scattergram in which values for the width of the right subganglionic process are plotted against values for the dorsal mantle length.

Statistics:

| | |
|----------------|---------|
| Correlation | 0.67796 |
| Significance | 0.00000 |
| Plotted Values | 178.0 |
| Missing Values | 1.0 |

The evidence indicates a positive correlation at the 0.01 level of significance.

Raw data are presented within Appendix 2.

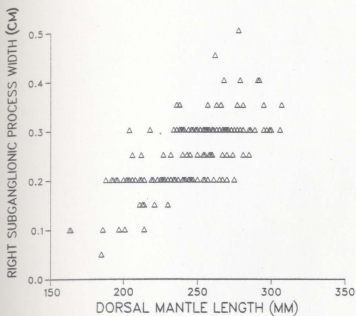
Figure 18A. The same as above, save that values obtained are sorted with respect to sex of the squid.

Statistics:

| | Males | Females |
|----------------|---------|---------|
| Correlation | 0.66349 | 0.59001 |
| Significance | 0.00000 | 0.00000 |
| Plotted Values | 41.0 | 137.0 |
| Missing Values | 0.0 | 1.0 |

In both sexes, the evidence indicates a positive correlation at the 0.01 level of significance.

18



18A

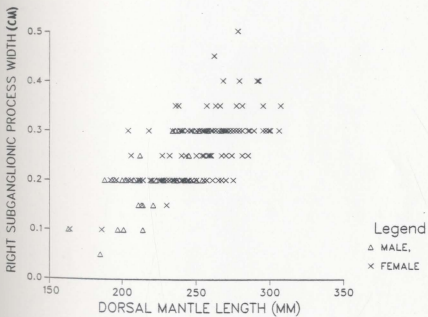


Figure 19. A scattergram in which values for the width of the left subganglionic process are plotted against values for the dorsal mantle length.

Statistics:

| | |
|----------------|---------|
| Correlation | 0.71732 |
| Significance | 0.00000 |
| Plotted Values | 175.0 |
| Missing Values | 4.0 |

The evidence indicates a positive correlation at the 0.01 level of significance.

Raw data are presented within Appendix 2.

Figure 19A. The same as above, save that values obtained are sorted with respect to sex of the squid.

Statistics:

| | Males | Females |
|----------------|---------|---------|
| Correlation | 0.72339 | 0.64051 |
| Significance | 0.00000 | 0.00000 |
| Plotted Values | 40.0 | 135.0 |
| Missing Values | 1.0 | 3.0 |

In both sexes, the evidence indicates a positive correlation at the 0.01 level of significance.

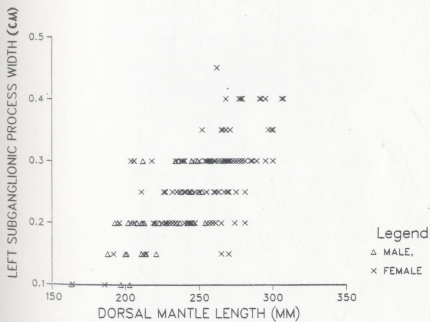
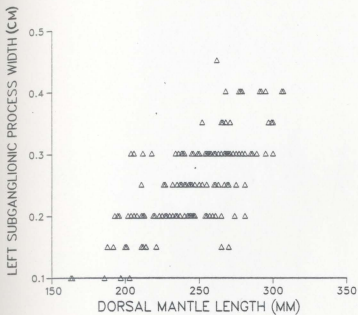


Figure 20. A scattergram in which values for the length of the right subganglionic process are plotted against values for the dorsal mantle length.

Statistics:

| | |
|----------------|---------|
| Correlation | 0.15403 |
| Significance | 0.02005 |
| Plotted Values | 178.0 |
| Missing Values | 1.0 |

The evidence indicates that the correlation is not significantly different from zero at the 0.01 level.

Raw data are presented within Appendix 2.

Figure 20A. The same as above, save that values obtained are sorted with respect to sex of the squid.

Statistics:

| | Males | Females |
|----------------|---------|---------|
| Correlation | 0.13286 | 0.11308 |
| Significance | 0.20381 | 0.09415 |
| Plotted Values | 41.0 | 137.0 |
| Missing Values | 0.0 | 1.0 |

In both sexes, the evidence indicates that the correlation is not significantly different from zero at the 0.01 level.

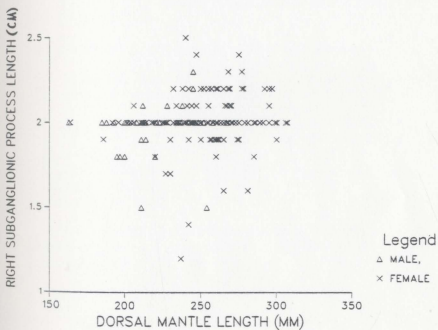
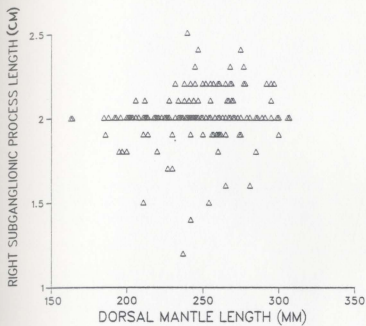


Figure 21. A scattergram in which values for the length of the left subganglionic process are plotted against values for the dorsal mantle length.

Statistics:

| | |
|----------------|---------|
| Correlation | 0.14577 |
| Significance | 0.02713 |
| Plotted Values | 175.0 |
| Missing Values | 4.0 |

The evidence indicates that the correlation is not significantly different from zero at the 0.01 level.

Raw data are presented within Appendix 2.

Figure 21A. The same as above, save that values obtained are sorted with respect to sex of the squid.

Statistics:

| | Males | Females |
|----------------|---------|---------|
| Correlation | 0.14880 | 0.11053 |
| Significance | 0.17973 | 0.10093 |
| Plotted Values | 40.0 | 135.0 |
| Missing Values | 1.0 | 3.0 |

In both sexes, the evidence indicates that the correlation is not significantly different from Zero at the 0.01 level.

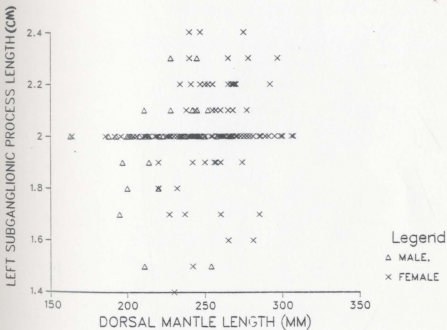
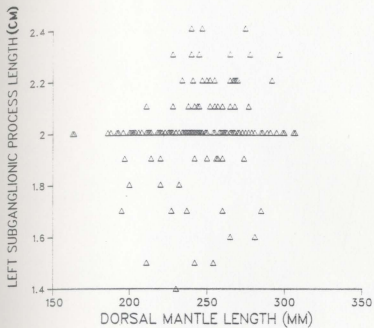


Figure 22. A scattergram in which values for the width of the right inferior preganglionic lobe are plotted against values for the dorsal mantle length.

Statistics:

| | |
|----------------|---------|
| Correlation | 0.45672 |
| Significance | 0.00000 |
| Plotted Values | 177.0 |
| Missing Values | 2.0 |

The evidence indicates a positive correlation at the 0.01 level of significance.

Raw data are presented within Appendix 2.

Figure 22A. The same as above, save that values obtained are sorted with respect to sex of the squid.

Statistics:

| | Males | Females |
|----------------|---------|---------|
| Correlation | 0.51096 | 0.37833 |
| Significance | 0.00038 | 0.00000 |
| Plotted Values | 40.0 | 137.0 |
| Missing Values | 1.0 | 1.0 |

In both sexes, the evidence indicates a positive correlation at the 0.01 level of significance.

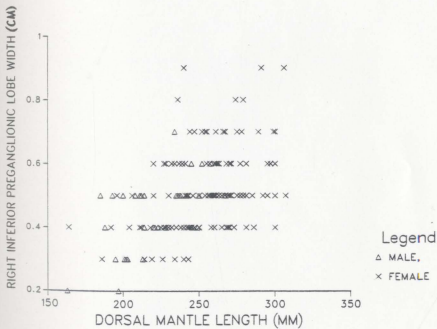
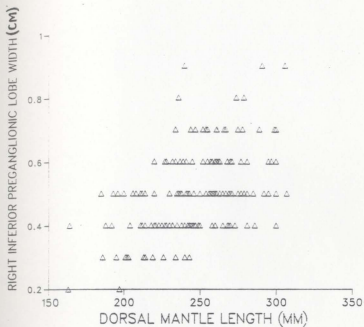


Figure 23. A scattergram in which values for the width of the left inferior preganglionic lobe are plotted against values for the dorsal mantle length.

Statistics:

| | |
|----------------|---------|
| Correlation | 0.48295 |
| Significance | 0.00000 |
| Plotted Values | 174.0 |
| Missing Values | 5.0 |

The evidence indicates a positive correlation at the 0.01 level of significance.

Raw data are presented within Appendix 2.

Figure 23A. The same as above, save that values obtained are sorted with respect to sex of the squid.

Statistics:

| | Males | Females |
|----------------|---------|---------|
| Correlation | 0.42716 | 0.42055 |
| Significance | 0.00334 | 0.00000 |
| Plotted Values | 39.0 | 135.0 |
| Missing Values | 2.0 | 3.0 |

In both sexes, the evidence indicates a positive correlation at the 0.01 level of significance.

Figure 24. A scattergram in which values for the length of the right inferior preganglionic lobe are plotted against values for the dorsal mantle length.

Statistics:

| | |
|----------------|---------|
| Correlation | 0.51275 |
| Significance | 0.00000 |
| Plotted Values | 177.0 |
| Missing Values | 2.0 |

The evidence indicates a positive correlation at the 0.01 level of significance.

Raw data are presented within Appendix 2.

Figure 24A. The same as above, save that values obtained are sorted with respect to sex of the squid.

Statistics:

| | Males | Females |
|----------------|---------|---------|
| Correlation | 0.48452 | 0.38911 |
| Significance | 0.00077 | 0.00000 |
| Plotted Values | 40.0 | 137.0 |
| Missing Values | 1.0 | 1.0 |

In both sexes, the evidence indicates a positive correlation at the 0.01 level of significance.

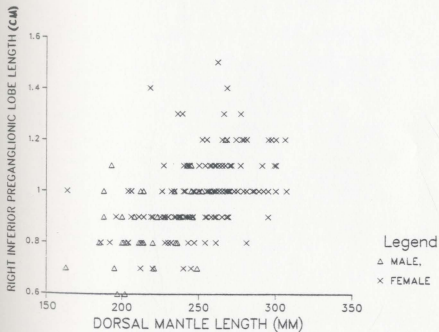
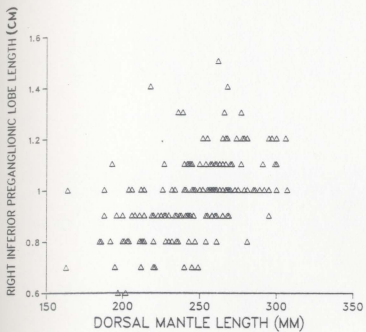


Figure 25. A scattergram in which values for the length of the left inferior preganglionic lobe are plotted against values for the dorsal mantle length.

Statistics:

| | |
|----------------|---------|
| Correlation | 0.59389 |
| Significance | 0.00000 |
| Plotted Values | 174.0 |
| Missing Values | 5.0 |

The evidence indicates a positive correlation at the 0.01 level of significance.

Raw data are presented within Appendix 2.

Figure 25A. The same as above, save that values obtained are sorted with respect to sex of the squid.

Statistics:

| | Males | Females |
|----------------|---------|---------|
| Correlation | 0.53589 | 0.53358 |
| Significance | 0.00022 | 0.00000 |
| Plotted Values | 39.0 | 135.0 |
| Missing Values | 2.0 | 3.0 |

In both sexes, the evidence indicates a positive correlation at the 0.01 level of significance.

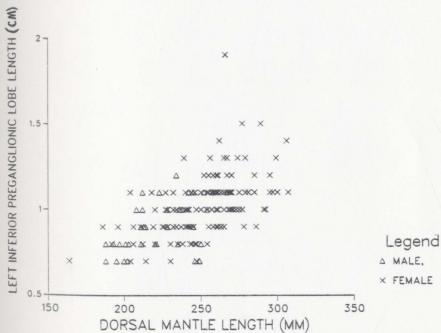
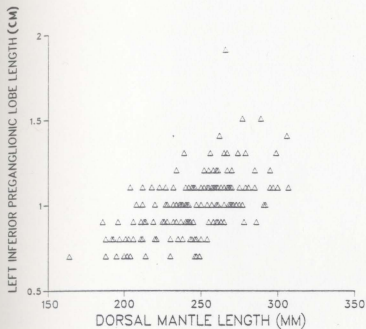


Figure 26. A scattergram in which values for the width of the right superior preganglionic lobe are plotted against values for the dorsal mantle length.

Statistics:

| | |
|----------------|---------|
| Correlation | 0.44093 |
| Significance | 0.00000 |
| Plotted Values | 177.0 |
| Missing Values | 2.0 |

The evidence indicates a positive correlation at the 0.01 level of significance.

Raw data are presented within Appendix 2.

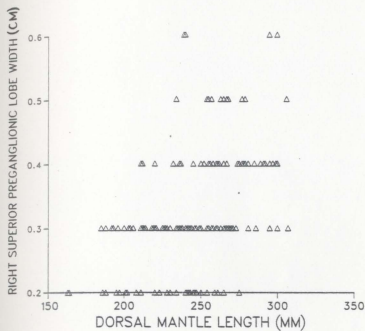
Figure 26A, The same as above, save that values obtained are sorted with respect to sex of the squid.

Statistics:

| | Males | Females |
|----------------|---------|---------|
| Correlation | 0.24927 | 0.39200 |
| Significance | 0.06043 | 0.00000 |
| Plotted Values | 40.0 | 137.0 |
| Missing Values | 1.0 | 1.0 |

The evidence indicates that (1) for males, the correlation is not significantly different from zero at the 0.01 level and (2) for females, a positive correlation is evident at the 0.01 level of significance.

26



26A

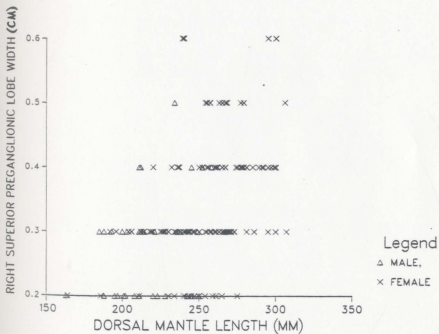


Figure 27. A scattergram in which values for the width of the left superior preganglionic lobe are plotted against values for the dorsal mantle length.

Statistics:

| | |
|----------------|---------|
| Correlation | 0.38301 |
| Significance | 0.00000 |
| Plotted Values | 173.0 |
| Missing Values | 6.0 |

The evidence indicates a positive correlation at the 0.01 level of significance.

Raw data are presented within Appendix 2.

Figure 27A. The same as above, save that values obtained are sorted with respect to sex of the squid.

Statistics:

| | Males | Females |
|----------------|---------|---------|
| Correlation | 0.52870 | 0.29114 |
| Significance | 0.00027 | 0.00032 |
| Plotted Values | 39.0 | 134.0 |
| Missing Values | 2.0 | 4.0 |

In both sexes, the evidence indicates a positive correlation at the 0.01 level of significance.

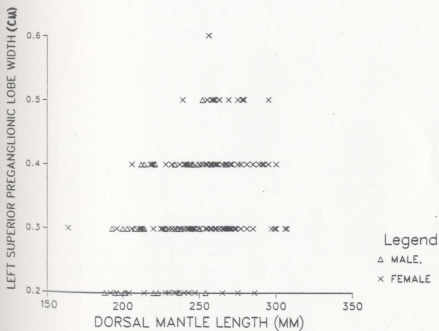
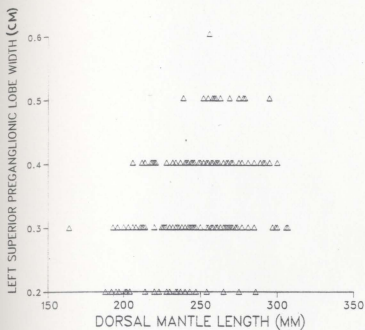


Figure 28. A scattergram in which values for the length of the right superior preganglionic lobe are plotted against values for the dorsal mantle length.

Statistics:

| | |
|----------------|---------|
| Correlation | 0.43178 |
| Significance | 0.00000 |
| Plotted Values | 177.0 |
| Missing Values | 2.0 |

The evidence indicates a positive correlation at the 0.01 level of significance.

Raw data are presented within Appendix 2.

Figure 28A. The same as above, save that values obtained are sorted with respect to sex of the squid.

Statistics:

| | Males | Females |
|----------------|---------|---------|
| Correlation | 0.31792 | 0.39442 |
| Significance | 0.02280 | 0.00000 |
| Plotted Values | 40.0 | 137.0 |
| Missing Values | 1.0 | 1.0 |

The evidence indicates that (1) for males, a positive correlation is evident at the 0.05 level and (2) for females, a positive correlation is evident at the 0.01 level of significance.

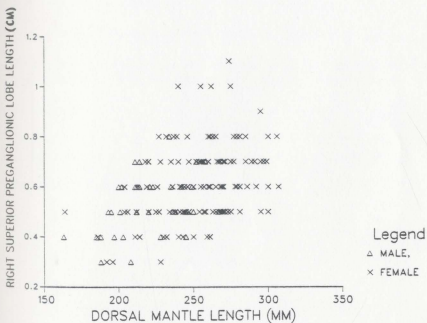
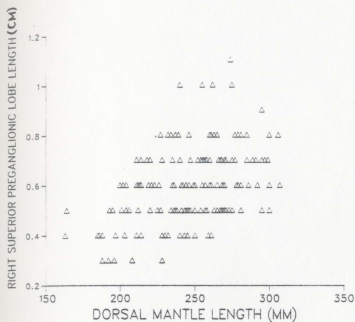


Figure 29. A scattergram in which values for the length of the left superior preganglionic lobe are plotted against values for the dorsal mantle length.

Statistics:

| | |
|----------------|---------|
| Correlation | 0.38081 |
| Significance | 0.00000 |
| Plotted Values | 173.0 |
| Missing Values | 6.0 |

The evidence indicates a positive correlation at the 0.01 level of significance.

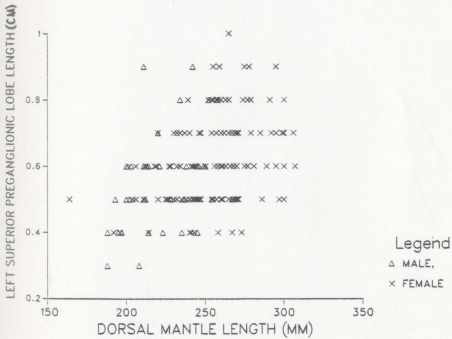
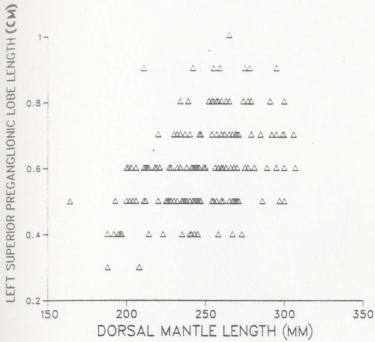
Raw data are presented within Appendix 2.

Figure 29A. The same as above, save that values obtained are sorted with respect to sex of the squid.

Statistics:

| | Males | Females |
|----------------|---------|---------|
| Correlation | 0.35880 | 0.33877 |
| Significance | 0.01245 | 0.00003 |
| Plotted Values | 39.0 | 134.0 |
| Missing Values | 2.0 | 4.0 |

The evidence indicates that (1) for males, a positive correlation is evident at the 0.05 level and (2) for females, a positive correlation is evident at the 0.01 level of significance.



Figures 30-45

The following statements summarize the information presented within Figures 30 through 45 (values representing the width or length of each component of a white body plotted against values for the weight of the squid from which a white body was obtained). Results of the morphometric study indicate a positive correlation at the 0.01 level of significance between (1) the width of each component of a white body and squid weight (2) the length of each component (except the subganglionic process) and squid weight. The evidence indicates that the correlation between the length of the subganglionic process and squid weight is not significantly different from zero at the 0.01 level.

When the above values are plotted with respect to the sex of the squid, the results yield a positive correlation at the 0.01 level of significance between (1) the width of each component of a white body and squid weight for females (2) the width of each component (except the right superior preganglionic lobe) and squid weight for males (3) the length of each component (except the subganglionic process) and squid weight for females (4) the length of each component (except the subganglionic process and the right superior preganglionic lobe) and squid weight for males. A positive correlation is obtained between the width or length of the right superior preganglionic lobe and squid weight (for males) at the 0.05 level of significance. Evidence indicates that the correlation between the length of the subganglionic process and squid weight (males or females) is not significantly different from zero at either the 0.01 or 0.05 level.

Figure 30. A scattergram in which values for the width of the right postganglionic lobe are plotted against values for the weight of the squid.

Statistics:

| | |
|----------------|---------|
| Correlation | 0.78612 |
| Significance | 0.00000 |
| Plotted Values | 177.0 |
| Missing Values | 2.0 |

The evidence indicates a positive correlation at the 0.01 level of significance.

Raw data are presented within Appendix 2.

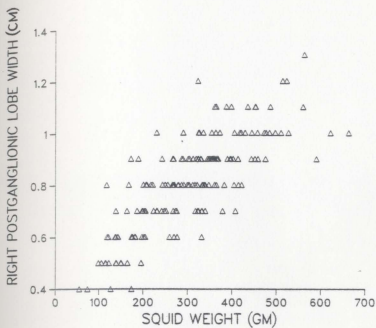
Figure 30A. The same as above, save that values obtained are sorted with respect to sex of the squid.

Statistics:

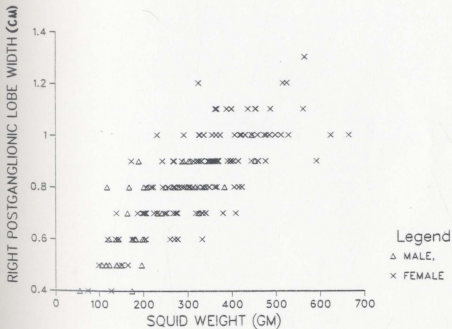
| | Males | Females |
|----------------|---------|---------|
| Correlation | 0.77534 | 0.74034 |
| Significance | 0.00000 | 0.00000 |
| Plotted Values | 41.0 | 136.0 |
| Missing Values | 0.0 | 2.0 |

In both sexes, the evidence indicates a positive correlation at the 0.01 level of significance.

30



30A



Legend

△ MALE,

× FEMALE

Figure 31. A scattergram in which values for the width of the left postganglionic lobe are plotted against values for the weight of the squid.

Statistics:

| | |
|----------------|---------|
| Correlation | 0.78691 |
| Significance | 0.00000 |
| Plotted Values | 174.0 |
| Missing Values | 5.0 |

The evidence indicates a positive correlation at the 0.01 level of significance.

Raw data are presented within Appendix 2.

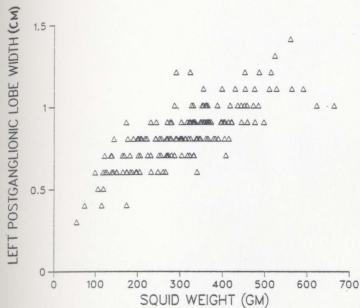
Figure 31A. The same as above, save that values obtained are sorted with respect to sex of the squid.

Statistics:

| | Males | Females |
|----------------|---------|---------|
| Correlation | 0.80510 | 0.73043 |
| Significance | 0.00000 | 0.00000 |
| Plotted Values | 40.0 | 134.0 |
| Missing Values | 1.0 | 4.0 |

In both sexes, the evidence indicates a positive correlation at the 0.01 level of significance.

31



31A

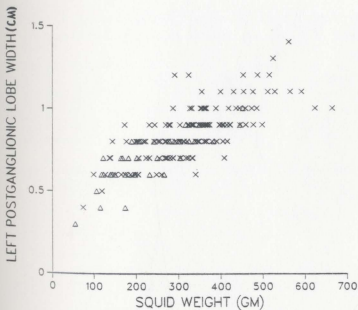


Figure 32. A scattergram in which values for the length of the right postganglionic lobe are plotted against values for the weight of the squid.

Statistics:

| | |
|----------------|---------|
| Correlation | 0.76540 |
| Significance | 0.00000 |
| Plotted Values | 177.0 |
| Missing Values | 2.0 |

The evidence indicates a positive correlation at the 0.01 level of significance.

Raw data are presented within Appendix 2.

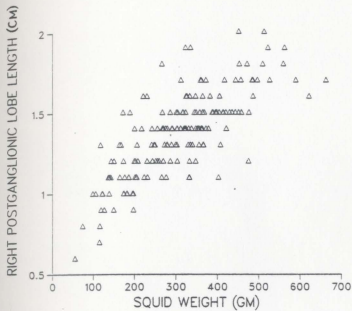
Figure 32A. The same as above, save that values obtained are sorted with respect to sex of the squid.

Statistics:

| | Males | Females |
|----------------|---------|---------|
| Correlation | 0.79917 | 0.70437 |
| Significance | 0.00000 | 0.00000 |
| Plotted Values | 41.0 | 136.0 |
| Missing Values | 0.0 | 2.0 |

In both sexes, the evidence indicates a positive correlation at the 0.01 level of significance.

32



32A

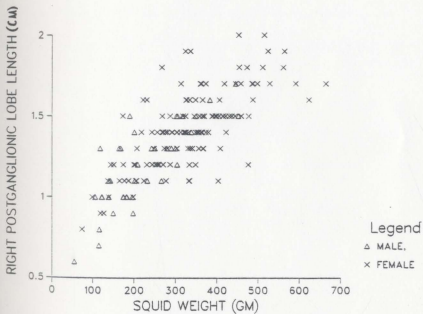


Figure 33. A scattergram in which values for the length of the left postganglionic lobe are plotted against values for the weight of the squid.

Statistics:

| | |
|----------------|---------|
| Correlation | 0.76762 |
| Significance | 0.00000 |
| Plotted Values | 174.0 |
| Missing Values | 5.0 |

The evidence indicates a positive correlation at the 0.01 level of significance.

Raw data are presented within Appendix 2.

Figure 33A. The same as above, save that values obtained are sorted with respect to sex of the squid.

Statistics:

| | Males | Females |
|----------------|---------|---------|
| Correlation | 0.81075 | 0.71051 |
| Significance | 0.00000 | 0.00000 |
| Plotted Values | 40.0 | 134.0 |
| Missing Values | 1.0 | 4.0 |

In both sexes, the evidence indicates a positive correlation at the 0.01 level of significance.

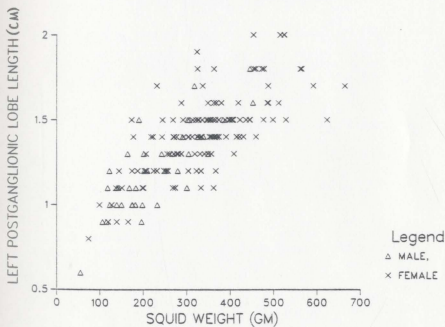
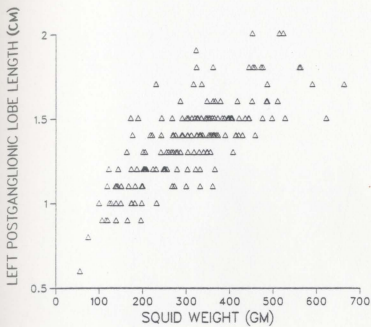


Figure 34. A scattergram in which values for the width of the right subganglionic process are plotted against values for the weight of the squid.

Statistics:

| | |
|----------------|---------|
| Correlation | 0.70684 |
| Significance | 0.00000 |
| Plotted Values | 177.0 |
| Missing Values | 2.0 |

The evidence indicates a positive correlation at the 0.01 level of significance.

Raw data are presented within Appendix 2.

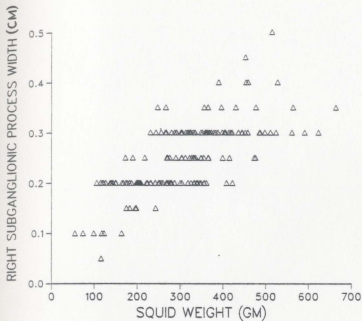
Figure 34A. The same as above, save that values obtained are sorted with respect to sex of the squid.

Statistics:

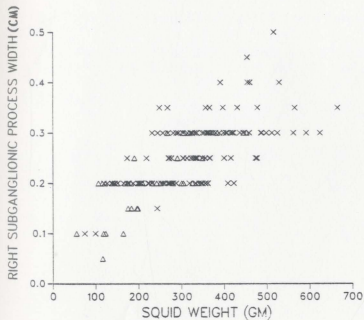
| | Males | Females |
|----------------|---------|---------|
| Correlation | 0.71312 | 0.63492 |
| Significance | 0.0000 | 0.00000 |
| Plotted Values | 41.0 | 135.0 |
| Missing Values | 0.0 | 3.0 |

In both sexes, the evidence indicates a positive correlation at the 0.01 level of significance.

34



34A



Legend

△ MALE,

× FEMALE

Figure 35. A scattergram in which values for the width of the left subganglionic process are plotted against values for the weight of the squid.

Statistics:

| | |
|----------------|---------|
| Correlation | 0.74232 |
| Significance | 0.00000 |
| Plotted Values | 174.0 |
| Missing Values | 5.0 |

The evidence indicates a positive correlation at the 0.01 level of significance.

Raw data are presented within Appendix 2.

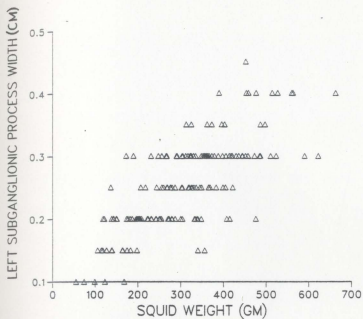
Figure 35A. The same as above, save that values obtained are sorted with respect to sex of the squid.

Statistics:

| | Males | Females |
|----------------|---------|---------|
| Correlation | 0.74423 | 0.68317 |
| Significance | 0.00000 | 0.00000 |
| Plotted Values | 40.0 | 134.0 |
| Missing Values | 1.0 | 4.0 |

In both sexes, the evidence indicates a positive correlation at the 0.01 level of significance.

35



35A

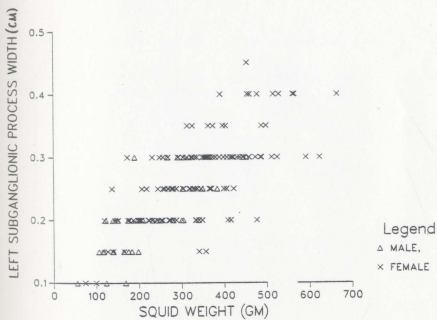


Figure 36. A scattergram in which values for the length of the right subganglionic process are plotted against values for the weight of the squid.

Statistics:

| | |
|----------------|---------|
| Correlation | 0.13907 |
| Significance | 0.03244 |
| Plotted Values | 177.0 |
| Missing Values | 2.0 |

The evidence indicates that the correlation is not significantly different from zero at the 0.01 level.

Raw data are presented within Appendix 2.

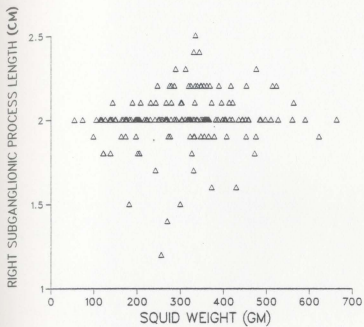
Figure 36A. The same as above, save that values obtained are sorted with respect to sex of the squid.

Statistics:

| | Males | Females |
|----------------|---------|---------|
| Correlation | 0.18782 | 0.08490 |
| Significance | 0.11981 | 0.16287 |
| Plotted Values | 41.0 | 136.0 |
| Missing Values | 0.0 | 2.0 |

In both sexes, the evidence indicates that the correlation is not significantly different from zero at the 0.01 level.

36



36A

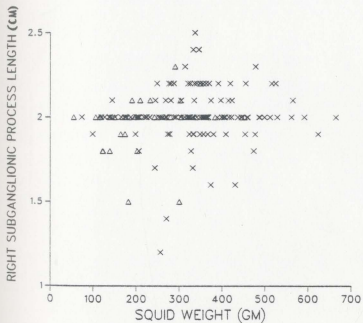


Figure 37. A scattergram in which values for the length of the left subganglionic process are plotted against values for the weight of the squid.

Statistics:

| | |
|----------------|---------|
| Correlation | 0.12334 |
| Significance | 0.05246 |
| Plotted Values | 174.0 |
| Missing Values | 5.0 |

The evidence indicates that the correlation is not significantly different from zero at the 0.01 level.

Raw data are presented within Appendix 2.

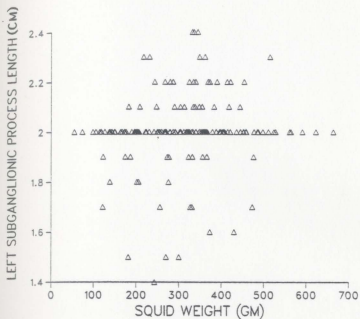
Figure 37A. The same as above, save that values obtained are sorted with respect to sex of the squid.

Statistics:

| | Males | Females |
|----------------|---------|---------|
| Correlation | 0.21135 | 0.06643 |
| Significance | 0.09524 | 0.22285 |
| Plotted Values | 40.0 | 134.0 |
| Missing Values | 1.0 | 4.0 |

In both sexes, the evidence indicates that the correlation is not significantly different from zero at the 0.01 level.

37



37A

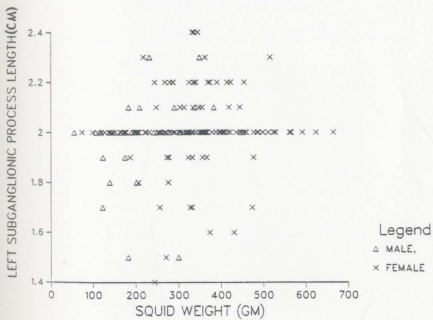


Figure 38. A scattergram in which values for the width of the right inferior preganglionic lobe are plotted against values for the weight of the squid.

Statistics:

| | |
|----------------|---------|
| Correlation | 0.49253 |
| Significance | 0.00000 |
| Plotted values | 176.0 |
| Missing Values | 3.0 |

The evidence indicates a positive correlation at the 0.01 level of significance.

Raw data are presented within Appendix 2.

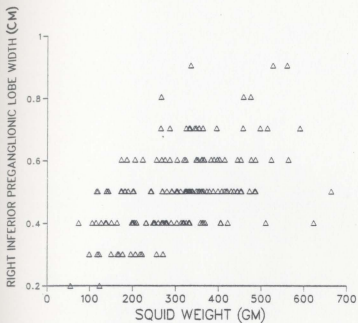
Figure 38A. The same as above, save that values obtained are sorted with respect to sex of the squid.

Statistics:

| | Males | Females |
|----------------|---------|---------|
| Correlation | 0.54351 | 0.42350 |
| Significance | 0.00014 | 0.00000 |
| Plotted Values | 40.0 | 136.0 |
| Missing Values | 1.0 | 2.0 |

In both sexes, the evidence indicates a positive correlation at the 0.01 level of significance.

38



38A

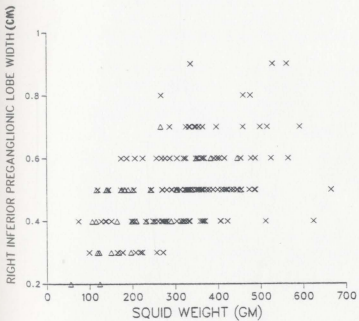


Figure 39. A scattergram in which values for the width of the left inferior preganglionic lobe are plotted against values for the weight of the squid.

Statistics:

| | |
|----------------|---------|
| Correlation | 0.51139 |
| Significance | 0.00000 |
| Plotted Values | 173.0 |
| Missing Values | 6.0 |

The evidence indicates a positive correlation at the 0.01 level of significance.

Raw data are presented within Appendix 2.

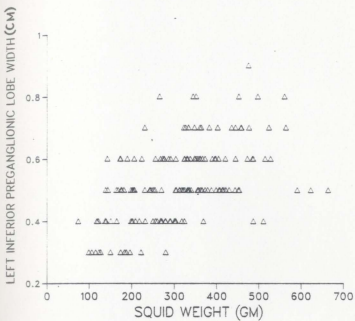
Figure 39A. The same as above, save that values obtained are sorted with respect to sex of the squid.

Statistics:

| | Males | Females |
|----------------|---------|---------|
| Correlation | 0.49191 | 0.45203 |
| Significance | 0.00073 | 0.00000 |
| Plotted Values | 39.0 | 134.0 |
| Missing Values | 2.0 | 4.0 |

In both sexes, the evidence indicates a positive correlation at the 0.01 level of significance.

39



39A

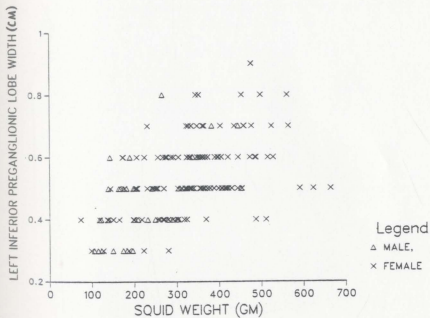


Figure 40. A scattergram in which values for the length of the right inferior preganglionic lobe are plotted against values for the weight of the squid.

Statistics:

| | |
|----------------|---------|
| Correlation | 0.56303 |
| Significance | 0.00000 |
| Plotted Values | 176.0 |
| Missing Values | 3.0 |

The evidence indicates a positive correlation at the 0.01 level of significance.

Raw data are presented within Appendix 2.

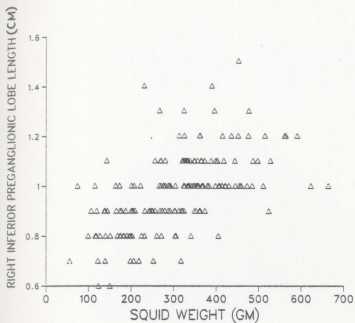
Figure 40A. The same as above, save that values obtained are sorted with respect to sex of the squid.

Statistics:

| | Males | Females |
|----------------|---------|---------|
| Correlation | 0.53948 | 0.47100 |
| Significance | 0.00016 | 0.00000 |
| Plotted Values | 40.0 | 136.0 |
| Missing Values | 1.0 | 2.0 |

In both sexes, the evidence indicates a positive correlation at the 0.01 level of significance.

40



40A

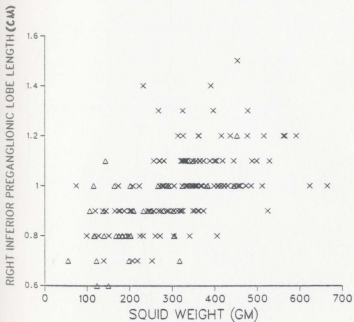


Figure 41. A scattergram in which values for the length of the left inferior preganglionic lobe are plotted against values for the weight of the squid.

Statistics:

| | |
|----------------|---------|
| Correlation | 0.61974 |
| Significance | 0.00000 |
| Plotted Values | 173.0 |
| Missing Values | 6.0 |

The evidence indicates a positive correlation at the 0.01 level of significance.

Raw data are presented within Appendix 2.

Figure 41A. The same as above, save that values obtained are sorted with respect to sex of the squid.

Statistics:

| | Males | Females |
|----------------|---------|---------|
| Correlation | 0.58463 | 0.56695 |
| Significance | 0.00005 | 0.00000 |
| Plotted Values | 39.0 | 134.0 |
| Missing Values | 2.0 | 4.0 |

In both sexes, the evidence indicates a positive correlation at the 0.01 level of significance.

Figure 42. A scattergram in which values for the width of the right superior preganglionic lobe are plotted against values for the weight of the squid.

Statistics:

| | |
|----------------|---------|
| Correlation | 0.49937 |
| Significance | 0.00000 |
| Plotted Values | 176.0 |
| Missing Values | 3.0 |

The evidence indicates a positive correlation at the 0.01 level of significance.

Raw data are presented within Appendix 2.

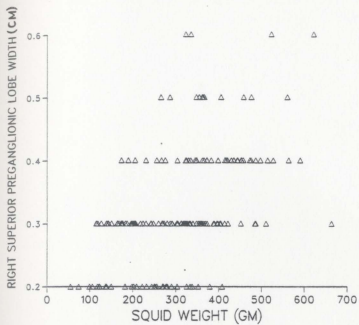
Figure 42A. The same as above, save that values obtained are sorted with respect to sex of the squid.

Statistics:

| | Males | Females |
|----------------|---------|---------|
| Correlation | 0.32685 | 0.46581 |
| Significance | 0.01977 | 0.00000 |
| Plotted Values | 40.0 | 136.0 |
| Missing Values | 1.0 | 2.0 |

The evidence indicates that (1) for males, a positive correlation is evident at the 0.05 level and (2) for females, a positive correlation is evident at the 0.01 level of significance.

42



42A

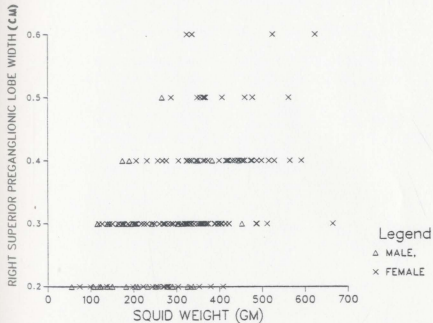


Figure 43. A scattergram in which values for the width of the left superior preganglionic lobe are plotted against values for the weight of the squid.

Statistics:

| | |
|----------------|---------|
| Correlation | 0.38087 |
| Significance | 0.00000 |
| Plotted Values | 172.0 |
| Missing Values | 7.0 |

The evidence indicates a positive correlation at the 0.01 level of significance.

Raw data are presented within Appendix 2.

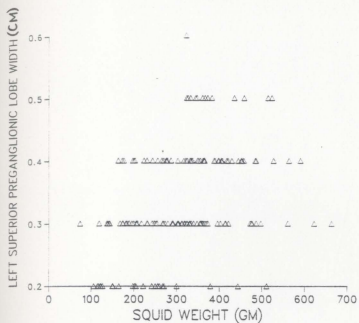
Figure 43A. The same as above, save that values obtained are sorted with respect to sex of the squid.

Statistics:

| | Males | Females |
|----------------|---------|---------|
| Correlation | 0.57678 | 0.27631 |
| Significance | 0.00006 | 0.00064 |
| Plotted Values | 39.0 | 133.0 |
| Missing Values | 2.0 | 5.0 |

In both sexes, the evidence indicates a positive correlation at the 0.01 level of significance.

43



43A

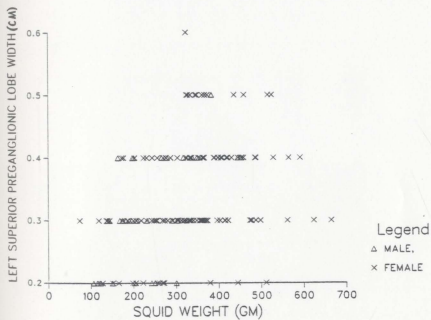


Figure 44. A scattergram in which values for the length of the right superior preganglionic lobe are plotted against values for the weight of the squid.

Statistics:

| | |
|----------------|---------|
| Correlation | 0.44894 |
| Significance | 0.00000 |
| Plotted Values | 176.0 |
| Missing Values | 3.0 |

The evidence indicates a positive correlation at the 0.01 level of significance.

Raw data are presented within Appendix 2.

Figure 44A. The same as above, save that values obtained are sorted with respect to sex of the squid.

Statistics:

| | Males | Females |
|----------------|---------|---------|
| Correlation | 0.33209 | 0.41652 |
| Significance | 0.01815 | 0.00000 |
| Plotted Values | 40.0 | 136.0 |
| Missing Values | 1.0 | 2.0 |

The evidence indicates that (1) for males, a positive correlation is evident at the 0.05 level and (2) for females, a positive correlation is evident at the 0.01 level of significance.

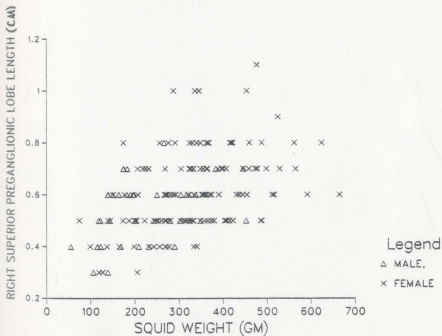
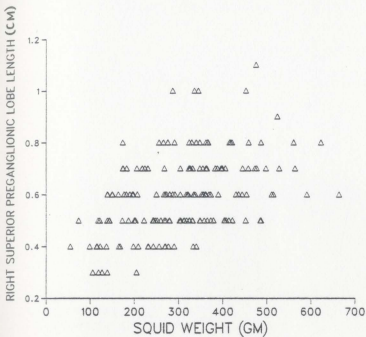


Figure 45. A scattergram in which values for the length of the left superior preganglionic lobe are plotted against values for the weight of the squid.

Statistics:

| | |
|----------------|---------|
| Correlation | 0.40207 |
| Significance | 0.00000 |
| Plotted Values | 172.0 |
| Missing Values | 7.0 |

The evidence indicates a positive correlation at the 0.01 level of significance.

Raw data are presented within Appendix 2.

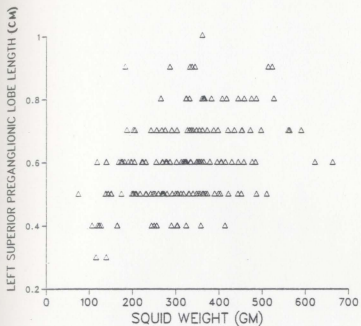
Figure 45A. The same as above, save that values obtained are sorted with respect to sex of the squid.

Statistics:

| | Males | Females |
|----------------|---------|---------|
| Correlation | 0.40551 | 0.35649 |
| Significance | 0.00522 | 0.00001 |
| Plotted Values | 39.0 | 133.0 |
| Missing Values | 2.0 | 5.0 |

In both sexes, the evidence indicates a positive correlation at the 0.01 level of significance.

45



45A

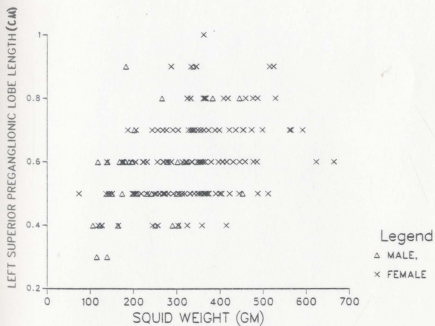


Table 7. The results of t-tests in which the morphometric statistics (recorded in centimeters) of each white body were compared with the sex of the squid from which the white body was collected. (Group 1 = males; Group 2 = females)

| Variable | Number of Cases | Mean | Standard Deviation | T Value | Degrees of Freedom | 2-Tail Prob. |
|----------|------------------------------------|--------|--------------------|---------|--------------------|--------------|
| RPL1 | Right Postganglionic Lobe Width | | | | | |
| Group 1 | 41 | 0.6927 | 0.160 | 5.48 | 176 | 0.000 |
| Group 2 | 137 | 0.8540 | 0.167 | | | |
| RPL2 | Right Postganglionic Lobe Length | | | | | |
| Group 1 | 41 | 1.1902 | 0.251 | 5.47 | 176 | 0.000 |
| Group 2 | 137 | 1.4226 | 0.235 | | | |
| LPL1 | Left Postganglionic Lobe Width | | | | | |
| Group 1 | 40 | 0.6900 | 0.146 | 6.05 | 173 | 0.000 |
| Group 2 | 135 | 0.8667 | 0.167 | | | |
| LPL2 | Left Postganglionic Lobe Length | | | | | |
| Group 1 | 40 | 1.2025 | 0.244 | 5.15 | 173 | 0.000 |
| Group 2 | 135 | 1.4141 | 0.223 | | | |
| RSP1 | Right Subganglionic Process Width | | | | | |
| Group 1 | 41 | 0.2024 | 0.061 | 5.72 | 176 | 0.000 |
| Group 2 | 137 | 0.2664 | 0.063 | | | |
| RSP2 | Right Subganglionic Process Length | | | | | |
| Group 1 | 41 | 1.9732 | 0.143 | 1.44 | 176 | 0.153 |
| Group 2 | 137 | 2.0124 | 0.156 | | | |
| LSP1 | Left Subganglionic Process Width | | | | | |
| Group 1 | 40 | 0.2038 | 0.058 | 5.61 | 173 | 0.000 |
| Group 2 | 135 | 0.2685 | 0.066 | | | |
| LSP2 | Left Subganglionic Process Length | | | | | |
| Group 1 | 40 | 1.9800 | 0.152 | 1.17 | 173 | 0.244 |
| Group 2 | 135 | 2.0111 | 0.146 | | | |

Table 7 (cont'd.)

| Variable | Number of Cases | Mean | Standard Deviation | T Value | Degrees of Freedom | 2-Tail Prob. |
|----------|--|--------|--------------------|---------|--------------------|--------------|
| RIPL1 | Right Inferior Preganglionic Lobe Width | | | | | |
| Group 1 | 40 | 0.4450 | 0.106 | 3.24 | 175 | 0.001 |
| Group 2 | 137 | 0.5161 | 0.126 | | | |
| RIPL2 | Right Inferior Preganglionic Lobe Length | | | | | |
| Group 1 | 40 | 0.8750 | 0.137 | 5.28 | 175 | 0.000 |
| Group 2 | 137 | 1.0095 | 0.143 | | | |
| LIPL1 | Left Inferior Preganglionic Lobe Width | | | | | |
| Group 1 | 39 | 0.4615 | 0.121 | 3.67 | 172 | 0.000 |
| Group 2 | 135 | 0.5393 | 0.115 | | | |
| LIPL2 | Left Inferior Preganglionic Lobe Length | | | | | |
| Group 1 | 39 | 0.8974 | 0.148 | 4.30 | 172 | 0.000 |
| Group 2 | 135 | 1.0304 | 0.176 | | | |
| RSPL1 | Right Superior Preganglionic Lobe Width | | | | | |
| Group 1 | 40 | 0.2775 | 0.077 | 3.73 | 175 | 0.000 |
| Group 2 | 137 | 0.3358 | 0.090 | | | |
| RSPL2 | Right Superior Preganglionic Lobe Length | | | | | |
| Group 1 | 40 | 0.5325 | 0.116 | 2.97 | 175 | 0.003 |
| Group 2 | 137 | 0.6095 | 0.151 | | | |
| LSPL1 | Left Superior Preganglionic Lobe Width | | | | | |
| Group 1 | 39 | 0.3051 | 0.079 | 2.66 | 171 | 0.009 |
| Group 2 | 134 | 0.3448 | 0.083 | | | |
| LSPL2 | Left Superior Preganglionic Lobe Length | | | | | |
| Group 1 | 39 | 0.5538 | 0.145 | 2.42 | 171 | 0.017 |
| Group 2 | 134 | 0.6119 | 0.128 | | | |

Reference to Table 7 will indicate that in the case of some of the lobes of the white body, the differences are minimal between the sexes, but are in all instances statistically significant (0.01 level).

Table 8. The results of t-tests in which the morphometric statistics (recorded in centimeters) of each component of the right white body were compared with corresponding values for the left white body.

| Variable | Number of Cases | Mean | Standard Deviation | T Value | Degrees of Freedom | 2-Tail Prob. |
|----------|---|--------|--------------------|---------|--------------------|--------------|
| RPL1 | Right Postganglionic Lobe Width | | | | | |
| | 174 | 0.8178 | 0.179 | -1.30 | 173 | 0.195 |
| | | 0.8270 | 0.178 | | | |
| LPL1 | Left Postganglionic Lobe Width | | | | | |
| RPL2 | Right Postganglionic Lobe Length | | | | | |
| | 174 | 1.3713 | 0.254 | 0.51 | 173 | 0.609 |
| | | 1.3661 | 0.245 | | | |
| LPL2 | Left Postganglionic Lobe Length | | | | | |
| RSP1 | Right Subganglionic Process Width | | | | | |
| | 174 | 0.2523 | 0.067 | -0.64 | 173 | 0.524 |
| | | 0.2540 | 0.070 | | | |
| LSP1 | Left Subganglionic Process Width | | | | | |
| RSP2 | Right Subganglionic Process Length | | | | | |
| | 174 | 2.0034 | 0.156 | -0.09 | 173 | 0.931 |
| | | 2.0040 | 0.148 | | | |
| LSP2 | Left Subganglionic Process Length | | | | | |
| RIPL1 | Right Inferior Preganglionic Lobe Width | | | | | |
| | 172 | 0.5012 | 0.122 | -2.73 | 171 | 0.007 |
| | | 0.5227 | 0.121 | | | |
| LIPL1 | Left Inferior Preganglionic Lobe Width | | | | | |

Table 8 (cont'd.)

| Variable | Number of Cases | Mean | Standard Deviation | T Value | Degrees of Freedom | 2-Tail Prob. |
|----------|--|--------|-----------------------|------------|-----------------------|-----------------|
| RIPL2 | Right Inferior Preganglionic Lobe Length | | | | | |
| | 172 | 0.9797 | 0.150 | 1.95 | 171 | 0.053 |
| | | 1.0012 | 0.179 | | | |
| LIPL2 | Left Inferior Preganglionic Lobe Length | | | | | |
| RSPL1 | Right Superior Preganglionic Lobe Width | | | | | |
| | 171 | 0.3240 | 0.090 | 1.74 | 170 | 0.084 |
| | | 0.3368 | 0.083 | | | |
| LSPL1 | Left Superior Preganglionic Lobe Width | | | | | |
| RSPL2 | Right Superior Preganglionic Lobe Length | | | | | |
| | 171 | 0.5965 | 0.147 | -0.29 | 170 | 0.772 |
| | | 0.5994 | 0.134 | | | |
| LSPL2 | Left Superior Preganglionic Lobe Length | | | | | |

Each of the above pairs (RPL1/LPL1, etc.) is from the same specimen.

Figures 46-49

The following statements summarize the information presented within Figures 46 through 49 (values representing the total length of a white body plotted against values for the DML or weight of the squid from which a white body was obtained). The results indicate a positive correlation at the 0.01 level of significance between (1) the total length of a white body and DML (2) the total length of a white body and squid weight.

When the above values are plotted with respect to the sex of the squid, the results of the morphometric study are similar to those indicated above.

Figure 46. A scattergram in which values for the total length of the right white body are plotted against values for the dorsal mantle length.

Statistics:

| | |
|----------------|---------|
| Correlation | 0.70896 |
| Significance | 0.00000 |
| Plotted Values | 177.0 |
| Missing Values | 2.0 |

The evidence indicates a positive correlation at the 0.01 level of significance.

Raw data are presented within Appendix 2.

Figure 46A. The same as above, save that values obtained are sorted with respect to sex of the squid.

Statistics:

| | Males | Females |
|----------------|---------|---------|
| Correlation | 0.79939 | 0.60761 |
| Significance | 0.00000 | 0.00000 |
| Plotted Values | 40.0 | 137.0 |
| Missing Values | 1.0 | 1.0 |

In both sexes, the evidence indicates a positive correlation at the 0.01 level of significance.

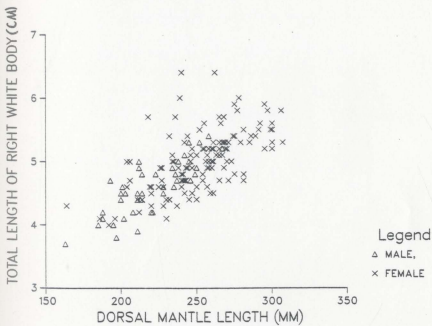
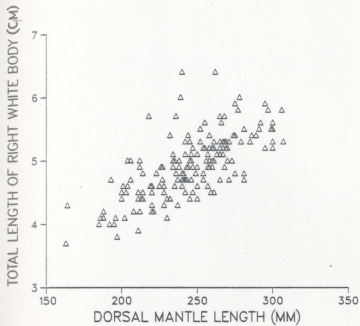


Figure 47. A scattergram in which values for the total length of the right white body are plotted against values for the weight of the squid.

Statistics:

| | |
|----------------|---------|
| Correlation | 0.73498 |
| Significance | 0.00000 |
| Plotted Values | 176.0 |
| Missing Values | 3.0 |

The evidence indicates a positive correlation at the 0.01 level of significance.

Raw data are presented within Appendix 2.

Figure 47A. The same as above, save that values obtained are sorted with respect to sex of the squid.

Statistics:

| | Males | Females |
|----------------|---------|---------|
| Correlation | 0.82557 | 0.65099 |
| Significance | 0.00000 | 0.00000 |
| Plotted Values | 40.0 | 136.0 |
| Missing Values | 1.0 | 2.0 |

In both sexes, the evidence indicates a positive correlation at the 0.01 level of significance.

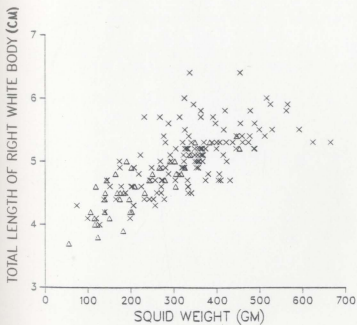
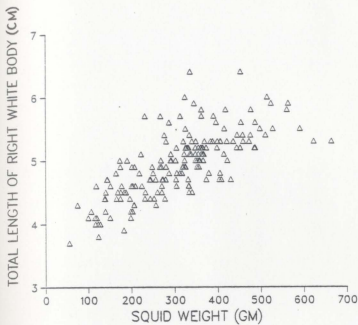


Figure 48. A scattergram in which values for the total length of the left white body are plotted against values for the dorsal mantle length.

Statistics:

| | |
|----------------|---------|
| Correlation | 0.72179 |
| Significance | 0.00000 |
| Plotted Values | 173.0 |
| Missing Values | 6.0 |

The evidence indicates a positive correlation at the 0.01 level of significance.

Raw data are presented within Appendix 2.

Figure 48A. The same as above, save that values obtained are sorted with respect to sex of the squid.

Statistics:

| | Males | Females |
|----------------|---------|---------|
| Correlation | 0.70123 | 0.66515 |
| Significance | 0.00000 | 0.00000 |
| Plotted Values | 39.0 | 134.0 |
| Missing Values | 2.0 | 4.0 |

In both sexes, the evidence indicates a positive correlation at the 0.01 level of significance.

Figure 49. A scattergram in which values for the total length of the left white body are plotted against values for the weight of the squid.

Statistics:

| | |
|----------------|---------|
| Correlation | 0.74299 |
| Significance | 0.00000 |
| Plotted Values | 172.0 |
| Missing Values | 7.0 |

The evidence indicates a positive correlation at the 0.01 level of significance.

Raw data are presented within Appendix 2.

Figure 49A. The same as above, save that values obtained are sorted with respect to sex of the squid.

Statistics:

| | Males | Females |
|----------------|---------|---------|
| Correlation | 0.77680 | 0.68362 |
| Significance | 0.00000 | 0.00000 |
| Plotted Values | 39.0 | 133.0 |
| Missing Values | 2.0 | 5.0 |

In both sexes, the evidence indicates a positive correlation at the 0.01 level of significance.

thereby making accurate measurement of the white body impossible. All missing values were eliminated from subsequently prepared scattergrams and statistical analysis. The results of the morphometric study are presented.

B. Microscopic Anatomy

i. The Capsule

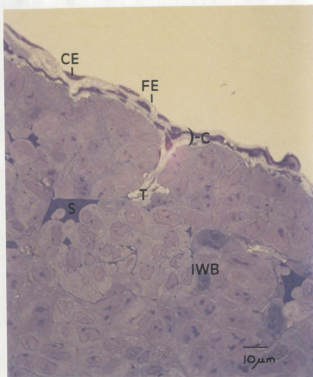
Each white body is enveloped by a protective layer of tissue known as the capsule (Figure 50). Typically, this external layer measures 8.0-8.5 μm in thickness, however, a range in width of 5.5 μm to 11.8 μm has been observed. The capsule conforms to every surface contour, including the free-marginal notches and deep furrows of the postganglionic lobe. Cellular elements and fibrous elements comprise the structural components of this capsule. The former are identified within scanning electron micrographs by the elevated areas of ovoid shape which indicate underlying nuclei (Figure 51). These cells are spindle shaped when viewed longitudinally. Nucleoli are frequently observed within their ovoid nuclei. The cytoplasm of these cells contains extensive rough endoplasmic reticulum and numerous mitochondria. Such cells may occur at various points throughout the capsule of the white body; including the outer margin, the central region, or the inner portion near the white body tissue. Often, these cells are grouped closely together. Surrounding the cells is an amorphous matrix or ground substance in which are embedded fibers

Figure 50. Light micrographs illustrating the fibrous capsule that envelops the white body of I. illecebrosus.

- A. A cross section of the right post-ganglionic lobe from a female specimen; 252 mm DML. Toluidine blue; 820 x
- B. A cross section of the right inferior preganglionic lobe from a female specimen; 232 mm DML. Villanueva; 470 x

| | |
|-----|---------------------------------|
| C | Capsule |
| CE | Cellular Element of the Capsule |
| FE | Fibrous Element of the Capsule |
| IWB | Internal White Body Tissue |
| MC | Mitotic White Body Cells |
| S | Sinus |
| T | Trabecula |

A



B

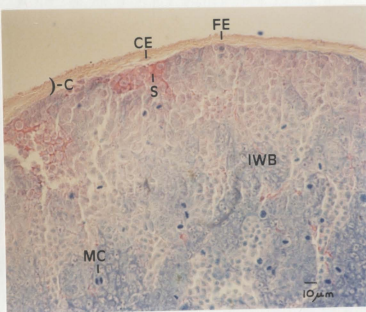
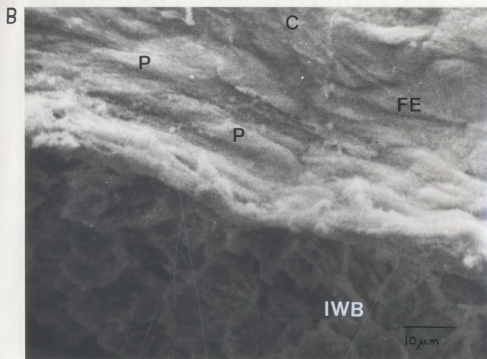
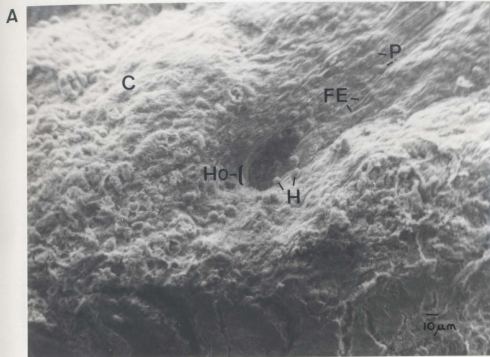


Figure 51. Scanning electron micrographs of the white body capsule (female I. illecebrosus; 252 mm DML).

A. The ventral surface of the left inferior preganglionic lobe. 488 x

B. As above; different field of view. 3150 x

| | |
|-----|--|
| C | Capsule; White Body Surface |
| FE | Fibrous Elements of the Capsule |
| H | Hemocytes |
| Ho | Hemoosculum |
| IWB | Internal White Body Tissue |
| P | Prominence due to the Nuclei of the Capsular Cells |



(Figure 52). The general morphology of such cells and their close association with the fibrous elements of the capsule, strongly suggest they are fibroblastoid.

The capsular fibers mentioned previously are long, slender, serpentine structures that impart a stringy or filamentous texture to the white body surface (Figure 51). These fibers are composed of many fibrils (Figure 52); the number varying from approximately 200-700 within each fiber bundle. Such fibrils do not exhibit visible banding. However, their diameter ($0.2 \mu\text{m}$), arrangement into bundles, and occurrence within the amorphous matrix of the capsule, are highly indicative of collagen-like fibers rather than that of reticular or elastic fibers.

Occasionally, a portion of the capsule will extend into the underlying white body tissue in the form of trabeculae (Figure 53). Three elements comprise each trabecula; fibroblastoid cells, fibrous bundles, and an amorphous ground substance. The last serves as the matrix into which the fibroblastoid cells and the fibers are embedded; an arrangement identical to that of the capsular material found elsewhere. The fibrils of the trabecular fibers measure $0.2 \mu\text{m}$ in diameter. They are aligned in longitudinal rows but do not exhibit any visible periodicity (Figure 54). The general appearance of such fibers again suggests a collagen-like fibrillar nature. As we shall see later, the white body is characterized by an internal fibrous network. A segment of it surrounds the trabeculae.

Figure 52. An electron micrograph illustrating the fibrous structure of the capsule of the white body (cross section of the right postganglionic lobe; female I. illecebrosus; 252 mm DML). 29,948 x

- B-CS Bundle of Capsular Fibrils in Cross Section
- B-LS Bundle of Capsular Fibrils in Longitudinal Section
- CR Central Region of Capsule
- FC Fibroblastoid Cell
- GM Ground Matrix
- IB Inner Border of Capsule
- M Mitochondrion
- N Nucleus
- OM Outer Margin of Capsule
- WBC White Body Cell
- * A portion of the internal fibrous network which extends between the outer capsule and the internal white body tissue.

The author is pleased to acknowledge the services of Mr. Philip Hyam, Mrs. Lisa Lee and Mrs. Kate Ryan of the EM Unit of the Faculty of Medicine in the preparation of the electronphoto micrographs in Figs. 52, 54, 59, 61, 62, 64, 65, 66, 68, 69, 70, 73 and 75. In the same vein, Mrs. Carloyn Emerson provided instruction in the preparation of tissues for scanning electron microscopy.

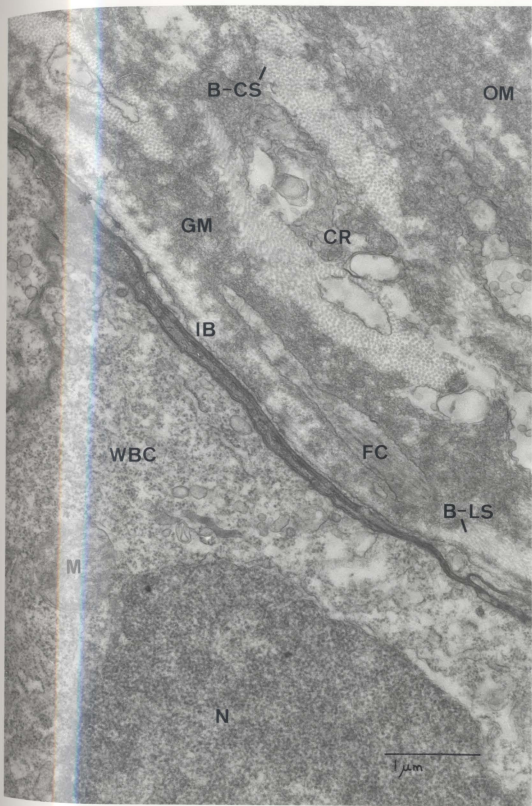


Figure 53. A light micrograph showing a longitudinal section of trabeculae within the right subganglionic process of a female I. illecebrosus (252 mm DML). Toluidine blue; 588 x

| | |
|-----|----------------------------|
| C | Capsule |
| IWB | Internal White Body Tissue |
| T | Trabecula |

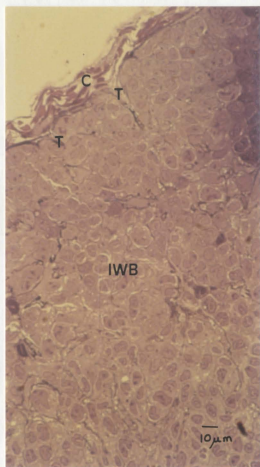
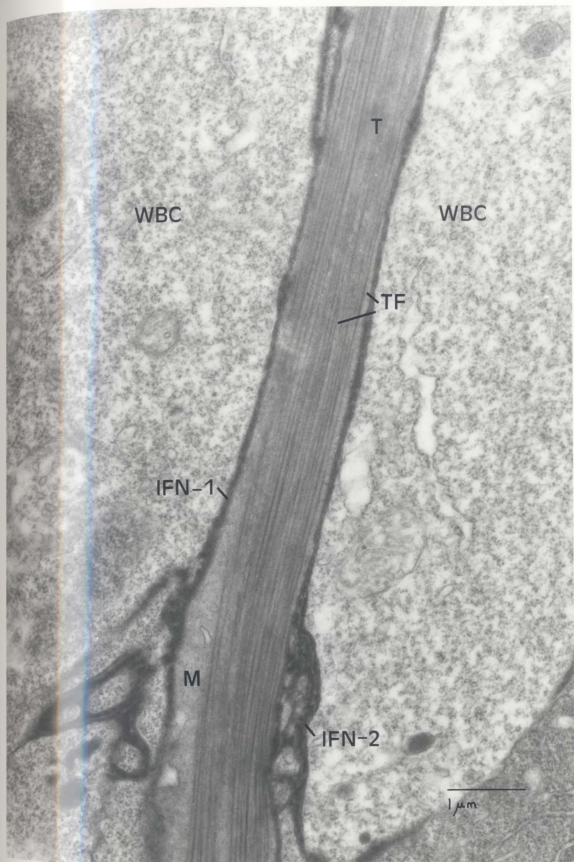


Figure 54. An electron micrograph to illustrate the relationship between a trabecula and the internal fibrous network of the white body (longitudinal section of the right postganglionic lobe; female I. illecebrosus; 252 mm DML). 28,728 x

| | |
|-------|---|
| IFN-1 | Internal Fibrous Network Enveloping the Trabecula |
| IFN-2 | Internal Fibrous Network Joining with IFN-1 |
| M | Matrix |
| T | Trabecula |
| TF | Trabecular Fibrils |
| WBC | White Body Cell |



As a result, the trabeculae do not make contact with the cells of the internal white body tissue. In addition, other portions of the internal fibrous network that lie in close proximity with the trabeculae display fibrous extensions which eventually join with those fibers that envelop the trabeculae (Figure 54).

Usually the capsule invests each lobe and the subganglionic process as a continuous layer, however, scanning electron micrographs reveal occasional interruptions in the form of orifices; here named hemooscula (Figure 55). The cells and fibers of the capsule become aligned around the circumference of each hemoosculum as the immediate vicinity of the latter is approached. As a result, the capsular material appears to encircle each of these hemooscula. This encirclement is extremely pronounced at the rim of each hemoosculum for, here, the cobblestone effect due to prominences caused by the underlying capsular cell nuclei is absent. Instead, there exists a smoother and, therefore, more emphasized encompassing of the hemoosculum by the capsule. These hemooscula penetrate the capsule on both dorsal and ventral surfaces of the white body lobes. Furthermore, they may occur singly or in groupings of up to ten.

Associated with each hemoosculum is a connecting blood vessel or a sinus (Figure 56). Structurally, this permits direct communication between the lumen of such vascular channels and the optic sinus which envelops the white body lobe. These vascular channels appear to be lined

Figure 55. Scanning electron micrographs of the external surface of the white body (female I. illecebrosus; 252 mm DML).

- A. The ventral surface of the left inferior preganglionic lobe. 488 x
- B. Enlargement of above, showing hemoosculum in greater detail. 2,375 x

| | |
|----|---------------------------|
| C | Capsule; External Surface |
| H | Hemocytes |
| Ho | Hemoosculum |

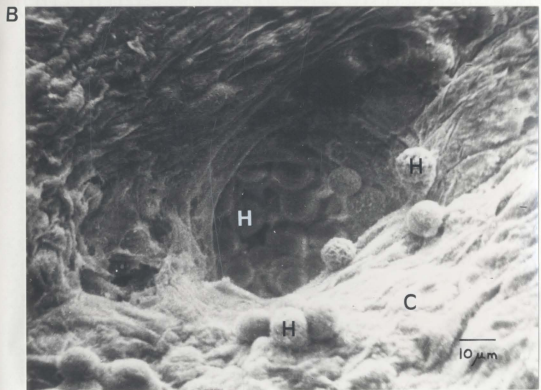
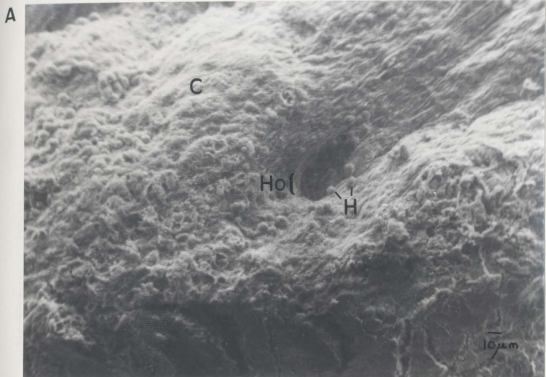


Figure 56. Scanning electron micrographs illustrating the structure of the capsular hemooscula (female I. illecebrosus; 252 DML).

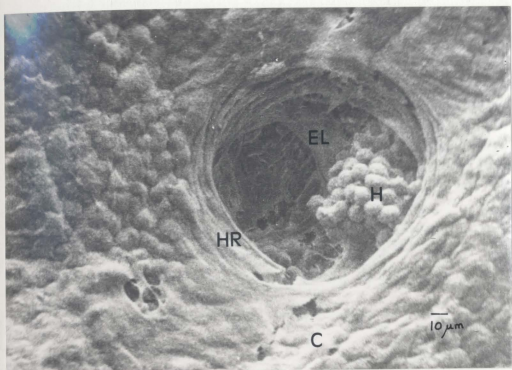
A and B. Dorsal surfaces of the left superior preganglionic lobe. Represented are the white body's vascular channels that communicate with the external optic sinus via the hemooscula.

A. 1,250 x

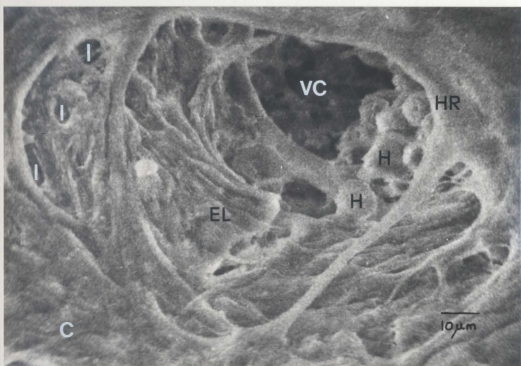
B. 2,100 x

| | |
|----|--|
| C | Capsule |
| EL | Endothelial Lining of Vascular Channel |
| H | Hemocytes |
| HR | Hemooscular Rim |
| I | Interruptions in the Endothelium |
| VC | Vascular Channel |

A



B



with an incomplete layer of endothelium. Hemocytes measuring approximately $10\ \mu\text{m}$ in diameter are frequently observed within the channels or near their openings. These hemocytes exhibit a ruffled surface which is highly suggestive of pseudopodia.

The surface configuration of the capsule, as outlined above, was well illustrated within scanning electron micrographs while histological details were seen to best advantage within the thick sections of TEM prepared material.

ii. Internal Features

Many fibers ramify throughout the interior of the white body. Collectively, these fibers constitute a network that provides support for the surrounding white body tissue and vasculature. Furthermore, as previously noted, these fibers join with and envelop the trabeculae of the capsule. In such instances, these internal fibers extend beyond the boundaries of the trabeculae to occupy that area between the external capsule and the interior white body tissue (Figure 52).

With the aid of light and scanning electron microscopy, these fibers are shown to be long, filamentous structures (Figures 57 and 58). This thread-like appearance is retained even though the individual diameters may vary. Such fibers also exhibit smooth, straight to slightly wavy contours. A closer examination of the network's morphology

Figure 57. A light micrograph illustrating aspects of the fibrous supportive network of the white body (cross section of the right postganglionic lobe; female I. illecebrosus; 252 mm DML). Toluidine blue; 820 x

| | |
|-----|----------------------------|
| FC | Fibroblastoid Cell |
| FSN | Fibrous Supportive Network |
| IWB | Internal White Body Tissue |

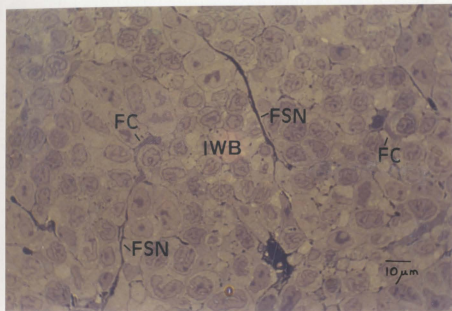
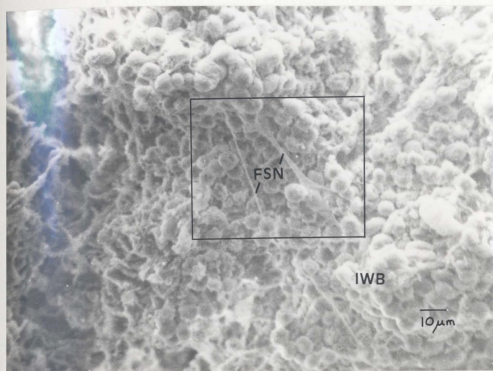


Figure 58. Scanning electron micrographs of the white body interior (female I. illecebrosus; 252 mm DML).

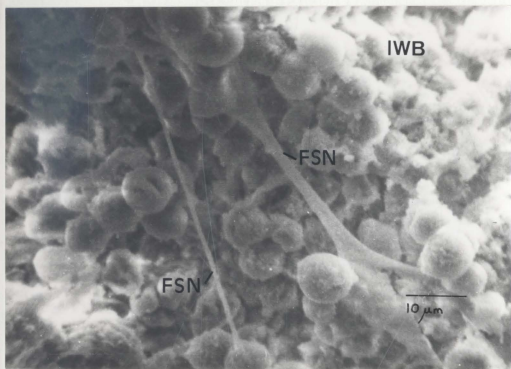
- A. A view of the fibrous supportive network within the left inferior preganglionic lobe. 1,188 x
- B. An enlargement of a portion of the field seen in A. 3,088 x

FSN Fibrous Supportive Network
IWB Internal White Body Tissue

A



B



reveals that each fiber is comprised of finer subunits or fibrils. These fibrils display transversely oriented bands of $0.03 \mu\text{m}$ periodicity. The bands of adjacent fibrils are aligned with each other such that parallel rows are established. The result is a uniform pattern of banding shared by all fibrils of a given fiber bundle (Figure 59).

Although this banding pattern is not identical to that of collagen fibers ($0.064 \mu\text{m}$; Krause & Cutts, 1981), the similarities in fibrillar organization strongly suggest that the white body supportive fibers are closely related to collagen fibers.

Associated with this internal supportive network are fibroblastoid cells (Figures 60 and 61). These cells are stellate in shape; their long cytoplasmic extensions closely aligned with the fibrous network of the lobe. Within light micrographs, such cells exhibit darkly stained nuclei. Usually, these nuclei are ovoid, however they may also appear triangular in shape due to the encroachment of the surrounding white body tissue. Ultrastructurally, the nuclei display marginated chromatin. The cytoplasm of such fibroblast-like cells is filled with rough endoplasmic reticulum and numerous mitochondria (Figure 62). Occasionally, electron-dense material is present within the cisternae of the former organelle. The fibroblastoid cells of the white body's interior are morphologically similar to those fibroblastoid cells associated with the fibrous component of the white body's capsule.

Figure 59. An electron micrograph illustrating the periodicity displayed by fibers of the supportive network (cross section of the left postganglionic lobe; female I. illecebrosus; 252 mm DML). 12,130 x

FB Fibrillar Bands
FSN Fibrous Supportive Network
WBC White Body Cell

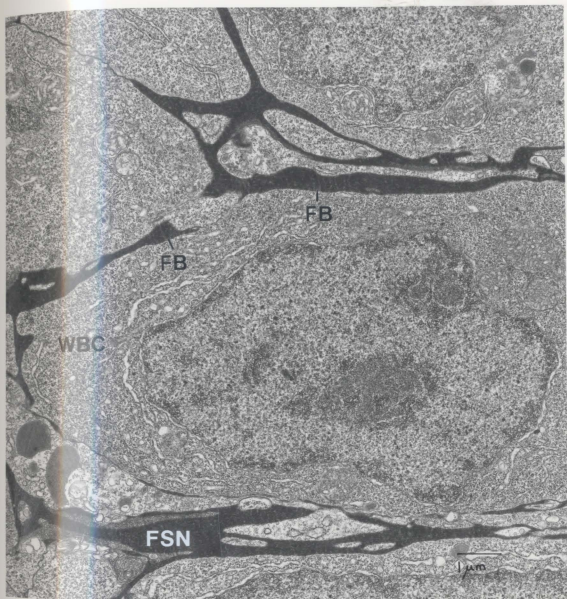


Figure 60. A light micrograph illustrating fibroblastoid cells of the white body interior (cross section of the right postganglionic lobe; female I. illecebrosus; 252 mm DML). Toluidine blue; 820 x

| | |
|-----|----------------------------|
| FC | Fibroblastoid Cell |
| FSN | Fibrous Supportive Network |
| N | Nucleus |
| WBC | White Body Cell |

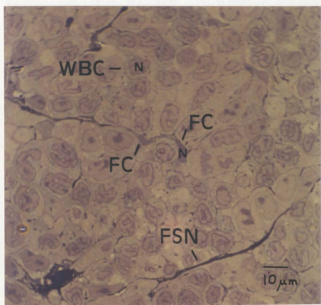


Figure 61. An electron micrograph illustrating the close relationship between a fibroblastoid cell and the internal fibrous network of the white body lobe (cross section of the right postganglionic lobe; female I. illecebrosus; 252 mm DML). 8,938 x

| | |
|-----|-----------------------|
| CE | Cytoplasmic Extension |
| FC | Fibroblastoid Cell |
| FN | Fibrous Network |
| N | Nucleus |
| WBC | White Body Cell |

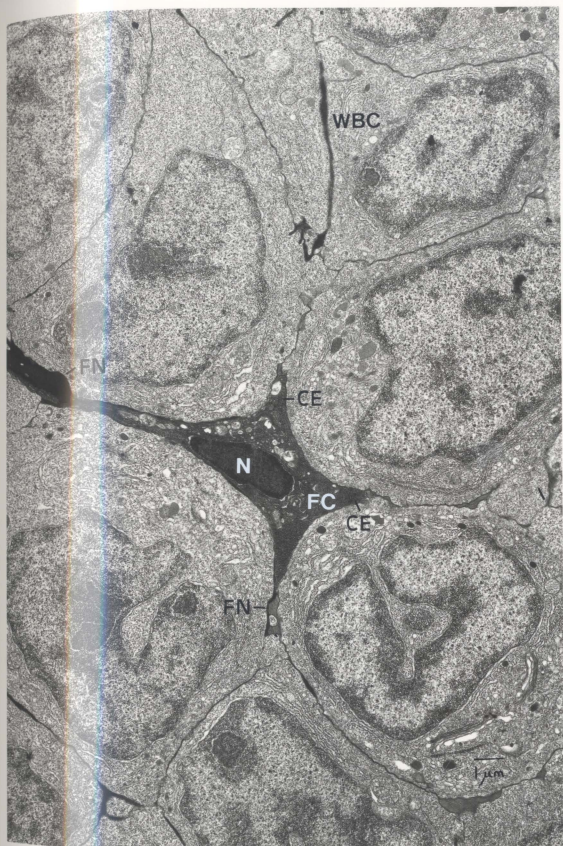
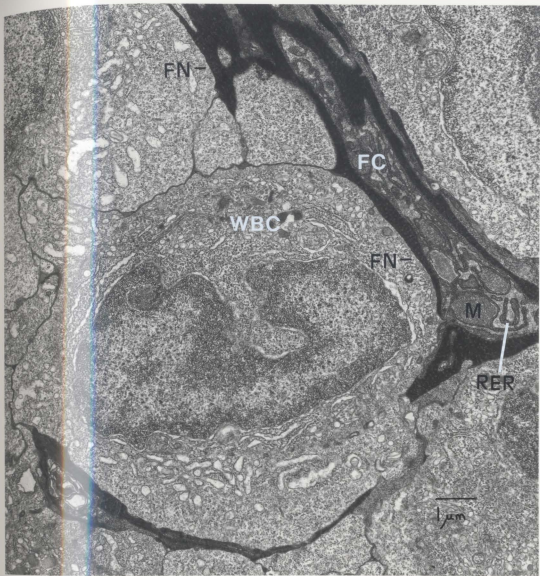


Figure 62. An electron micrograph illustrating the fine structure of fibroblastoid cells from the interior of a white body lobe (cross section of the right postganglionic lobe; female I. illecebrosus; 252 mm DML). 11,810 x

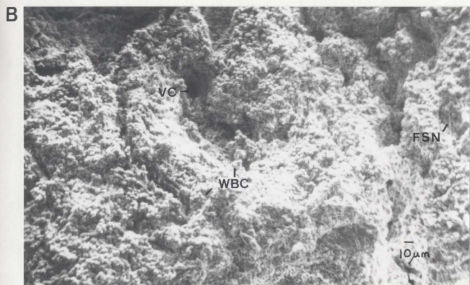
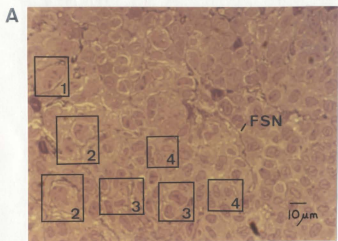
| | |
|-----|-----------------------------|
| FC | Fibroblastoid Cell |
| FN | Fibrous Network |
| M | Mitochondrion |
| RER | Rough Endoplasmic Reticulum |
| WBC | White Body Cell |



Between the external capsule and the internal network of supportive fibers, there exists a population of densely packed cells (Figure 63). Upon first observation, these cells (here termed white body cells) appear to be homogeneous. This is particularly evident within scanning electron micrographs where the vast majority of these white body cells share the following external features: a spherical profile with smooth or slightly ruffled surfaces. Those cells which do not conform to the above category appear to be flattened and angular in outline. It was not possible to ascertain whether this latter group of cells represents disfigured white body cells (due to the SEM processing) or, possibly, the fibroblastoid cells mentioned previously.

The uniformity displayed by white body cells at the scanning electron microscopy level becomes less apparent when such cells are viewed by light and electron microscopy. The latter two techniques reveal a gradation in chromatin concentration within the various nuclei. If one views the white body cells with this feature in mind, a pattern of organization becomes evident.

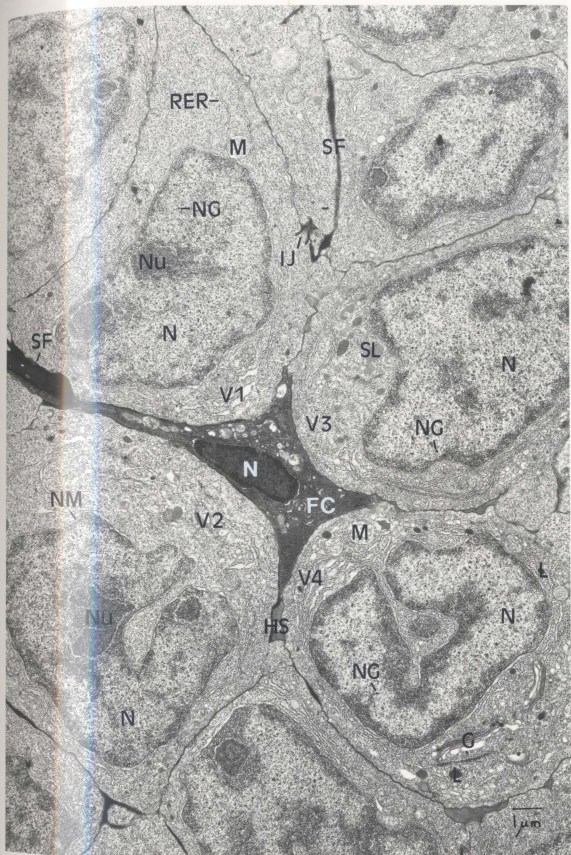
Cells may be classified on the basis of similarity in the distribution of nuclear material. On that basis, four variations may be described as follows. Light microscopy preparations reveal that one group of white body tissue cells, Variation 1 white body cells (approximately 19.5 μm in diameter; refer to Appendix 3), possess nuclei



in which the chromatin is equally distributed. The nuclei are lightly stained in histological sections and nucleoli are usually present. Transmission electron microscopy preparations (Figure 64) confirm the uniformly dispersed pattern of chromatin and, furthermore, indicate that a concentration of chromatin along the nuclear membrane is minimal, if present. However, in the immediate vicinity of the nucleolus there is a concentration of nuclear material. Electron-dense amorphous granules are seen scattered throughout the chromatin. The nucleolus is a prominent feature of these nuclei both in size and appearance. The latter is a result of an electron-lucent area that separates the nucleolus from the concentration of chromatin that surrounds it. These cells and their nuclei appear to exhibit the largest diameters of the cell variations, however this observation may be due to the plane of section. Adjacent to this grouping of cells is a second variation of white body tissue cell; Variation 2 white body cells (approximately 13 μm in diameter). The nuclei of these cells display marginated chromatin. Increased concentrations of chromatin within the central regions of the nucleus are also evident. With regard to nucleolar appearance and the presence of electron-dense nuclear granules, Variation 2 white body cells are similar to those cells within the Variation 1 category. These nuclei are moderately stained in histological preparations. Variation 3 white body cells (approximately 11 μm in diameter) possess

Figure 64. An electron micrograph of white body tissue from a female specimen of I. illecebrosus (252 mm DML; a cross section of the right postganglionic lobe). 8,938 x

| | |
|-----|---------------------------------|
| FC | Fibroblast-like Cell |
| G | Golgi Body |
| HS | Hemal Space |
| IJ | Intercellular Junction |
| L | Lysosome-like Body |
| M | Mitochondrion |
| N | Nucleus |
| NG | Nuclear Granules |
| NM | Nuclear Membrane |
| Nu | Nucleolus |
| RER | Rough Endoplasmic Reticulum |
| SF | Supportive Fibers |
| SL | Secondary Lysosome-like Body |
| V1 | Variation One White Body Cell |
| V2 | Variation Two White Body Cell |
| V3 | Variation Three White Body Cell |
| V4 | Variation Four White Body Cell |



nuclei in which the concentration of nuclear material has progressed to a further stage. The nucleus is now outlined with a uniform band of darkly stained chromatin. Those concentrations of chromatin within the central nuclear regions also stain more intensely. While the nuclear granules are still present, the nucleolus has become less prominent. Such nuclei are also moderately stained by histological techniques. Fringing this group of cells is the fourth variation of white body tissue cell: Variation 4 white body cells (approximately 8 μm in diameter). The nuclei within these cells display an advanced stage of chromatin concentration. The electron-dense nuclear granules persist, however the nucleolus is no longer observed. Such nuclei stain darkly in histological preparations. This arrangement of the four white body tissue cell variations occurs repeatedly not only within a given field of view but also throughout each white body lobe and subganglionic process. It was noted (refer to Appendix 4) that 2-5% of these cells represent the Variation 1 white body cell; 19-30% the Variation 2 cell; 30-44%, the Variation 3 cell; and 31-44% the Variation 4 white body cell. These values hold for each lobe and the subganglionic process. The organization and structural details of this internal white body tissue were best observed within those samples processed for transmission electron microscopy and, in particular, those tissue preparations fixed in the modified Karnovsky adjusted to the pH (7.2)

and osmolarity (1400) of the squid's blood.

All four variations of the white body cell possess an abundance of cytoplasmic organelles. The observed structures include free ribosomes, Golgi bodies, lysosome-like bodies, mitochondria, rough endoplasmic reticulum, secondary lysosome-like bodies, and vacuoles. Although a quantitative study of organelle distribution was not undertaken, there appears to be a higher incidence of rough endoplasmic reticulum within Variation 3 white body cells and lysosome-like bodies within Variation 4 white body cells. The free ribosomes contribute to the dense granularity of the cytoplasmic matrix that is characteristic of all four white body cell variations.

Intercellular junctions (Figures 65 and 66) are yet another cytoplasmic feature. Although infrequent, these junctional complexes, when present, unite Variation 1 white body cells. Usually such junctions occur as electron-dense parallel bars positioned perpendicularly to the adjoining cell membranes. Each portion of a junction measures $0.08 \mu\text{m}$ in width and $0.63 \mu\text{m}$ in length. A distance of $0.50 \mu\text{m}$ separates the two portions. The cytoplasm of the two adjoining cells appears to be continuous through the intercellular junction. These observations and the ones concerning cellular organelles and nuclear appearance are summarized in Table 9.

White body cells have frequently been observed during mitosis (Figures 67 and 68). These mitotic figures

Figure 65. An electron micrograph illustrating an intercellular junction between two Variation 1 white body cells (cross section of the right postganglionic lobe; female I. illecebrosus; 252 mm DML). 12,130 x

| | |
|----|-------------------------------|
| IJ | Intercellular Junction |
| M | Mitochondrion |
| N | Nucleus |
| Nu | Nucleolus |
| V1 | Variation One White Body Cell |

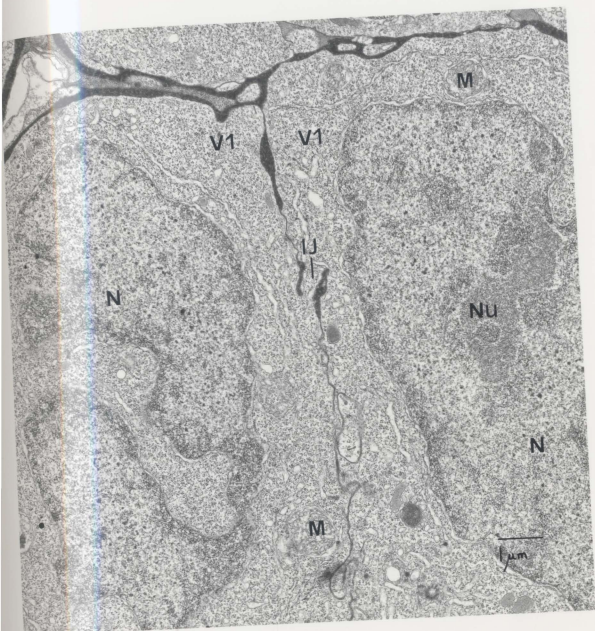


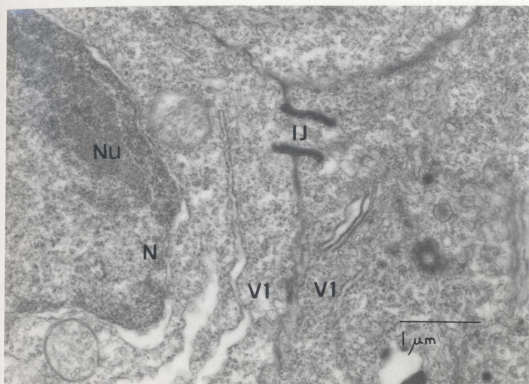
Figure 66. Electron micrographs illustrating the structural details of an intercellular junction (cross section of the left post-ganglionic lobe; female I. illecebrosus; 252 mm DML).

A. 24,282 x

B. 119,700 x

| | |
|----|-------------------------------|
| IJ | Intercellular Junction |
| N | Nucleus |
| Nu | Nucleolus |
| V1 | Variation One White Body Cell |

A



B

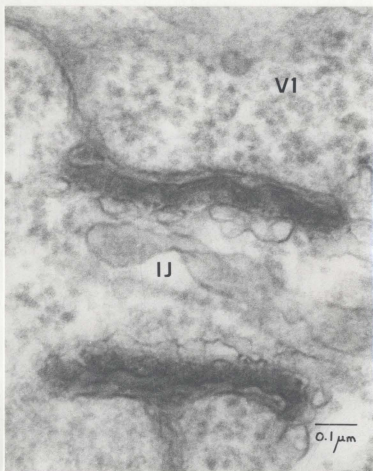


Table 9. Comparison of nuclear and cytoplasmic features of cell variants in the white body of Illex illecebrosus.

| | | | |
|----|------------------|----|--------------------------|
| C | Concentrated | NM | Nuclear Membrane |
| D | Diffuse | NP | Not Present |
| G | Granular | P | Present |
| LP | Less Prominent | PC | Pronounced Concentration |
| NI | Nuclear Interior | SC | Slight Concentration |

Cell Variation

Nuclear and Cytoplasmic Features

| | Chromatin | Nuclear Granules | Nucleolus | Cytoplasm | Golgi Apparatus | Lysosome-like Bodies | Mitochondria | Rough Endoplasmic Reticulum | Secondary Lysosome-like Bodies | Vacuoles | Intercellular Junctions |
|-------------|-----------|------------------|-----------|-----------|-----------------|----------------------|--------------|-----------------------------|--------------------------------|----------|-------------------------|
| Variation 1 | D | P | P | G | P | P | P | P | P | P | P |
| Variation 2 | SC/NM | P | P | G | P | P | P | P | P | P | NP |
| Variation 3 | C/NI/NM | P | LP | G | P | P | P | P | P | P | NP |
| Variation 4 | PC/NI/NM | P | NP | G | P | P | P | P | P | P | NP |

Figure 67. A light micrograph illustrating the presence and distribution of mitotic cells within white body tissue (cross section of the right inferior preganglionic lobe from a female I. illecebrosus; 232 mm DML; Villanueva). 470 x

| | |
|-----|--|
| B | Blood |
| C | Capsule |
| IWB | Interior White Body Tissue |
| MC | Cell in Process of Mitotic Nuclear Division |

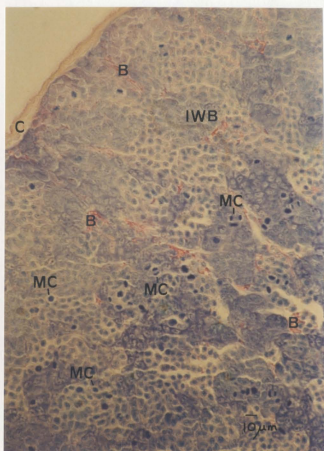
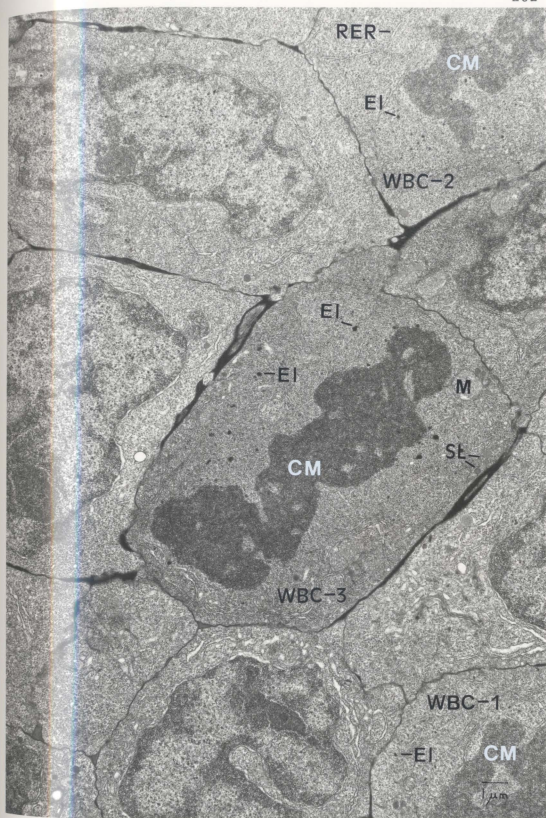


Figure 68. An electron micrograph illustrating white body cells during mitosis (cross section of the left postganglionic lobe; female I. illecebrosus; 252 mm DML). 8,938 x

| | |
|-------|---|
| CM | Chromatin |
| EI | Electron-dense Inclusions |
| M | Mitochondrion |
| RER | Rough Endoplasmic Reticulum |
| SL | Secondary Lysosome-like Bodies |
| WBC-1 | White Body Cell (Early Prophase) |
| WBC-2 | White Body Cell (Middle Prophase) |
| WBC-3 | White Body Cell (Late Prophase/ Early Metaphase) |



are especially well demonstrated within Villanueva stained white body tissue sections. In such preparations, the mitotic nuclei are quickly identified by their deep staining properties. These nuclei appear in sharp contrast to the surrounding interphase nuclei which exhibit a minimal degree of stain. As a result, one can readily study not only the presence but also the distribution of those white body cells undergoing mitosis. Initial observations suggest that the percentage of dividing cells is relatively high (calculation of the mitotic index follows). In addition, these dividing cells appear to be concentrated within the central portion of the white body lobe. Unique to the morphology of these mitotic cells is the presence of electron-dense cytoplasmic inclusions (Figure 69). During early/middle prophase, these electron-dense inclusions resemble the granules within the interphase nuclei of all four white body cell variations. During late prophase/early metaphase, these inclusions display increases in diameter (2x) and electron density. Later stages of the mitotic process appear to exhibit a substantial reduction of cytoplasmic inclusions. These mitotic cells have been observed among groupings of the second and/or third white body tissue cell variations.

Small blood vessels, sinuli, and hemal spaces occur throughout this tissue of the white body. Figure 70 illustrates one of the small vessels. Its lining is composed of a discontinuous layer of endothelial cells.

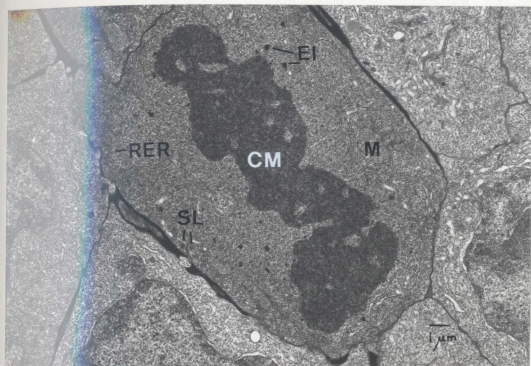
Figure 69. Electron micrographs illustrating the structural details of white body cells during mitosis (cross section of the left postganglionic lobe; female I. illecebrosus; 252 mm DML).

A. White Body Cell 6,703 x
(Late Prophase/Early Metaphase)

B. White Body Cell 12,130 x
(Anaphase)

| | |
|-----|--------------------------------|
| CM | Chromatin |
| EI | Electron-dense Inclusions |
| M | Mitochondrion |
| RER | Rough Endoplasmic Reticulum |
| SL | Secondary Lysosome-like Bodies |

A



B

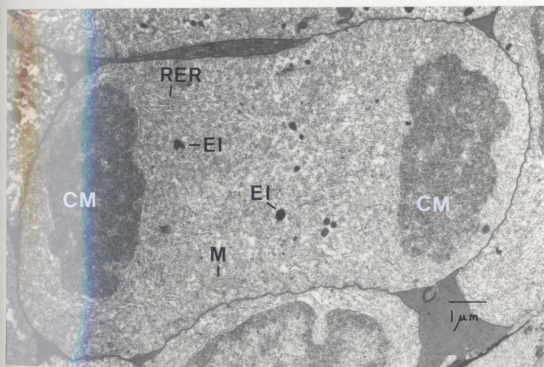
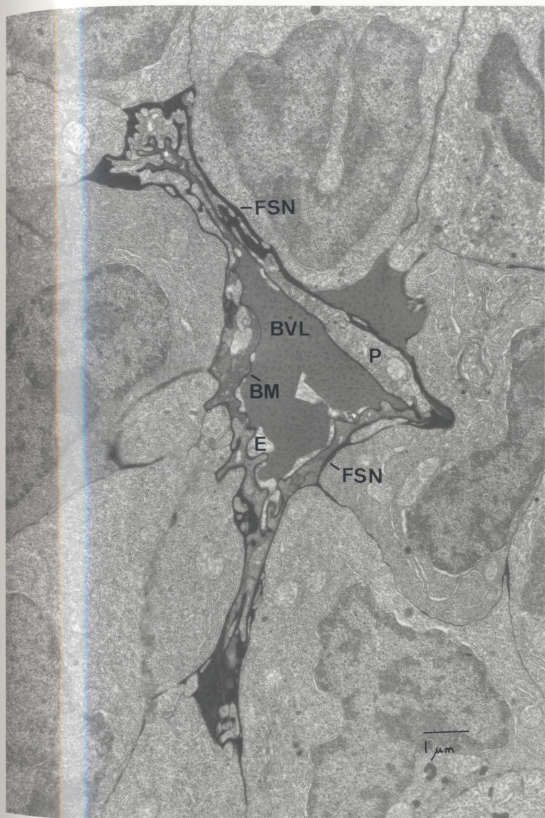


Figure 70. An electron micrograph illustrating one of the small blood vessels within the white body tissue of I. illecebrosus (cross section of the right postganglionic lobe; female specimen; 252 mm DML). 8,618 x

| | |
|-----|----------------------------|
| BM | Basement Membrane |
| BVL | Blood Vessel Lumen |
| E | Endothelial Cell |
| FSN | Fibrous Supportive Network |
| P | Pericyte |



Underlying this endothelial layer, in sequential order, is a basement membrane, a layer of pericytes, and lastly, a layer of fibrous material. The basement membrane is complete (uninterrupted) and highly convoluted. The pericyte layer which lies next to the basement membrane conforms precisely with the convolutions of the latter. These pericytes interdigitate to form a continuous ring around the lumen of the vessel. The most peripheral layer, consisting of fibers, separates the small blood vessel from the surrounding tissue. These fibers are part of the white body's internal supportive network. Within scanning electron micrographs, such blood vessels appear as tubular passages (Figure 71) that wind their way through the tissue of the white body interior. The lumen of each vessel is bound by a layer of squamous endothelial cells.* Additional blood vascular channels may occur at angles to those just described. Communication between the vessels is via their lumina. The spherical structures which represent the only visible interluminal feature are here labeled hemocytes.

Sinuli are also present throughout each lobe and subganglionic process of a white body. Characteristically, their general outline is highly irregular in appearance (Figures 72 and 73). These sinuli, the dilated portions of venous blood vessels, are lined with an incomplete layer

* Although these endothelial cells are tightly adjoining, occasionally one can observe discontinuities or spaces.

Figure 71. Scanning electron micrographs showing the vascular channels that penetrate the white body tissue (female I. illecebrosus; 252 mm DML).

A. An interior view of the left inferior preganglionic lobe. 2,375 x

B. As above; different field of view. 2,375 x

C Cells of the White Body
H Hemocytes
VC Vascular Channel
W Wall of the Vascular Channel

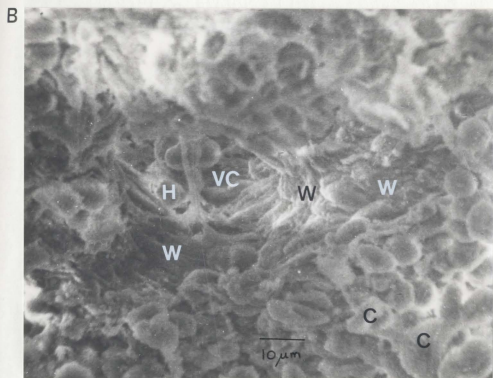
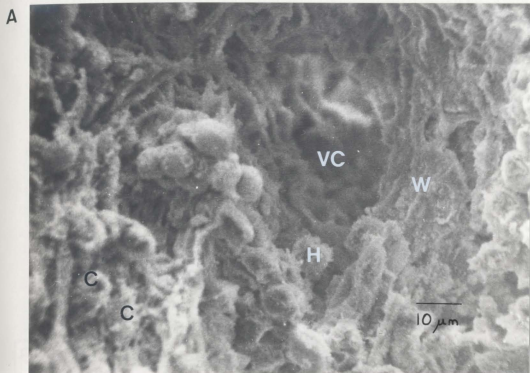


Figure 72. Light micrographs illustrating sinuli within white body tissue.

A. Cross section of the right subganglionic process from a female I. illecebrosus; 252 mm DML. Toluidine blue; 550 x

B. Cross section of the right inferior preganglionic lobe from a female I. illecebrosus; 232 mm DML. Villanueva; 470 x

C Capsule
H Hemocytes
IWB Internal White Body Tissue
S Sinulus
V Vessel Communicating with Sinulus

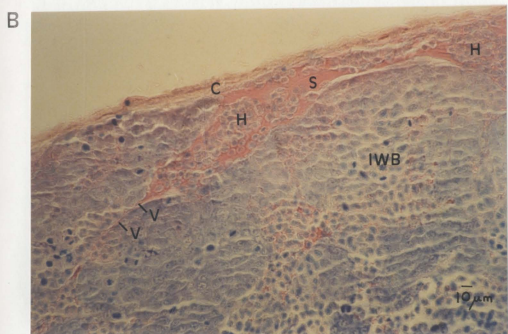
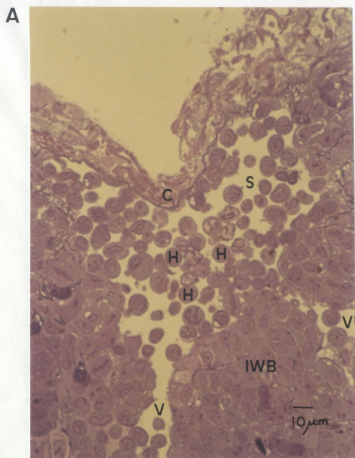
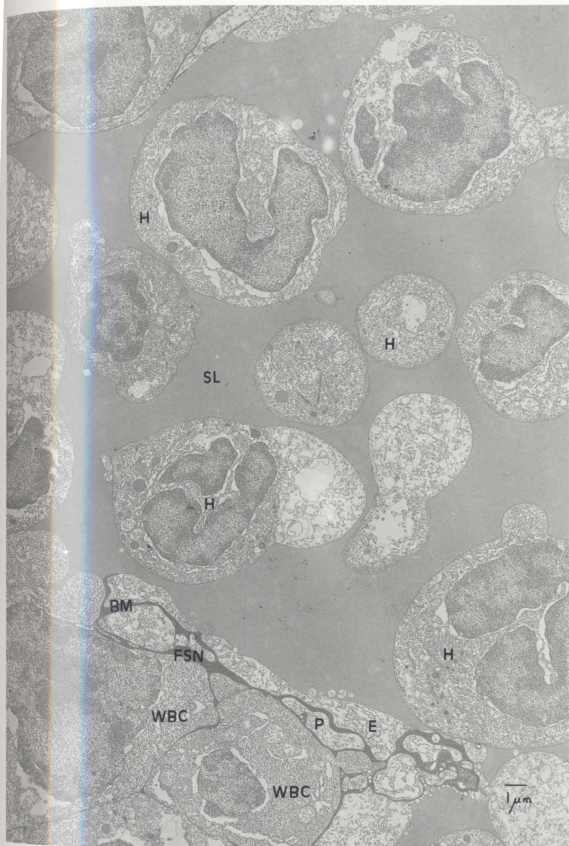


Figure 73. An electron micrograph illustrating the ultrastructure of a sinusus within white body tissue (longitudinal section of the right postganglionic lobe; female I. illecebrosus; 252 mm DML). 6,065 x

| | |
|-----|----------------------------|
| BM | Basement Membrane |
| E | Endothelial Cell |
| FSN | Fibrous Supportive Network |
| H | Hemocyte |
| P | Pericyte |
| SL | Sinusus Lumen |
| WBC | White Body Cell |



of endothelial cells. Supporting the endothelial layer is an uninterrupted basement membrane, an incomplete layer of pericytes, and finally, a layer of fibrous material. The last mentioned (which originates from the white body's internal supportive network) joins with the basement membrane at intervals, thereby giving the appearance that the pericytes are within one fibrous supportive layer. Hemocytes are often observed within the lumen of a sinus. The general morphology of such blood cells is similar to that previously described for the fourth variation of white body tissue cell. Figure 74 shows a subcapsular sinus that ruptured during tissue processing. The previously contained hemocytes are now liberated to the exterior.

The discontinuous layer of endothelial cells which lines the small vessels and sinuli facilitates the passage of blood from the white body vasculature into the surrounding white body tissue. Electron micrographs demonstrate that this hemal fluid enters the intercellular spaces; hereafter termed hemal spaces (Figure 75). Molecules of the respiratory pigment, hemocyanin, are usually visible within the blood that occupies these hemal spaces. On such occasions, the hemocyanin molecules are aligned in parallel rows. Rarely are these hemal spaces supported by the white body's fibrous network. Rather, it is only when a hemal space occurs at a point along the network's tract that contact is established. Even under these circumstances, the support afforded the hemal space is minimal.

Figure 74. A light micrograph illustrating a sub-capsular sinusus that was disrupted during processing of the white body tissue (cross section of the right subganglionic process; female I. illecebrosus; 252 mm DML). 950 x

| | |
|-----|-----------------------------------|
| C | Capsule |
| H | Hemocytes |
| IWB | Internal White Body Tissue |
| S | Sinusus |
| V | Vessel Communicating with Sinulus |

Stained with Toluidine blue.

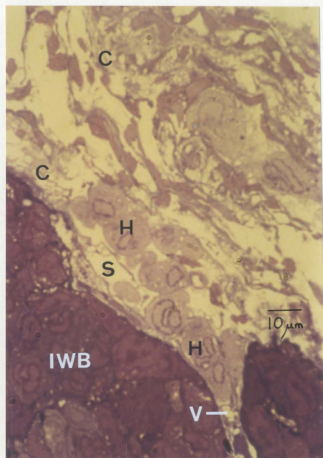


Figure 75. An electron micrograph illustrating the hemal spaces within white body tissue from I. illecebrosus (cross section of the left postganglionic lobe; female specimen; 252 mm DML). 11,172 x
insert; 17,556 x

| | |
|-----|---|
| FN | Fibrous Network |
| H | Hemocyanin(Molecules Aligned in Parallel Rows) |
| HS | Hemal Space |
| WBC | White Body Cell |

Insert: Magnified view of the hemocyanin molecules within a hemal space.

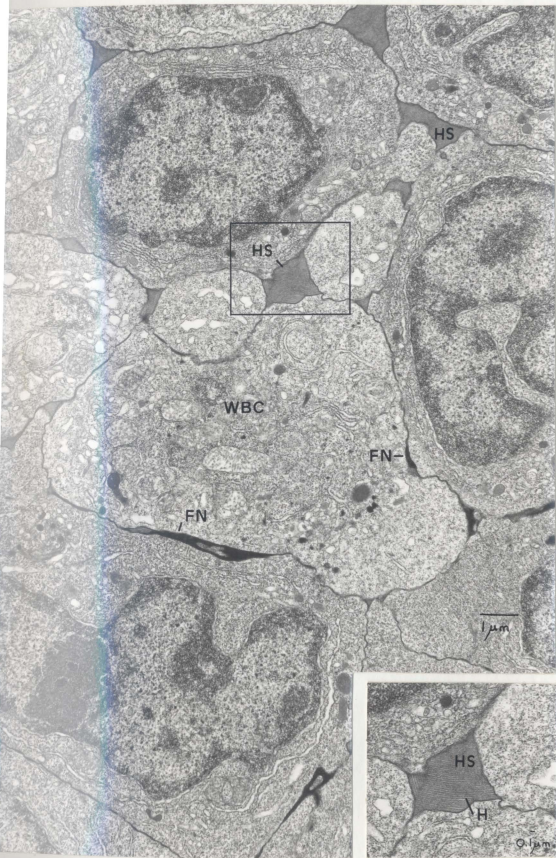


Figure 76 shows composite drawings that illustrate the microscopic anatomy of the white bodies within I. illecebrosus. These drawings are based upon the information derived from tissue samples viewed by means of light, scanning, and electron microscopy. Figure 77 demonstrates the structural similarity among the various components of a white body.

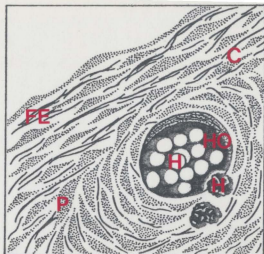
Each lobe and subganglionic process of a white body are histologically similar. All are protected by an external capsule consisting of an amorphous matrix in which are embedded fibers and fibroblastoid cells. These fibers, which impart a filamentous appearance to the capsule, do not exhibit a visible periodicity. Occasionally, a portion of the capsule will extend into the underlying white body tissue as a trabecula. The latter joins with and is enveloped by the white body's internal network of fibrous material. These internal fibers lend support to the surrounding tissue and vasculature of the white body lobe or subganglionic process. They are associated with fibroblastoid cells and exhibit a periodicity of $0.03 \mu\text{m}$. In conjunction with the external capsule, these fibers create a framework for the mass of densely packed white body cells. Each white body cell possesses an abundance of cytoplasmic organelles including free ribosomes, Golgi bodies, lysosome-like bodies, mitochondria, rough endoplasmic reticulum, secondary lysosome-like bodies, and vacuoles. However, the white body cells differ with regard to the degree of

Figure 76. Diagrammatic representation of cellular features as observed in the white body of I. illecebrosus.

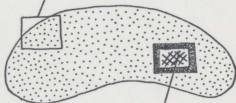
- A. Surface configuration and structures as based upon SEM analysis. 950 x
- B. Longitudinal section showing subcapsular organization. 1,000 x

| | |
|----|--|
| C | Capsule |
| CF | Capsular Fibers |
| FC | Fibroblastoid Cell |
| FE | Fibrous Elements of the Capsule |
| H | Hemocyte |
| Ho | Hemoosculum |
| MC | Mitotic Cell |
| N | Network of Supportive Fibers |
| P | Prominence due to the Nuclei of the Capsular Cells |
| S | Sinus |
| T | Trabecula |
| V1 | Variation One White Body Cell |
| V2 | Variation Two White Body Cell |
| V3 | Variation Three White Body Cell |
| V4 | Variation Four White Body Cell |

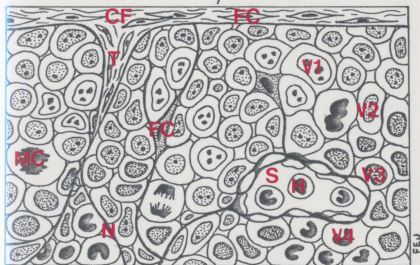
A



10 μm



B

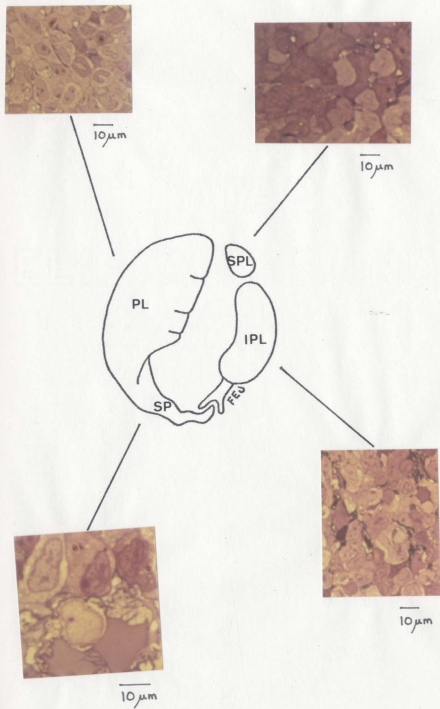


10 μm

figure 77. Light micrographs to demonstrate that each lobe and subganglionic process of a white body are histologically similar.

| | | |
|-----|-----------------------------|-------|
| IPL | Inferior Preganglionic Lobe | 550 x |
| PL | Postganglionic Lobe | 550 x |
| SP | Subganglionic Process | 820 x |
| SPL | Superior Preganglionic Lobe | 550 x |

Each photograph is of a cross section of the tissue from that portion of the white body so indicated.



chromatin concentration exhibited by the various nuclei. Such nuclear concentration ranges from a uniformly dispersed pattern of chromatin, through a graded series to, eventually, an advanced stage of chromatin condensation. On this basis, four variations of white body cell have been noted. Cells representing each variation tend to cluster together, so that within any one grouping of white body cells there is present those cells whose nuclei exhibit similar concentrations of nuclear material. As mentioned previously, this arrangement is repeated not only within a given field of view but also throughout each white body lobe and subganglionic process. Intercellular junctions have been observed between Variation 1 white body cells and mitotic figures among groupings of the second and/or third white body cell variations. This is particularly true of those second and/or third cell groupings which occur within the central region of a white body lobe. Dispersed throughout this white body tissue are numerous blood vessels, sinuli, and hemal spaces. While the vessels and sinuli receive strong support from the internal fibrous network, the intercellular hemal spaces receive minimal support, if any.

C. Vascular Studies

The terms applied herein to the major blood vessels, sinuses, and other features of the blood vascular system are those of Bradbury (1970) in her study of the cephalic arterial and venous circulation of I. illecebrosus. The

vasculature supplying blood to and transporting blood from the white bodies has received no direct investigation until the present study.

i. Arterial Blood Supply to the White Bodies

The information gathered from injections of Latex and RENOGrafin-60 (a radiopaque contrast agent) indicates that the white bodies receive arterial blood from branches of the cephalic aorta. More specifically, oxygenated blood from the ctenidia enters the systemic heart by way of the branchial veins (the efferent branchial vessels). From the systemic heart, blood is pumped anteriorly via the cephalic aorta (Figure 78). Numerous arteries carrying blood to adjacent viscera and mantle tissue, originate from this trunk artery as it proceeds anteriorly. Prior to its passage through the foramen magnum of the cartilaginous "skull", the cephalic aorta bifurcates at a point overlying the dorsal apex of the hepatic portion of the hepatopancreas. Both branches enter the cranial cavity through the foramen, whereupon they are termed (Bradbury, 1970) intracranial arteries. From each intracranial artery there arises a vessel that arches laterally to service the posterior regions of the adjacent eye and its associated structures. These two lateral branches are here named the right and left posterior ophthalmic arteries. Distal to the origin of the right posterior ophthalmic artery, the intracranial artery proceeds anteriorly as the buccal artery. However, beyond the origin of the left posterior

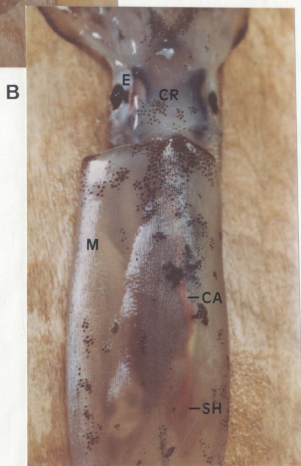
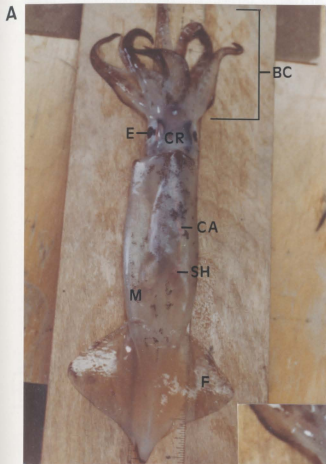
Figure 78. Photographs of I. illecebrosus (male specimen; 214 mm DML) illustrating the systemic heart and cephalic aorta following arterial injection of red Latex.

A. Anesthetized specimen. 0.4 x

B. As above. 0.8 x

| | |
|----|-------------------|
| BC | Brachial Cone |
| CA | Cephalic Aorta |
| CR | Cephalic Region |
| E | Eye, Left |
| F | Fin |
| M | Mantle or Pallium |
| SH | Systemic Heart |

The systemic heart and cephalic aorta are visible through the translucent dorsal mantle wall.



ophthalmic artery, the left intracranial artery angles ventrad; coming to lie beneath and parallel to the buccal artery (Figure 79). It is from this ventral artery, called the brachial trunk artery, that the anterior regions of the right and left eyes and their associated structures receive blood. These vessels arise at 90° angles from the brachial trunk artery and are here named the right and left anterior ophthalmic arteries. A composite drawing illustrating the forementioned blood vessels is presented in Figure 80.

It is now possible to outline a more detailed account of the white bodies' blood supply by tracing the pathways of these anterior and posterior ophthalmic arteries. Due to the fact that vessels to the right and left white bodies are mirror images of each other, only one aspect (the right) will be described.

The right posterior ophthalmic artery turns laterally across the medial surface of the right eye to a point just beyond the postganglionic lobe of the white body. Here, the posterior ophthalmic artery veers posteriad to join the circumophthalmic artery. Prior to this juncture, there arises from the laterally-directed portion of the posterior ophthalmic artery a vessel whose branches ramify throughout the upper region of the postganglionic lobe (Figure 81). This vessel is here named the superior postganglionic artery. The lower region of the postganglionic lobe of the white body receives blood from (1) two vessels that originate from the posteriorly-directed portion of

Figure 79. Illustrations to elucidate the relationship between the intracranial arteries, buccal artery, and the brachial trunk artery (female I. illecebrosus; 227 mm DML; arterial injection of red Latex). 2.5 x

- A. Photograph of anesthetized specimen.
 B. Diagrammatic representation of above.

| | |
|------|---|
| B | Bifurcation of Cephalic Aorta |
| BA | Buccal Artery |
| BM | Buccal Mass |
| BTA | Brachial Trunk Artery |
| CA | Cephalic Aorta |
| E | Eye |
| H | Hepatic Portion of Hepatopancreas |
| LAOA | Left Anterior Ophthalmic Artery |
| LIA | Left Intracranial Artery |
| LOG | Left Optic Ganglion |
| LPL | Left Postganglionic Lobe of White Body |
| LPOA | Left Posterior Ophthalmic Artery |
| M | Mantle (Folded Back on Itself) |
| RAOA | Right Anterior Ophthalmic Artery |
| RIA | Right Intracranial Artery |
| ROG | Right Optic Ganglion |
| RPL | Right Postganglionic Lobe of White Body |
| RPOA | Right Posterior Ophthalmic Artery |



POSTERIOR

ANTERIOR

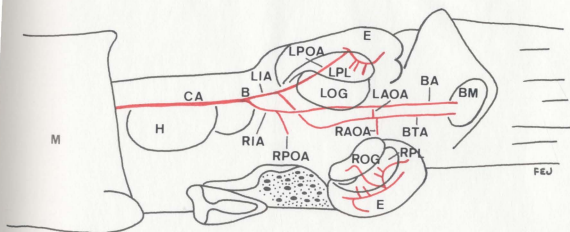


Figure 80. Diagram illustrating the general route of oxygenated blood from the gills to the arteries that vascularize the white bodies (modified from Bradbury, 1970, p. 197).

| | |
|-----|-----------------------------------|
| AMA | Anterior (Marginal) Mantle Artery |
| AOA | Anterior Ophthalmic Artery |
| BA | Buccal Artery |
| BTA | Brachial Trunk Artery |
| BV | Branchial Vein |
| CA | Cephalic Aorta |
| GPA | Gastrocaecal Pancreatic Artery |
| HA | Hyponomal Artery |
| HeA | Hepatic Artery* |
| IA | Intracranial Artery |
| MMA | Median Mantle Artery |
| PA | Posterior Aorta |
| POA | Posterior Ophthalmic Artery |
| SH | Systemic Heart |

*The so-called hepatic gland artery (Bradbury, 1970).

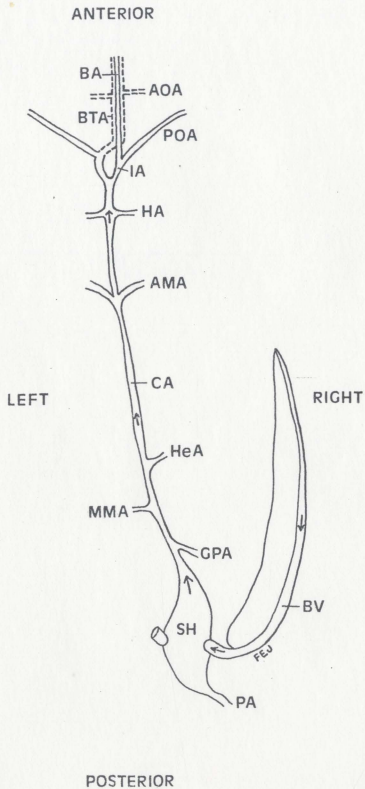
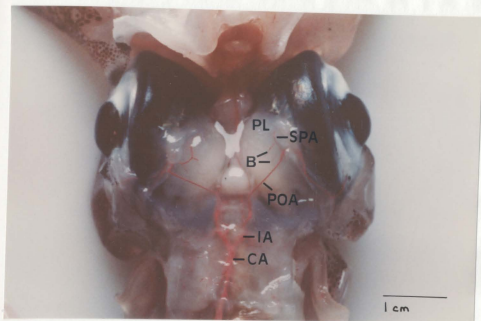


Figure 81. Photographs illustrating the right and left superior postganglionic arteries and their branches that vascularize the upper region of the postganglionic lobes (female I. illecebrosus; 227 mm DML).

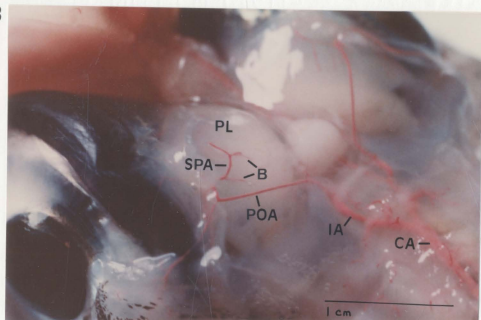
- A. Anesthetized, Latex injected specimen (right superior postganglionic artery and its branches). 2.0 x
- B. As above (left superior postganglionic artery and its branches). 4.5 x

| | |
|-----|--|
| B | Branches of the Superior Postganglionic Artery |
| CA | Cephalic Aorta |
| IA | Intracranial Artery |
| PL | Postganglionic Lobe of the White Body |
| POA | Posterior Ophthalmic Artery |
| SPA | Superior Postganglionic Artery |

A



B



the posterior ophthalmic artery and (2) one vessel from the adjacent circumphthalmic artery. All three vessels to the lower regions of the postganglionic lobe are here named the inferior postganglionic arteries (Figure 82). The subganglionic process which intermediates the postganglionic lobe and the inferior preganglionic lobe also receives blood from the circumphthalmic artery (Figure 82). The four vessels observed within this area supplying the upper region of the subganglionic process tissue are named the process arteries.

The right anterior ophthalmic artery, branching from the brachial trunk artery at a 90° angle, passes beneath the inferior preganglionic lobe to supply blood to the anterior regions of the right eye and optic ganglion (Figure 83). At a point prior to its passage beneath this lobe of the white body, there originates from the anterior ophthalmic artery a vessel that angles dorsally; the anterior white body artery (Figure 84). Two branches immediately arise from it; namely, the superior preganglionic artery and the inferior preganglionic artery. The former enters the small superior preganglionic lobe while the other ramifies throughout the larger more ventrally located inferior preganglionic lobe (Figure 84).

This entire description of the arterial blood supply to the white bodies is summarized in Figures 85 and 86 and within Table 10.

Figure 82. A photograph showing arteries to the right subganglionic process and the lower region of the right postganglionic lobe (female I. illecebrosus; 227 mm DML; anesthetized, Latex injected specimen). 4.5 x

| | |
|-----|----------------------------------|
| COA | Circumophthalmic Artery |
| IA | Intracranial Artery |
| IPA | Inferior Postganglionic Arteries |
| PA | Process Artery |
| PL | Postganglionic Lobe |
| POA | Posterior Ophthalmic Artery |
| SP | Subganglionic Process |

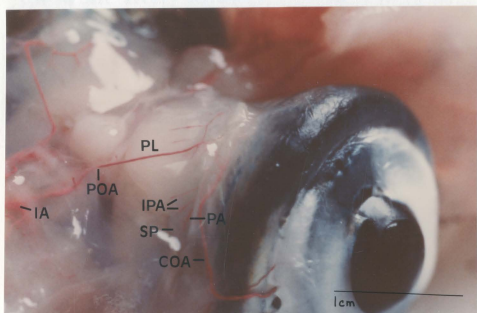


Figure 83. Photographs illustrating the right anterior ophthalmic artery following arterial injection of red Latex (male I. illecebrosus; 214 mm DML).

A. Medial view of the right eye of an anesthetized specimen. 4.5 x

B. As above; minus optic ganglion. 4.5 x

| | |
|-----|-----------------------------|
| AOA | Anterior Ophthalmic Artery |
| BTA | Brachial Trunk Artery |
| E | Eye |
| IA | Intracranial Artery |
| IPL | Inferior Preganglionic Lobe |
| OG | Optic Ganglion |
| PL | Postganglionic Lobe |
| SP | Subganglionic Process |
| SPL | Superior Preganglionic Lobe |

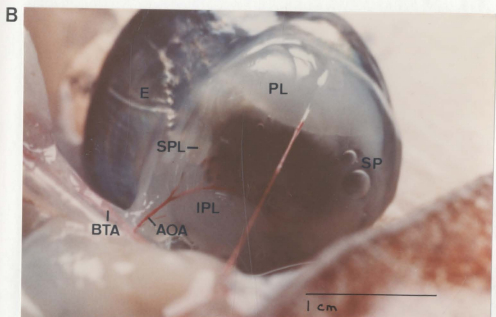
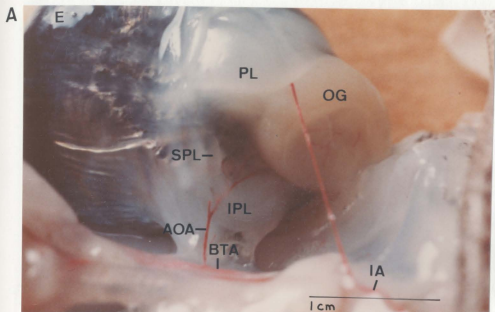


Figure 84. Photographs illustrating the right anterior white body artery and its branches as indicated by Latex injection.

A. Medial view of the right eye from an anesthetized female I. illecebrosus; 227 mm DML. The right optic ganglion has been removed. 4.5 x

B. As above; different angle. 4.5 x

| | |
|-----|--|
| AOA | Anterior Ophthalmic Artery |
| AWA | Anterior White Body Artery |
| IPA | Inferior Preganglionic Artery |
| IPL | Inferior Preganglionic Lobe of White Body |
| PL | Postganglionic Lobe of White Body |
| R | Rami of IPA |
| SP | Subganglionic Process of White Body |
| SPA | Superior Preganglionic Artery |
| SPL | Superior Preganglionic Lobe of White Body |

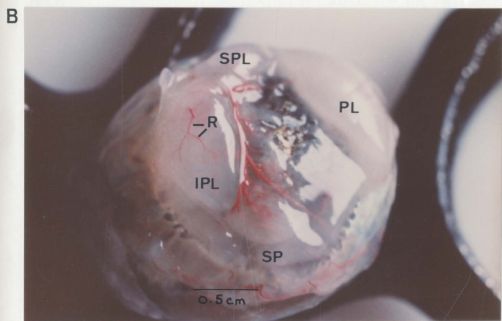
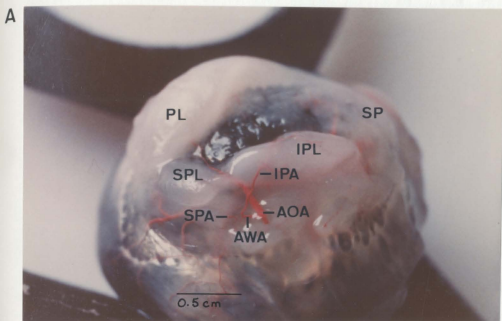


Figure 85. Composite diagram illustrating the pathway of the right and left posterior ophthalmic arteries and their branches. 3.5 x

| | |
|-----|----------------------------------|
| CA | Cephalic Aorta |
| COA | Circumophthalmic Artery |
| IA | Intracranial Artery |
| IPA | Inferior Postganglionic Arteries |
| PA | Process Arteries |
| POA | Posterior Ophthalmic Artery |
| SPA | Superior Postganglionic Artery |
| WB | White Body (see Figure 13) |

Both rings of white body tissue have been drawn as if displaced laterally.

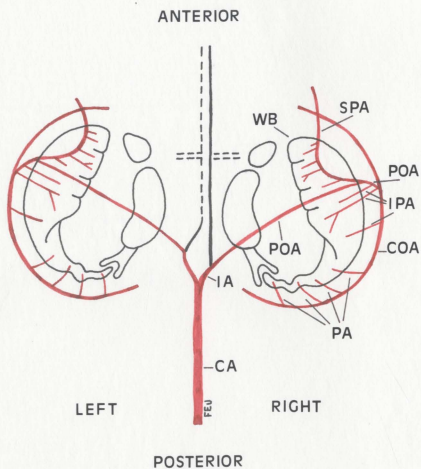


Figure 86. Composite diagram illustrating the pathway of the right and left anterior ophthalmic arteries and their branches. 3.5 x

| | |
|-----|-------------------------------|
| AOA | Anterior Ophthalmic Artery |
| AWA | Anterior White Body Artery |
| BTA | Brachial Trunk Artery |
| CA | Cephalic Aorta |
| IA | Intracranial Artery |
| IPA | Inferior Preganglionic Artery |
| SPA | Superior Preganglionic Artery |
| WB | White Body (see Figure 13) |

Both rings of white body tissue have been drawn as if displaced laterally.

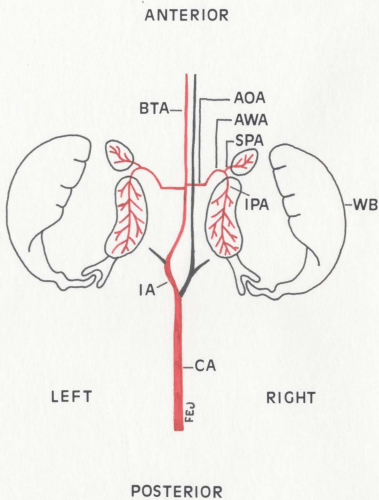
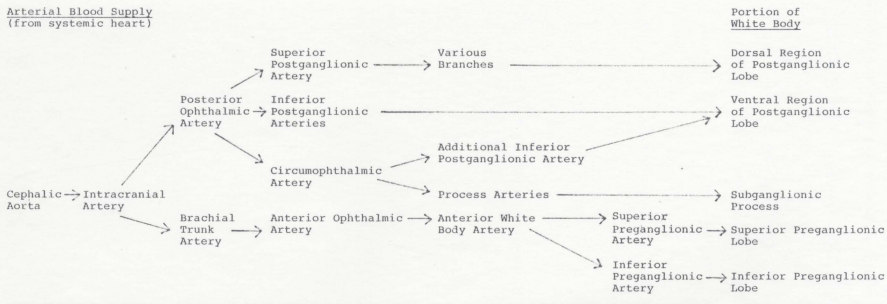


Table 10. A table indicating arterial routes from the systemic heart to the various parts of the white bodies.

Arterial Blood Supply
(from systemic heart)



ii. White Body Tissue Circulation

The circulation* of blood within the white bodies was studied following (1) injections of white body arteries by use of Latex and/or Staedtler drawing ink and (2) histological preparations of white body tissue by light microscopy, transmission electron microscopy (TEM), and scanning electron microscopy (SEM). The information derived from these varied sources produced an integrated view of the vascular network. Furthermore, the data indicated that the vascular network within each lobe of a white body ring is similar.

As the Latex injections have demonstrated (Figure 84), the arteries to a lobe of the white body ramify throughout that tissue to produce increasingly finer vessels. These smaller vessels eventually join with channels that transport venous blood. Communication between a lobe's arterial and venous systems is presumably achieved via capillaries, although demonstration of the latter was not possible due to their fragile structure. However, the venous channels can be defined and easily recognized within histological preparations by the dilations they display. The dilations observed within these venous blood vessels have been named sinuli (Figure 72). A detailed description of their ultrastructure is reported within the Internal Features subdivision of the Microscopic Anatomy section of the Results.

*Here referring to the blood vessels accommodating blood flow.

Sinuli vary greatly in size and are found randomly distributed throughout the tissue of each lobe and sub-ganglionic process. Although no evidence could be seen indicating their occurrence in localized congregations, occasionally a sinus is seen adjacent to the fibrous capsule. Venous blood, within the superficial sinuli and/or veins of each lobe and process, directly enters the venous system of the cephalic region, a portion of which are the optic sinuses, via hemooscula (orifices in the capsule).

iii. Venous Drainage

Injections of RENOgrafen-60 afforded an opportunity to study the right and left optic sinuses within the cephalic region of I. illecebrosus. The resultant sequence of illustrations (Figure 87; 1-5) shows the filling of these sinuses with the radiopaque contrast agent cited above. Such illustrations provide information regarding the position and configuration of the optic sinuses.

The first figure within this photographic sequence (Figure 87-1; recorded 1 minute and 38 seconds following the injection of RENOgrafen-60) reveals the initial signs of what will become the right optic sinus. This particular portion of the sinus is situated "over" the region of the postganglionic lobe of the right white body. The second figure (Figure 87-2; recorded 1 minute and 50 seconds following injection) exhibits a more distinct outline of the right optic sinus; that portion within the

Figure 87. A photographic sequence illustrating the position and configuration of the left and right optic sinuses as demonstrated by the injection of the radiopaque contrast agent, RENografin-60 (female I. illecebrosus; 265 mm DML). 0.75 x

1. 1 minute; 38 seconds postinjection
2. 1 minute; 50 seconds postinjection
3. 1 minute; 57 seconds postinjection
4. 2 minutes; 30 seconds postinjection
5. 2 minutes; 50 seconds postinjection

| | |
|-----|---|
| CA | Cephalic Aorta |
| H | Hypodermic Needle |
| LP | Left Postganglionic Portion of the Left Optic Sinus |
| LS | Left Subganglionic Portion of the Left Optic Sinus |
| LSu | Left Superior Preganglionic Portion of the Left Optic Sinus |
| OBS | Outer Buccal Sinus |
| RP | Right Postganglionic Portion of the Right Optic Sinus |
| RS | Right Subganglionic Portion of the Right Optic Sinus |
| RSu | Right Superior Preganglionic Portion of the Right Optic Sinus |
| SH | Systemic Heart |

region of the right postganglionic lobe being easily discerned. Furthermore, the corresponding portion of the left optic sinus is likewise visible. There is, however, a second area associated with this outline of the left optic sinus. It is a circular area which appears in a medial position to the right of this left optic sinus. Figure 87-3 (recorded 1 minute and 57 seconds following injection) further defines the images outlined in the previous two photographs. Within the fourth illustration (Figure 87-4; recorded 2 minutes and 30 seconds after injection) the configuration of the postganglionic portion of both right and left optic sinuses is accentuated. Adjacent to the posterior edge of both former structures there appears to be forming a third structure. The outline of the circular area of the left optic sinus has become more visible and a similar area is now discernible on the right side. First signs of the outer buccal sinus are also evident. The last photograph of the sequence (Figure 87-5; recorded 2 minutes and 50 seconds following the injection of RENOGrafin-60) provides a well defined outline of all the portions of each optic sinus. The largest visible portion is positioned "over" the postganglionic lobe of a white body. At the posterior edge of the latter, there is present a second portion which angles medially and anteriorly; a confirmation corresponding to the subganglionic process with the possibility of extending toward the inferior preganglionic lobe. The final observable

portion, of circular configuration, lies "over" the region of the superior preganglionic lobe. While each of the three portions is closely associated with an adjacent portion, there appears to be sufficient distinction among the three to suggest that each optic sinus is actually comprised of three chambers. The three chambers which are thought to form the right optic sinus are a mirror image to those of the left.

2. Immunological Studies of the White Bodies

Two observations were noted during the preparation of the white body cell suspension. Firstly, the white body tissue of I. illecebrosus is very easily dissociated into individual cells. Secondly, the passage of this cell suspension through glass wool, alone, was not sufficient to remove particulate debris. Rather, centrifugation on Ficoll-Paque, a density gradient medium, was required in order to obtain a homogeneous preparation of white body cells.

When samples of the white body cell suspension were exposed to rabbit antiserum or saline during a slide agglutination test, the former (white body cell suspension plus antiserum) became flocculant, indicating a positive reaction. White body cell suspension plus saline exhibited a negative reaction. These findings prompted the indirect immunofluorescence experiments; the results of which are reported in the pages that

follow. Unless otherwise stated, all tissue sections and material for smear preparations were from I. illecebrosus.

A. Unabsorbed Rabbit Antiserum

In the indirect immunofluorescent tests the rabbit antisera obtained at different times after immunization consistently displayed a positive (++) reaction upon exposure to four samples of I. illecebrosus white body cell suspension smears (each from a different specimen; each in duplicate). This reaction became strongly positive (+++) if the antiserum tested was diluted 1:10 or 1:20 with phosphate-buffered saline. The latter observation influenced subsequent procedures in that antiserum, as well as control serum, were hereafter diluted 1:10 before experimentation commenced.

Positive to strongly positive reactions were displayed upon rabbit antiserum addition to samples from three different specimens of I. illecebrosus white body (Figure 88), liver, and muscle (Figure 88) tissue sections (each tested in duplicate).

Strongly positive reactions were repeatedly observed following antiserum addition to two samples of I. illecebrosus blood smears (Figure 89) (each from a different specimen; each in duplicate) and one sample of O. pteropus blood (tested in duplicate). However, it was noted that ethanol-fixed blood smears from the latter species of squid reacted negatively, indicating denaturation or extraction of the antigen(s).

Figure 88. Photographs demonstrating the reactions that result upon exposure of squid tissues to antiserum and normal rabbit serum with subsequent addition of fluorescent sheep antiserum to rabbit immunoglobulin.

- A. Frozen white body tissue section (7 μ m) from I. illecebrosus. Antiserum reaction is strongly positive (+++). 820 x
- B. Frozen mantle (muscle) tissue section (7 μ m) from I. illecebrosus. Antiserum reaction is strongly positive (+++). 820 x
- C. Frozen white body tissue section (7 μ m) from I. illecebrosus. Normal rabbit serum reaction is negative (-). 820 x

CM Circular Muscle
LM Longitudinal Muscle
WBC White Body Cells
WTS White Body Tissue Section

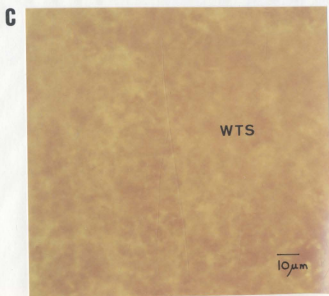
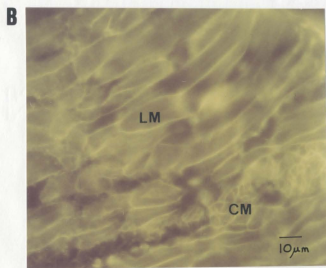
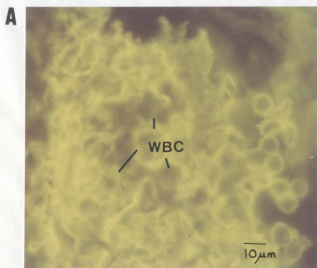
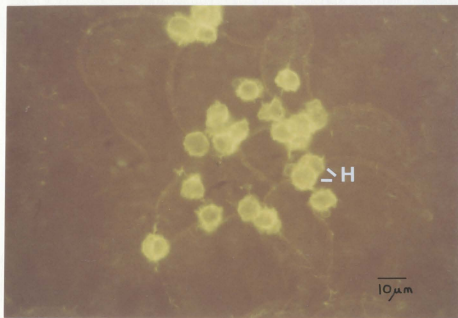


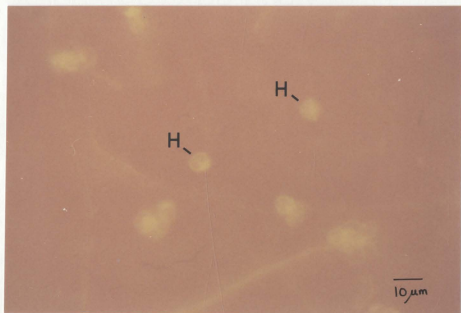
Figure 89. Photographs demonstrating the reactions that result upon exposure of squid hemocytes to antiserum and normal rabbit serum with subsequent addition of fluorescent sheep antiserum to rabbit immunoglobulin.

- A. Blood smear from I. illecebrosus.
Antiserum reaction is strongly positive
(+++). 900 x
 - B. Blood smear from I. illecebrosus.
Normal rabbit serum reaction is negative
(-). 900 x
- H Hemocytes

A



B



Controls (normal rabbit serum and PBS) employed during the testing of this rabbit antiserum were negative. A summary of the results described above is compiled within Table 11.

B. Absorbed Rabbit Antiserum

Samples of rabbit antiserum were absorbed individually with samples of I. illecebrosus ink sac, liver, mantle (muscle), optic ganglion, ovary, and stomach homogenates. These six tissue homogenates were processed from three different specimens. The resultant absorbed antisera were then tested in duplicate trials against I. illecebrosus blood (Figure 90), O. pteropus blood, I. illecebrosus white body cell suspension smears, and I. illecebrosus white body, liver, and muscle tissue sections.

Although the antiserum absorptions were incomplete (antiserum absorbed with liver still reacts with liver, etc.) the results, Table 12, indicate that the white body cells carry at least one antigen not carried on the other tissues used for absorption. Of special interest is the result that white body cells were the only I. illecebrosus tissue which completely removed the reaction with blood cells from O. pteropus.

3. Mitotic Index Study of the White Bodies

The mitotic indices of white body tissue samples from six different specimens of I. illecebrosus were

Table 11. Indirect immunofluorescent reactions of antiserum prepared against I. illecebrosus white body cells. Antiserum tested against various squid tissues with subsequent addition of fluorescent sheep antiserum to rabbit immunoglobulin.

^aReactions defined as: - Negative (background)
 (+) Only slightly brighter than background
 + Marginally positive
 ++ Positive
 +++ Strongly positive

^bNot tested.

| | Squid Tissues Tested | | | | | | |
|---------------|------------------------|----------------------|------------------------|-------------------|--------------------|-----------------|-----------------|
| | <u>I. illecebrosus</u> | | | | <u>O. pteropus</u> | | |
| | Cell | White Body Smears | White Body Sections | Liver Sections | Muscle Sections | Blood Smears | Blood Smears |
| Antiserum 1:1 | ++ ^a | + | n.t. ^b | n.t. | n.t. | n.t. | n.t. |
| 1:10 | +++ | ++ | +++ | +++ | +++ | +++ | +++ |
| 1:20 | +++ | ++ | n.t. | n.t. | n.t. | n.t. | n.t. |
| Normal rabbit | 1:1 | + | - | n.t. | n.t. | n.t. | n.t. |
| | 1:10 | (+) | - | (+) | (+) | (+) | - |
| PBS | | - | - | - | - | - | - |

Figure 90. Photographs demonstrating the reactions that result upon exposure of hemocytes from I. illecebrosus to antiserum, absorbed antiserum, and normal rabbit serum with subsequent addition of fluorescent sheep antiserum to rabbit immunoglobulin.

- A. Blood smear. Antiserum reaction is strongly positive (+++). 900 x
 - B. Blood smear. White body absorbed antiserum reaction is positive (++). 900 x
 - C. Blood smear. Normal rabbit serum is negative (-). 900 x
- H Hemocytes

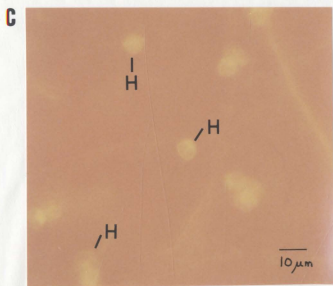
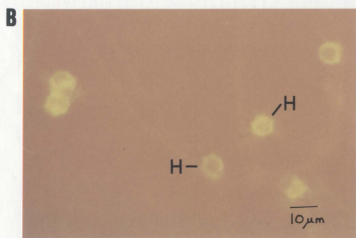
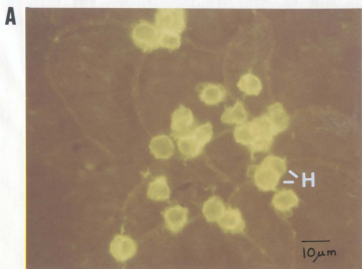


Table 12. Indirect immunofluorescent reactions of antiserum prepared against I. illecebrosus white body cells. Unabsorbed antiserum and antiserum absorbed with various tissues from I. illecebrosus tested against various squid tissues with subsequent addition of fluorescent sheep antiserum to rabbit immunoglobulin.

^aSee Table 9.

^bNot tested.

| | Squid Tissue Tested | | | | | |
|----------------------------------|------------------------|-------------------|----------|----------|--------|--------------------|
| | <u>I. illecebrosus</u> | | | | | <u>O. pteropus</u> |
| | White Body | | Liver | Muscle | Blood | Blood |
| | Cell Smears | Sections | Sections | Sections | Smears | Smears |
| Antiserum 1:10 | +++ ^a | +++ | +++ | +++ | +++ | +++ |
| Antiserum 1:10 absorbed with: | | | | | | |
| Ink sac | ++ | n.t. ^b | n.t. | n.t. | +++ | ++ |
| Liver | ++ | n.t. | + | n.t. | + | +++ |
| Muscle (Mantle) | ++ | n.t. | n.t. | + | ++ | +++ |
| Optic Ganglion | ++ | n.t. | n.t. | n.t. | +++ | ++ |
| Ovary | ++ | n.t. | n.t. | n.t. | +++ | +++ |
| Stomach | ++ | n.t. | n.t. | n.t. | +++ | +++ |
| White Body | + | + | n.t. | n.t. | ++ | - |
| Normal Rabbit 1:10 | - | - | (+) | (+) | (+) | - |
| PBS | - | - | - | - | - | - |

calculated. Tissue samples were collected over the four month interval of September-December, 1979. One tissue sample was obtained from each squid with the exception of the December specimen which provided four samples; one from each component of a white body. Telophase nuclei were not included during any of these mitotic counts because of their close resemblance to sectioned portions of the reniform shaped interphase nuclei. The data compiled throughout this mitotic index study are presented within Table 13.

White body tissue collected in September, October, and November exhibited mitotic indices averaging 3.9. Each index recorded during this period varied no more than 0.4 from another; the highest being 4.1, the lowest 3.7. The mitotic indices of white body tissue samples collected in December averaged 3.2. In this instance, however, the maximum variation among indices was 1.3. These two values are the result of the high mitotic index (4.1) recorded for the right inferior preganglionic lobe. The latter index is comparable to those recorded for white body tissue samples collected in September, October, or November. If this particular index is removed and the indices of the remaining white body components evaluated, the average mitotic index becomes 2.9 with a range in variation of 0.2.

These results indicate, with respect to the white body samples observed, that the percentage of dividing cells is (1) consistent throughout the Fall months of the year and the majority of white body components, (2) elevated

Table 13. Data collected during the mitotic index study of white body tissue from I. illecebrosus

RIPL Right Inferior Preganglionic Lobe
RPL Right Postganglionic Lobe
RSP Right Subganglionic Process
RSPL Right Superior Preganglionic Lobe

Values recorded in this table represent the number of cells observed as undergoing mitosis per 1,000 cells counted.

Each sample was examined in triplicate, the values for mitotic cells averaged, and the mitotic index calculated using the formula (Kruse & Patterson, 1973).

$$\frac{\text{Number of Mitotic Cells}}{\text{Total Number of Cells Counted}} \times 100$$

| Squid Sex/Dorsal Mantle Length Tissue/Sampling Date | Count One | Count Two | Count Three | Average | Mitotic Index |
|--|--------------|--------------|----------------|---------|------------------|
| 1. M/230 mm DML RPL/Sept. 19, 1979 | 40 | 43 | 41 | 41.3 | 4.1 |
| 2. M/242 mm DML RPL/Sept. 19, 1979 | 44 | 40 | 39 | 41.0 | 4.1 |
| 3. F/252 mm DML RPL/Oct. 1, 1979 | 37 | 38 | 42 | 39.0 | 3.9 |
| 4. F/260 mm DML RPL/Oct. 25, 1979 | 37 | 38 | 37 | 37.3 | 3.7 |
| 5. F/250 mm DML RPL/Nov. 5, 1979 | 43 | 33 | 42 | 39.3 | 3.9 |
| 6. F/257 mm DML RPL/Dec. 5, 1979 | 30 | 31 | 27 | 29.3 | 2.9 |
| 6a. F/257 mm DML RSP/Dec. 5, 1979 | 27 | 33 | 23 | 27.6 | 2.8 |
| 6b. F/257 mm DML RIPL/Dec. 5, 1979 | 42 | 41 | 39 | 40.6 | 4.1 |
| 6c. F/257 mm DML RSPL/Dec. 5, 1979 | 26 | 31 | 34 | 30.3 | 3.0 |

in the inferior preganglionic lobe, and (3) of sufficient magnitude to suggest the existence of a renewing population of white body cells.

4. Radioisotope Labeling Studies of the White Bodies

Blank control slides in addition to the labeled blood smears and labeled prepared slides of white body tissue were incubated at 4°C under dark conditions. Duplicate samples of each smear and tissue preparation were then developed following 1, 3, or 6-week incubation intervals. Table 14 provides a summary of the results obtained for each autoradiograph.

Subsequent to the one week period of incubation, a substantial level (designated in autoradiographic terminology as a "pool") of tritiated thymidine was observed within arterial and venous blood smears made 30 minutes after the injection of the radioactive material. This quantity of label was not present within blood smears made 1-72 hours after injection.

Subsequent to the 3-week and 6-week intervals of incubation, a substantial level of radioisotope was also observed within arterial and venous blood smears made 30 minutes after injection. However, following both these latter mentioned incubation periods, reduced levels of label were likewise visible within blood smears made one hour after the squid's exposure to tritiated thymidine.

Table 14. The incidence of tritiated thymidine within the blood and selected tissues of I. illecebrosus subsequent to varying intervals of (1) exposure time to the radioisotope and (2) incubation time to reveal the latter's presence.

BG Background; sparsely occurring evidence of label
 P Pool; densely occurring evidence of label
 RL Reduced Levels of Label

| Squid Specimens | One Week Incubation | | | | Exposure Time to Tritiated Thymidine |
|-----------------|---------------------------------|--------------------|---------------------------|--------------------------|--------------------------------------|
| | Levels of Observed Radioisotope | | | | |
| | Cephalic Aorta | Anterior Vena Cava | Right Postganglionic Lobe | Left Postganglionic Lobe | |
| 1 | P | P | BG | BG | 30 minutes |
| 2 | P | P | BG | BG | |
| 3 | BG | BG | BG | BG | 1 hour |
| 4 | BG | BG | BG | BG | |
| 5 | BG | BG | BG | BG | 3 hours |
| 6 | BG | BG | BG | BG | |
| 7 | BG | BG | BG | BG | 5 hours |
| 8 | BG | BG | BG | BG | |
| 9 | BG | BG | BG | BG | 10 hours |
| *10 | | | | | |
| 11 | BG | BG | BG | BG | 24 hours |
| 12 | BG | BG | BG | BG | |
| 13 | BG | BG | BG | BG | 48 hours |
| *14 | | | | | |
| 15 | BG | BG | BG | BG | 72 hours |
| 16 | BG | BG | BG | BG | |

Table 14 (cont'd.)

| Squid Specimens | Three and Six Weeks Incubation | | | | Exposure Time to Tritiated Thymidine |
|-----------------|--------------------------------|---------------------------------|---------------------------|--------------------------|--------------------------------------|
| | Cephalic Aorta | Levels of Observed Radioisotope | | | |
| | | Anterior Vena Cava | Right Postganglionic Lobe | Left Postganglionic Lobe | |
| 1 | P | P | BG | BG | 30 minutes |
| 2 | P | P | BG | BG | |
| 3 | RL | RL | BG | BG | 1 hour |
| 4 | RL | RL | BG | BG | |
| 5 | BG | BG | BG | BG | 3 hours |
| 6 | BG | BG | BG | BG | |
| 7 | BG | BG | BG | BG | 5 hours |
| 8 | BG | BG | BG | BG | |
| 9 | BG | BG | BG | BG | 10 hours |
| *10 | | | | | |
| 11 | BG | BG | BG | BG | 24 hours |
| 12 | BG | BG | BG | BG | |
| 13 | BG | BG | BG | BG | 48 hours |
| *14 | | | | | |
| 15 | BG | BG | BG | BG | 72 hours |
| 16 | BG | BG | BG | BG | |

*Animal expired during exposure to tritiated thymidine.

The tritiated thymidine present within the above smears occurred extracellularly; that is, free within the fluid portion of the blood. At no time was the label concentrated over the nuclei of the circulating hemocytes. Furthermore, incorporation of the radioisotope into the nuclei of dividing white body cells was never demonstrated despite the length of exposure time and/or incubation time.

Blank control slides which were coated with photographic emulsion and then exposed to daylight became opaque during autoradiographic processing while those blank slides which were treated identically to the labeled slides remained transparent.

GENERAL DISCUSSION AND CONCLUSIONS

It has long been contended by researchers that the white bodies (a pair of multilobate organs, one surrounding the optic ganglion on the back of each eye of cephalopod molluscs) are the site of hemocyte production. The evidence cited by earlier workers in support of this conclusion has been primarily morphological in nature.

The present study endeavors to (1) advance the understanding of white body morphology through detailed observations of the gross and microscopic anatomy of these organs, and (2) provide, for the first time, experimental data to substantiate the premise that white bodies produce the circulating blood cells.

A brief reference to the white bodies' location and configuration (similar to that described immediately above) frequently serves as introduction to the majority of papers that deal with the functional morphology of these structures. The present study extends these previous descriptions not only by offering a more precise definition of the location and configuration of the white bodies but also by providing new descriptions of their general appearance, shape, dimensions, and the interrelationships of the several components and their relationship with the optic sinus. Furthermore, precise nomenclatorial terms are assigned to each of these white body components.

Within I. illecebrosus, the white body of the right eye is a mirror image to that of the left eye. This strictly visual interpretation is substantiated by statistical analysis. Through the use of a paired-sample t-test, the values representing the mean width and length of each component of at least 171 right white bodies were compared with corresponding values for an equal number of left white bodies. Each pair of measurements (width of the right postganglionic lobe/width of the left postganglionic lobe; length of the right postganglionic lobe/length of the left postganglionic lobe) were collected from the same specimen. In each instance, the results indicate there is no significant difference between the means at the 0.01 level.

Each white body is attached to the external medial surface of the adjacent eye via connective tissue that is present along the outer rim of the several lobes that compose the organ. It is only upon the excision of an eye that an entire white body is visible. The various components of each white body are named with respect to their spatial relationship with the adjacent optic ganglion. Hence, there is represented a postganglionic lobe, an inferior preganglionic lobe, and a superior preganglionic lobe. Connecting the postganglionic and inferior preganglionic lobes is a narrow band of tissue designated the subganglionic process.

While every lobe and subganglionic process consists of soft tissue that may appear translucent or white in

color, there are observable differences in the external form assumed by the various components. The most distinctive of the three lobes is the postganglionic lobe. This tear-shaped component of the white body exhibits both the largest dimensions (approximately 1.4 cm in greatest length, 0.8 cm in greatest width) and the unique external features referred to earlier. Whereas the subganglionic process and the inferior and superior preganglionic lobes display uniformly smooth exterior surfaces (when viewed macroscopically), the postganglionic lobe displays irregularities. These irregularities occur in three forms: a network of blood vessels that extend over the orbital surface of the postganglionic lobe, shallow notches that appear along the free margin of the postganglionic lobe, and deep furrows which occur where the postganglionic lobe attaches to the medial surface of the eye. The former two irregularities are noted consistently during studies of the postganglionic lobe, however the deep furrows have not been observed in all instances. It is here suggested that this external appearance might be related to the dimensions of the lobe. The fact that the postganglionic lobe is the largest component of a white body may necessitate the organization of its tissue into what appears to be the beginnings of lobules. Furthermore, such a structure would require an increased supply of blood which might explain the surface vasculature described previously. A fuller discussion of this last point is presented during a

consideration of the blood vessels that irrigate the white bodies.

The free terminus of each postganglionic lobe aligns with the vertical stripe of the eye's lateral surface; an observation which might prove beneficial in future experimental work requiring the location of this lobe by external "landmarks" or coordinates. The remaining portion of the postganglionic lobe curves around the adjacent optic ganglion and faces posteriorly. The subganglionic process (approximately 2.0 cm in greatest length, 0.25 cm in greatest width) originates from the ventral portion of this lobe and continues dorsoanteriorly to contact the optic (under) surface of the inferior preganglionic lobe. Equidistant from each of these two lobes, the serpentine configuration of the process is disrupted. That portion proceeding from the postganglionic lobe (the serpentine portion) ends within the angulation exhibited by that portion of the process which contacts the inferior preganglionic lobe. The unusual appearance of the subganglionic process raises questions that can not be answered within the scope of this thesis; questions regarding the embryological development of the white bodies. However, based upon the detailed observations of 358 such structures (required for the morphometric analysis), this author speculates that the two portions of the subganglionic process originate as separate entities which, over time, grow toward each other. If such were the case, the

serpentine portion might grow dorsoanteriorly while the straight portion grows ventroposteriorly to meet the former. At their juncture, the straight portion might bifurcate, each branch extending to either side of the serpentine portion thereby forming the angulation that typifies this portion of the process within the squid studied to date. This purely hypothetical account awaits proper embryological consideration. The reniform-shaped inferior preganglionic lobe is the intermediate lobe of the white body with regard to its dimensions (approximately 1.0 cm in greatest length, 0.5 cm in greatest width) and position. Closely associated with its dorsal edge is the superior preganglionic lobe. The latter is the last and smallest (approximately 0.6 cm in greatest length, 0.3 cm in greatest width) of the white body lobes. The superior preganglionic lobe is ovoid in shape and its dorsal edge lies within a short distance (0.1-0.3 cm) of the postganglionic lobe's free terminus.

Thus, the white body of each eye comprises an incomplete ring predominated by three lobes. Speculation as to why a proposed organ of hemocytogenesis would be located on the back of a squid's eye and the advantage and/or purpose of its multilobate configuration awaits a discussion of the vascular studies to follow.

The association between selected measurements of the white bodies and a squid's dorsal mantle length was investigated. Values representing the greatest width or length of each component from 179 specimens of I. illecebrosus

were plotted against values for the dorsal mantle length of the squid from which the white body was collected. In all cases, with the exception of the length of the subganglionic process (right and left components), the correlation coefficient is greater than the critical value at the 0.01 level of significance. These results provide evidence in favor of a positive correlation between said measurements of the white bodies and dorsal mantle length. With respect to the lengths of the right and left subganglionic processes, the correlation coefficient (in both cases) is less than the critical value at the 0.01 level of significance. These are the only instances in which the evidence indicates a correlation that is not significantly different from zero.* An assessment of the descriptive statistics (Appendix 1) that pertain to variables of the morphometric study reveals that (1) values of 2.003 cm (mean) and 2.000 cm (mode) are recorded for the length of the right subganglionic process, and (2) values of 2.004 cm (mean) and 2.000 cm (mode) are recorded for the length of the left subganglionic process. It is here suggested that the constancy of the above values is responsible for this absence of correlation between the length of a subganglionic process and dorsal mantle length. Furthermore, the existence of such conformity in measurement would seem to imply that the subganglionic process attains its presently recorded length prior to the remaining components of a white body attaining theirs, or, as has been suggested, this process merely "closes the circle" that is formed through lobular development.

*See p. 276A

In addition to sorting morphometric data on the white body and white body portions against mantle length, the 179 specimens of I. illecebrosus were separated with respect to sex (41 males and 138 females). Reference to the scattergrams presented in Figures 14A through 29A, will indicate that in females there is a positive correlation (0.01 level of significance) between the width of each component of the organ and DML, as was the case when the data are tested without separation by sex. The same level of significant correlation holds with respect to (a) the width of each component (except in the case of the right superior preganglionic lobe) and DML for male specimens, (b) the length of each component (except the subganglionic process) and DML for males and females, and, in this latter case, the length, the superior preganglionic lobe for DML in males.

A similar association is present between selected measurements of the white bodies and a squid's weight. For this investigation, those values representing the greatest width or length of each component from 179 specimens of I. illecebrosus were plotted against values for the weight of the squid from which the white body was collected. As was characteristic of the previous study, the lengths of the right and left subganglionic processes are the only cases in which the evidence indicates a correlation that is not significantly different from zero. In both instances, the correlation coefficient is less than the critical value at the 0.01 level. It would appear that the conformity between the mode and mean values for the length of a subganglionic process is again responsible for the results obtained during this investigation. Correlation coefficients recorded for the remaining measurements of the white bodies are greater than the critical value at the 0.01 level of significance; providing evidence in favor of a positive correlation between the latter and a squid's weight.*

When values representing the mean width or length of each component are compared to the sex of the squid from which the white body was collected, it is noted that the white body is smaller in male squid than it is in female squid (at the 0.01 level). This is an indication of a sexual dimorphism that is not readily apparent with regard to other

*see p. 277A

As was the case with DML and length and width of squid white bodies, the weight of males (41) and females (138) were sorted separately. Scattergrams presented in Figures 30A through 45A here refer. Positive correlations (0.01 level of significance) between squid weight and (a) width of each component of the white body in females, (b) the width of each component, except the right superior preganglionic lobe (males), (c) the length of each component, except the subganglionic process (females) and (d) the length of each component except the subganglionic process and the right superior preganglionic lobe (males) are computed.

It is interesting to note that when variations or deviations from conformity appear here or in the case of DML and morphometry of the white body, it appears most frequently in the case of males, and specifically in the size of the superior preganglionic lobe. Future work should be directed to elucidate the sequential developments of the white body, with particular reference to its ontogeny in males as opposed to females.

variables tested during this study.

Lastly, values for the total length of each white body (calculated by summing the individual lengths of its components) were plotted against values for the dorsal mantle length or weight of the squid from which the white body was collected. In all cases, the correlation coefficient is greater than the critical value at the 0.01 level of significance; thereby providing evidence in favor of a positive correlation between the total length of a white body and the dorsal mantle length or weight of the squid from which it was obtained. This holds true between sexes.

The microscopic anatomy of the white bodies within I. illecebrosus is similar to that described for other species of cephalopod molluscs. Each component of a white body is surrounded by a capsule that conforms to every surface contour; including the marginal notches and deep furrows of the postganglionic lobe. This capsule is composed of an amorphous matrix in which are embedded fibroblastoid cells and fibers. Noel and Jullien (1933; S. officinalis, L. vulgaris, O. vulgaris, E. muschata), Cazal and Bogoraze (1943; O. vulgaris) and Bolognari (1950; L. vulgaris, I. coindetii, O. sagittatus, S. officinalis, H. dispar, S. rondoletii) stated that the capsular material stained for collagen. Cowden and Curtis (1974; O. briareus) reported that the collagen fibers displayed a periodic pattern characteristic of collagen, at the ultrastructural level. With respect to morphology and general arrangement,

the capsular fibers of the white body within I. illecebrosus (as viewed by means of light and electron microscopy) appear collagen-like, however they do not exhibit any visible periodicity.

Occasionally, a portion of the capsule will extend into the underlying tissue of a white body. These extensions, or trabeculae, are closely associated with segments of the white body's internal fibrous network. Contact between the two may be direct, in which case the internal fibers envelop a trabecula, or indirect, whereby additional fibers of the internal network join with those that surrounded the trabecula. Noel and Jullien (1933), Cazal and Bogoraze (1943), Bolognari (1950), and Cowden (1972) have recorded similar observations. With regard to the cephalopods studied, it would appear that this internal fibrous network and the outer capsule constitute a unified supportive structure or framework for the white body. Further consideration of the internal fibers is presented within subsequent sections of the discussion.

Although the capsule usually occurs as a continuous layer, there are occasional interruptions in the form of orifices, here named "hemooscula". Their presence and microscopic anatomy are noted for the first time in the literature. These hemooscula penetrate the capsule of each white body on both dorsal and ventral surfaces. Furthermore, they exhibit a highly structured appearance and may occur singly or in groupings of up to ten. It is suggested that

the hemooscula permit direct communication between the sub-capsular sinuli and blood vessels of a white body and the optic sinus which envelops that white body.

The existence of an internal stroma has been noted within the white body since the anatomical studies of the 1800's. Kollmann (1908) described this stroma as being "de nature cellulaire". The long, slender structures that connected the cells were interpreted as their anastomosed, cytoplasmic extensions. His sketch, Planche (Plate) 1 - Figure 79, depicting the internal organization of a white body from S. officinalis, shows stromal cells which are fibroblastoid in appearance. The remaining authors (some of whom preceded Kollmann) characterized this stroma as a "fibrous" supportive network. Indeed, the evidence collected to date supports this view. The earlier workers, such as Hensen (1865), Faussek (1893; Loligo sp., Octopus sp., and Sepia sp.), and Cuénot (1897; E. aldrovandi, S. officinalis) described the presence of a "trame conjonctive réticulée" or "réticulum filamenteux". Subsequent workers have extended this description through an elucidation of the morphology and composition of the stromal elements (Noel & Jullien, 1933; Casal & Bogoraze, 1943; Bolognari, 1950; and Cowden, 1972, O. vulgaris). These authors recognized that the internal network was comprised of two portions; slender fibers and dense "tracts". The former were observed to course through the interior of a white body and, where required, provide support for the

small blood vessels of the white body's vasculature. With the aid of histological stains, the above authors demonstrated that the composition of these slender fibers was "précollagène". The dense tracts of fibers were observed in association with the large vascular channels and the trabeculae. Their composition has been described as "collagène". Thus, the fibrous nature of this internal framework of the white body has been established. Many fibers ramify throughout the interior of the white bodies within I. illecebrosus. Collectively, they too represent a network that provides support for the surrounding tissue and vasculature. With the aid of light and scanning electron microscopy, these fibers are shown to be long, filamentous structures of varying diameters. Ultra-structurally, they are composed of finer subunits or fibrils. Where the fibers are concentrated, there is evidence of periodicity. Although this banding pattern is not identical to that of collagen fibers, the similarities in fibrillar organization strongly suggest a close relation to the latter.

Associated with this internal supportive network are fibroblastoid cells. These cells are stellate in shape; their long cytoplasmic extensions closely aligned with the fibrous network. Generally, the nuclei within such cells are ovoid, however they may also appear triangular in shape due to the encroachment of the surrounding tissue of the white body. The previous description is similar to that

recorded for other species of cephalopods by Faussek (1893), Noel and Jullien (1933), Cazal and Bogoraze (1943), and Bolognari (1950).

Between the external capsule of the white body and the internal network of supportive fibers, there exists a population of densely packed cells. Historically, it is these cells which have been implicated in the process known as hemocytogenesis. Numerous devices have been employed to segregate these cells of the white body into categories representing a developmental series. Features such as cellular diameter, nuclear diameter, nuclear morphology and/or cytoplasmic inclusions have served as references for their identification at one time or another by the various researchers. With the possible exception of nuclear morphology, these cellular features constitute rather tenuous criteria. For example, both nuclear and cellular dimensions are difficult to ascertain in tissue preparations for light and/or electron microscopy due to the particular plane of section viewed. Similarly, cytoplasmic inclusions are not a reliable characteristic due to the changing metabolism of a cell. Hence, such inclusions may or may not be present at the time of observation. Ideally, the functional properties of a cell should represent the definitive means of analysis, however such information is not available for species of the invertebrate phyla. In lieu of this last criterion, nuclear morphology appears to be the most practical indicator by which to judge developmental

stages. Often, a noticeable lack of consensus is expressed in the selection of terms to describe these different stages. This tends to create confusion, thereby rendering comparisons among the cephalopod species rather difficult. However, there is one extremely positive factor. With few exceptions, similar techniques (refer to Table 1) were used to prepare these individual white bodies for subsequent observation.

Cuénot (1897) characterized these cells of the white body as being small, numerous, and identical in appearance to the "amibocytes jeunes". He further stated that such cells multiplied very actively by mitosis; a feature which was also noted by Faussek (1893). Kollmann (1908) proposed the name "cellules lymphoïdes granuleuses" and emphasized the absence of hyaline cells (those devoid of granulations) within the white body. According to Noel and Jullien (1933), Kollmann published again in 1924, this time offering a more detailed account of the cells. Three different morphological types were indicated: (1) cells possessing large vesicular nuclei and strongly basophilic cytoplasm, (2) cells exhibiting smaller, denser nuclei and a cytoplasm which was no longer basophilic; granular inclusions were observed in the cytoplasm, and (3) "leucocytes" with polymorphic nuclei and an abundance of cytoplasmic granulations. Cells of the first category were confined to "centres germinatifs" and their appearance was described as a protoplasmic mass. Furthermore, it was recorded that mitotic

figures were characteristic of these areas within the tissue samples obtained from juvenile specimens. The latter two cell types were present within adjacent areas of the white body. Mitotic figures were said to be characteristic of these latter areas should the tissue samples be obtained from adult animals.

Noel and Jullien (1933) noted the occurrence of "îlots foncés" or dark islands throughout the interior of a white body. The elements comprising these islands were segregated into two groups: (1) large, actively dividing cells termed "leucoblastes" which possessed large nuclei (with 1 or 2 nucleoli) and weakly basophilic cytoplasm, and (2) much smaller cells which progressively acquired polymorphic nuclei and cytoplasmic, eosinophilic granulations. They stated that such islands were reminiscent of germinal centers. In addition, a developmental series was described in which "leucoblastes", through cellular divisions, gave rise to those cells which eventually became the "eosinophiles". Mitotic figures were never detected within groupings of the latter.

Cazal and Bogoraze (1943) recorded similar observations, however they defined the cellular aggregations as being "îlots globuligènes" (leucopoietic islands). More importantly, these authors recognized a type of cell within the white body of O. vulgaris that had not been previously described for this tissue; the "néphrocyte". The cells assigned to this latter group and the "leucoblastes" were

said to compose the structural elements of these islands. The "leucoblastes" exhibited a strongly basophilic cytoplasm and round, oval, or slightly elongated nuclei, measuring 5-7 μm in diameter. Two or three nucleoli were usually present within such nuclei. These "leucoblastes" were frequently observed in the process of mitosis. "Néphrocytes" were described as large cells with large (6-10 μm), vesicular nuclei. A single nucleolus was typical of these nuclei. Occasionally, granular inclusions were observed within the basophilic cytoplasm. Such inclusions measured 3 μm in diameter and varied greatly in number. Particles of carmine were also noted within the cytoplasm following intravascular injections of this vital stain. The information prompted Cazal and Bogoraze (1943) to conclude that the cells were "néphrocytes d'accumulation" and that the white bodies within O. vulgaris were responsible for a "fonction néphrocytaire" in addition to their primary role of "leucopoiesis". The authors completed this discussion by stating that transitional forms had been noted between the "leucoblaste" and the "néphrocyte". Furthermore, they indicated that both cell types may exhibit similar morphological characteristics and that the differences between the two were of degree, only.

Bolognari (1951) also acknowledged that the white bodies within O. vulgaris were actively involved in this secondary function. His descriptions of the "tessuto globuligeno" (leucopoietic tissue) and the four stages of

development from "leucoblasti" to "leucociti maturi" were presented in detail within the Introduction, as were those descriptions of Cowden (1972) and Cowden and Curtis (1974, 1981).

With minor exceptions, the population of densely packed cells between the external capsule of the white body and the internal network of supportive fibers is similar within the cephalopods studied. This similarity is reflected not only in the morphology of the individual cells but also in their anatomical arrangement within the white body (see Table 1, pp. 9 - 12).

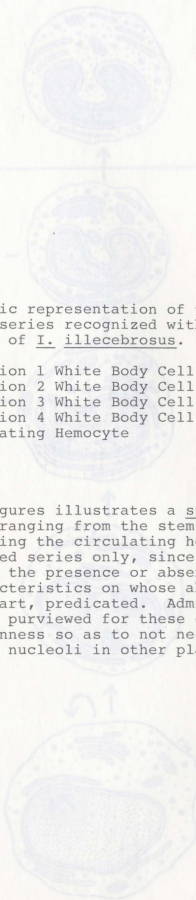
The results obtained in present study from the white body of I. illecebrosus are comparable. Employing nuclear appearance as the criterion for assessing the developmental series, this author described four variations of white body cells (Table 9; Figures 63, 64, 76, and summary Figure 91). Variation 1 cells possess nuclei in which the chromatin is equally distributed. The nuclei are lightly stained in histological sections and nucleoli are usually visible. These cells and their nuclei appear to exhibit the largest diameters of the cellular variations. Variation 1 cells compare morphologically and spatially with: (1) those cells confined to the "centres germinatifs" (Kollmann, 1924), (2) the "leucoblastes" of the dark islands (Noel & Jullien, 1933), (3) the "leucoblasti" (Bolognari, 1950), and (4) the "hemocytoblasts" (Cowden & Curtis, 1974, 1981).

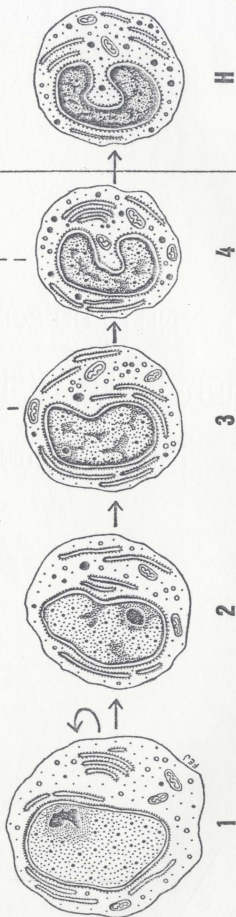
WHITE BODY TISSUE BLOOD

Figure 91. Diagrammatic representation of the hemocytogenic series recognized within the white body of I. illecebrosus. 2,500 x

- 1 Variation 1 White Body Cell
- 2 Variation 2 White Body Cell
- 3 Variation 3 White Body Cell
- 4 Variation 4 White Body Cell
- H Circulating Hemocyte

This series of figures illustrates a suggested developmental series, ranging from the stem cell (Variation 1), through and including the circulating hemocyte. It is presented as a suggested series only, since serial sections were not made to prove the presence or absence of a nucleolus, one of the chief characteristics on whose absence the developmental series is, in part, predicated. Admittedly, the sections (600 - 900 A) purviewed for these cellular variations were of sufficient thinness so as to not necessarily demonstrate the presence of nucleoli in other planes.



WHITE BODY TISSUE
BLOOD

Adjacent to these cells are the Variation 2 white body cells. Their nuclei display marginated chromatin. Increased concentrations of chromatin are also evident within the central regions of the nucleus. These nuclei are moderately stained in histological preparations and nucleoli are still visible. Variation 2 cells compare morphologically and spatially with: (1) those cells adjacent to the "centres germinatifs", cells with smaller, denser nuclei (Kollmann, 1924), (2) category two cells, cells that become "eosinophils" (Noel & Jullien, 1933), (3) first stage "proleucociti" (Bolognari, 1950), and (4) "primary leukoblasts" (Cowden & Curtis, 1974, 1981).

Variation 3 cells exhibit nuclei in which a uniform band of chromatin is concentrated along the nuclear periphery. Concentrations of chromatin within the central regions of these nuclei stain more intensely and nucleoli are becoming less prominent. Such nuclei are also moderately stained by histological techniques. Variation 3 cells compare morphologically and spatially with: (1) the cells adjacent to the "centres germinatifs" (Kollmann, 1924), (2) category 2 cells (Noel & Jullien, 1933), (3) the "leucoblastes" (Cazal & Bogoraze, 1943), (4) second stage "proleucociti" (Bolognari, 1950), and (5) "secondary leukoblasts" (Cowden & Curtis, 1974, 1981).

Fringing this group of cells is the fourth variation of white body cell. The nuclei within these cells display an advanced stage of chromatin concentration. Such nuclei

stain darkly in histological preparations and the nucleoli are no longer visible. Variation 4 cells compared morphologically and spatially with: (1) the small, numerous cells that are identical to "amibocytes jeunes" (Cuénot, 1897), (2) the "leucocytes" (Kollmann, 1924), (3) category 2 cells (Noel & Jullien, 1933), (4) the third stage "proleucociti" (Bolognari, 1950), and (5) "proleukocytes" (Cowden & Curtis, 1974, 1981).

Cells representing each of the four variations within the white body of I. illecebrosus tend to cluster together, so that within any one grouping there is present those cells whose nuclei exhibit similar concentrations of nuclear material. This arrangement is repeated not only within a given field of view but also throughout each lobe and subganglionic process. Spatial relationships such as these have been described for cells within the white bodies of other cephalopods. Hence, one encounters the terms "centres germinatifs", "flots foncés", and "flots globuligène".

This anatomical view of the white bodies is enhanced by mitotic figures which define, through their presence, the central regions of the germinative centers. Within I. illecebrosus, these mitoses are observed among groupings of the second and/or third cellular variations. Other researchers, with the exception of Kollmann (1924), have reported similar findings. Kollmann (1924) contended that cells within the latter stages of development were capable

of mitosis. The majority of these mitotic figures, within the white body of I. illecebrosus, are concentrated within the central portion of each lobe and subganglionic process.

Blood vessels, sinuli, and hemal spaces characterize the vasculature of the white bodies from I. illecebrosus. A more detailed account of these structures is presented within subsequent sections of the Discussion, however it should be noted that their presence, general distribution, and morphology are similar to that described by previous authors for a variety of cephalopod species. The term "sinuli" (singular sinulus) rather than "sinuses" has been employed by this author to clarify the distinction between the relatively small dilated portions of the venous channels within a white body and the relatively large venous cavities (known as the optic sinuses) which envelop each white body.

Blood cells are frequently observed within the lumens of these vessels and sinuli. A comparison between these two populations of cells reveals that they are morphologically similar (refer to Table 3 for a detailed description). Furthermore, when both of these groups of cells are compared with the cellular variations of the white body, it is noted that the majority of hemocytes resemble Variation 4 cells. Occasionally, however, hemocytes resembling Variation 3 cells are observed within the blood. Thus, within I. illecebrosus, there does not appear to be a maturation sequence within the sinuli, as proposed for other cephalopods.

Rather, mature cells are presumably released into the bloodstream and circulated throughout the system, as a whole. The circulation of hemocytes resembling Variation 3 white body cells might result if immature forms required vascular exposure in order to develop more fully. Alternately, such forms may be released prematurely in situations of stress. The information presented within Appendix 4 demonstrates that Variation 3 and Variation 4 cells occur with equal frequency within the white body. This would suggest that both forms are "primed" for release, regardless of the stimuli prompting such action.

The white bodies within I. illecebrosus are well vascularized. Histologically prepared sections of the tissue and/or Latex injected white body specimens reveal that branches from the two major cephalic arteries service each component of the two white bodies. These major branches and their finer extensions which were observed to ramify throughout the interior of the left or right white body tissues exhibit bilateral symmetry. That is to say, the blood vasculature of the right white body is a mirror image to that of the left white body.

The arteries received by the subganglionic process, the inferior preganglionic lobe or the superior preganglionic lobe enter upon contact (with either of these components of the white body) and branch therein to produce the finer arteries and arterioles. Figures 12, 81, 82, and 85 demonstrate that the vascular pattern of the

postganglionic lobe is somewhat different. Arteries contacting the postganglionic lobe do not enter the tissue immediately. Rather, these arteries (the inferior postganglionic arteries and branches of the superior postganglionic artery) spread over the postganglionic lobe, creating a distinctive pattern or network of surface vessels in the process. At various points over the lobe's surface, these arteries like those of the other components of a white body enter the underlying tissue. This vascular pattern which is unique to the postganglionic lobe of each white body may have evolved to accommodate the large dimensions exhibited by the lobe. It would appear that the remaining lobes and the subganglionic process (while relatively long, 2.0 cm, is quite narrow, 0.25 cm) receive an adequate supply of blood by the vasculature described previously. The postganglionic lobe, however, is sufficiently large as to require two sources of blood; one from the surface as well as one from the interior. This apparent requirement for additional blood, on the part of the postganglionic lobe, is also reflected in the organization of the vascular network in general. As the cephalic aorta approaches the cephalic region of the squid, it bifurcates to form the intracranial arteries. Blood transported along either the right or left intracranial artery will reach a postganglionic lobe. That blood, in fact, is carried by both arteries ensures the left and right postganglionic lobes a supply of blood from the two intracranial arteries.

This is in direct contrast to the vascular pattern of the superior and inferior preganglionic lobes which receive blood through only one of the intracranial arteries. Usually it is the left intracranial artery which proceeds anteriorly as the brachial trunk artery. It is from this latter vessel that branches arise which supply blood to both the superior and inferior preganglionic lobes of the right white body and the superior and inferior preganglionic lobes of the left white body.

All components of a white body display numerous vessels, sinuli, and hemal spaces within their tissue. The presence and general distribution of these vascular channels is similar to that noted for other cephalopods. With the aid of electron microscopy, however, it was possible to ascertain that structural differences exist between blood vessels and sinuli within the white bodies of I. illecebrosus. The former (the blood vessels) are lined with a discontinuous layer of endothelial cells. Next, in sequential order, is a basement membrane, a complete (uninterrupted) layer of pericytes, and, finally, a layer of fibrous material. Although the walls of the sinuli are comprised of the same four layers, the outer two layers differ slightly. Specifically, the walls of the sinuli possess an incomplete layer of pericytes and an outer layer of fibrous material that joins with the basement membrane at periodic intervals. This arrangement gives the appearance that the pericytes are within one fibrous supportive layer. As

previously stated, a discontinuous layer of endothelium characterizes the inner lining of both the blood vessels and the sinuli. Morphologically, this presents an ideal route by which newly formed hemocytes might gain access to the circulation. Indeed, Noel and Jullien (1933), Cazal and Bogoraze (1943), and Bolognari (1950) have implicated diapedesis as the method employed by hemocytes during such instances of transition. Upon the examination of histologically prepared sections (standard light microscopy techniques) of a white body from the cuttlefish Sepia officinalis, Noel and Jullien (1933) recorded an event similar to the one mentioned above. They observed cells in the process of migrating across the discontinuous endothelial walls that lined blood vessels within the tissue of the white body. These cells were described as products of the white body, the "leucocytes á granulations acidophiles", which enter the general circulation to become the only cellular component therein. Cazal and Bogoraze (1943) noted the same phenomenon within similarly prepared tissue sections from the white body of Octopus vulgaris. Bolognari (1950) studied the white bodies from the following cephalopods: Loligo vulgaris, Illex coindeti, Ommastrephes sagittatus, Sepia officinalis, Heteroteuthis dispar, and Sepiola rondoletii. His remarks were stated in quite general terms in that no specific references were made to any of the above species. Rather, a single description was offered for the entire group. In this description the

decapod white body was characterized as "globuligeno" (leukopoietic) and its cellular products were said to move into sinuses where the process of maturation was completed. While diapedesis was never observed within a white body of I. illecebrosus, its occurrence would seem feasible in light of the morphological descriptions of this tissue. Furthermore, diapedesis has been noted within white bodies from a number of other cephalopod species; white bodies that share structural (tissue and vascular) similarities with the white bodies of I. illecebrosus.

Hemal spaces, the intercellular areas filled with blood, lend support to the view that the white bodies within I. illecebrosus are well vascularized. These spaces are a typical component of a white body's morphology and are seen to best advantage within electron micrographs. Often, the latter reveal the presence of hemocyanin (the respiratory pigment) within the blood that occupies the spaces. In such instances, a reliable "marker" is established for verifying the presence of blood within the tissues of a white body. As noted in a previous description, the hemal spaces are merely those areas between cells. Unlike the blood vessels or sinuli, they do not exhibit a structured appearance. It is only at the most infrequent of times that a portion of the internal fibrous network will contact a hemal space and thus provide, for it, a supportive boundary.

Blood flows to a white body by way of the anterior and posterior ophthalmic arteries; passes through its tissue via small vessels, sinuli, and hemal spaces; and eventually leaves the tissue to enter the enveloping optic sinus by way of the hemooscula. Such a route is described and illustrated, here, for the first time, from observations of the vasculature of the white bodies from the Newfoundland bait squid, I. illecebrosus. Figures 85 and 86 provide a visual summation of the major arteries to each component of a white body. As is indicated, the right anterior ophthalmic artery supplies blood to both the right superior and inferior preganglionic lobes, while the right posterior ophthalmic artery supplies the right postganglionic lobe and the right subganglionic process. The converse is true of the left anterior and posterior ophthalmic arteries. Originating from these major vessels are the finer arteries and arterioles; both of which are seen to ramify throughout the translucent tissue of the various components of a white body. (The latter observations were made possible by Latex injection techniques.) These finer vessels of the arterial blood supply are frequently noted within histologically prepared sections of tissue from a lobe or subganglionic process. A discussion of their distributional and ultrastructural features has been presented prior to this section. Capillaries, however, are not observed presumably due to the fragile construction of their walls. The most prominent of the vascular features, the sinuli, are actually

the dilated portions of a white body's venous system. It is suggested that the blood passes from these sinuli to the exterior and, therefore, the optic sinus, via a direct route (through the hemooscula) or an indirect route (through additional venous vessels, veins, which would eventually communicate with an optic sinus through hemooscula).

Similar views have been propounded by Casal and Bogoraze (1943) and Young (1971) although the specific means by which this communication is accomplished were never mentioned.

The former authors employed vascular injections of Prussian blue (the actual site of injection was not indicated) during their study of the white bodies from O. vulgaris. This technique revealed the presence of arterioles which, subsequently, were observed to decrease in diameter as they ramified throughout the tissue of the white bodies. It was noted that the finest of these vessels met and joined with sinuses and that the sinuses communicated with the "lacunes orbitaires" or optic sinuses that surrounded the white bodies. Young (1971) commented upon the vasculature of the white bodies during his anatomical study of the nervous system within O. vulgaris. In this instance, arterial (cephalic aorta) injections of India ink were used to elucidate the vascular network. His findings, in the form of descriptions and photographs, suggested that direct communication between veins and the orbital (optic) sinus occurred at the surface of the white bodies. Although Bolognari (1950) did not employ such procedures (his

observations were based upon histologically prepared sections of tissue in which blood vessels had not been previously injected) he apparently agreed that blood passed directly from the white bodies to the enveloping sinuses for he stated (p. 372, English translation): "Since the capsule is uninterrupted, leukocytes must pass through in order to go into the lacunae".

Situated within the cephalic region of I. illecebrosus are the paired optic sinuses. Each sinus is closely associated with the medial surface of the adjacent eye and, as a result, bathes an entire white body. That both structures represent true venous cavities was well documented by Bradbury (1970). She cited three characteristics in defense of this view: (1) venous blood enters both optic sinuses by way of veins from nearby organs or tissues, (2) both sinuses drain into veins, and (3) both sinuses exhibit an endothelial lining. With the aid of the radiopaque contrast agent, RENOgrafin-60, additional information was obtained with regard to the morphology and venous circulation of the optic sinuses within I. illecebrosus.

The photograph series (Figure 87) which documents the filling of these sinuses (by RENOgrafin-60) clearly shows that both left and right optic sinuses fill sequentially by "compartments". There appears to be three such compartments per sinus. The largest visible compartment of each optic sinus is positioned "over" the postganglionic

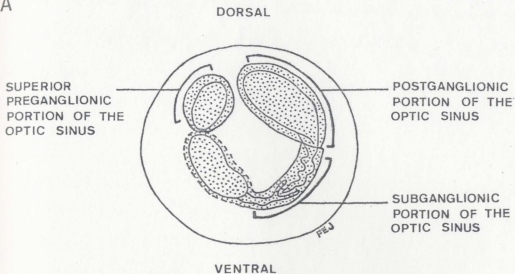
lobe of a white body. The second compartment angles medially and anteriorly; a configuration which corresponds to the subganglionic process. A third compartment lies "over" the region that is occupied by the superior preganglionic lobe (Figure 92). Although a close association appears to exist between any two adjacent compartments, certain distinctions are evident. These distinctions are represented by the non-confluent outlines that identify each compartment. The three compartments which are thought to comprise the right optic sinus are mirror images to those of the left optic sinus.

As indicated above, a remarkable similarity exists between the configuration of an optic sinus and that of the white body which it envelops. For this and other reasons to be discussed later, it is suggested that such an arrangement may be the key to understanding the mechanism by which cells produced in the white body enter the general circulation. More precisely, the similarity in configuration does not appear to be incidental. Rather, the information collected to date strongly supports the view that it (the similarity) is a logical solution adapted for the purpose of dispersing newly formed products of the white bodies. Consider that each white body is hemocytogenic (as the morphological and experimental evidence suggests). The newly formed blood cells would obviously require a means of entry to the general circulation. Each optic sinus offers such accessibility due to its connection with the branchial

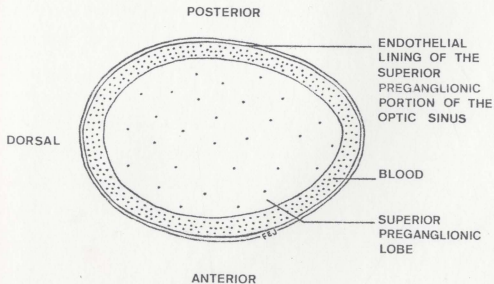
Figure 92. Diagrammatic representations of the relationship between a white body and the compartmentalized optic sinus in Illex illecebrosus.

- A. Medial view of a right eye. The dotted lines associated with the inferior preganglionic portion of the optic sinus indicate the presumed configuration of this structure. 2.5 x
- B. Enlargement of the superior preganglionic portion of the optic sinus.

A



B



circulation via the anterior vena cava. This route to the general circulation is further streamlined by the absence of veins which, if present, would connect a white body with the venous system of the cephalic region. The fact that each white body component lies within a portion of the optic sinus precludes the functional necessity of such veins, hence the existence of the hemooscula. The latter permit the direct passage of blood (and its blood cells) from the lumen of a subcapsular vein or sinus of a white body lobe to the compartment of the optic sinus in juxtaposition with that white body lobe. Thus a feasible route for the dispersal of newly formed hemocytes can be established between the site(s) of hemocyte production and the general blood circulation. Speculation as to why a proposed organ of hemocytogenesis would be present on the medial surface of a squid's eye and the advantage and/or purpose of its multilobate configuration was raised previously. Based upon the evidence presented above, it is here suggested that each white body is so positioned within the cephalic region of I. illecebrosus as to effect access to the systemic or general circulation of the animal, by the route established above, for the purpose of distributing the products of its tissues; the newly formed hemocytes. Furthermore, that full advantage of this vascular route might be attained, a multilobed configuration was adapted to or developed conjointly with the compartmentalized sinus which envelops it.

A population of cells may be characterized by the mitotic activity of its individual members. The employment of this criterion establishes three basic categories into which a given population might be classified: static cell populations, expanding cell populations, and renewing cell populations. Specific examples of each category, based upon mammalian systems, are described as follows. Static populations may be represented by neurons. A damaged or destroyed cell of this category is usually not replaced and, therefore, is lost to the population of which it was a member. Mitotic figures (cells undergoing mitosis) would not be expected within such tissue. Expanding populations may be represented by hepatocytes. Here, a damaged or destroyed cell is replaced, thereby sustaining the integrity of the original cell population. Typically, the necessity to replace these cells is infrequent, consequently the percentage of mitotic figures would be low. Renewing populations may be represented by epithelial cells which are constantly being lost and replaced. One would expect to observe a high percentage of mitotic figures within a population of these cells. Those tissues responsible for blood cell production are included within this third category. Blood cells are continually being lost from the bloodstream due to their active migration into the surrounding tissues, aging and/or death. Their importance to the animal requires that they be replaced immediately. Therefore, the mitotic activity of any tissue hypothesized as being a site of hemocytogenesis or hemocyte

production, as are the white bodies of cephalopods, is carefully examined. To ascertain the mitotic activity of a tissue, one may calculate its mitotic index. The latter refers to the ratio of cells undergoing mitosis to the total number of cells observed. The above technique was employed to study the mitotic activity of white body tissue from I. illecebrosus. Results obtained by this author are discussed in relation to those described for octopod and mammalian tissues.

White body tissue samples collected throughout the months of September, October, and November exhibited mitotic indices averaging 3.9%. These indices were very consistent in that each index varied no more than 0.4 percentage points from another. White body tissue samples obtained in December exhibited mitotic indices averaging 3.2%. Initially, the averages appear similar. However, examination of the December samples reveals that only one component of the white body, the inferior preganglionic lobe is responsible for the December average being as high as the value recorded above. If the mitotic index for this particular lobe is removed and the indices of the remaining white body components evaluated, the average mitotic index recorded for the December samples becomes 2.9%. It was noted that the mitotic index of white body tissue from this inferior preganglionic lobe is comparable to indices described for the postganglionic tissue samples collected in September, October, and November. Furthermore, based

solely upon the white body material observed, the indices calculated for each postganglionic lobe exhibit a slight decline in value from September to November and a more rapid decline in value between these latter three months and the month of December. This trend is difficult to interpret at present due to the limited availability of squid. However, it does raise interesting questions concerning the levels of mitotic activity through seasonal change and the degree to which the various components of the white body differ under such circumstances.

The mitotic activity of white body tissue from Octopus vulgaris was investigated by Necco and Martin in 1963. Their results were collected from white body cell suspensions which had been prepared by mechanical dissociation and cultured in vitro for 96 hours. This white body material had been obtained from young animals (40-60 grams). Calculations of the proliferative activity were made every 4 hours for a period of 20 hours. Both the mitotic index and a stathmokinetic index were investigated at these intervals. The latter index requires the addition of colchicine to the culture medium. Colchicine blocks the mitotic process at metaphase so that, over time, the cell population is characterized by an accumulation of mitotic figures. This increase, which represents the number of cells entering mitosis, is reflected in an elevated stathmokinetic index. Thus, the proliferative activity of the cells can be evaluated. Necco and Martin (1963) recorded an initial value

(zero culture time) of 9.5% mitosis for the white body cells of O. vulgaris. Four hours after the establishment of this culture, the value had decreased to 7.5%. At 8 hours the mitotic index was 5.0%, at 12 hours it was recorded as 4.5%, and by 16 hours the index had stabilized at 4.0% where it remained until the end of the testing period (20 hours culture time). This decrease in mitotic activity was interpreted by Necco and Martin as "a consequence of the adjustment to the new environment" (p. 590). Conversely, the values recorded for the stathmokinetic index increased rapidly to reach a maximum of 21.0% mitosis after 12 hours of culture time. Subsequent to this peak of activity, the index was observed to decrease steadily, attaining a final value (at 20 hours culture time) of 11.0% mitosis. The latter figure was only 1.5 percentage points above the initial figure of 9.5% mitosis recorded at zero culture time. Necco and Martin suggested that such a decline can be "explained by the fact that cells blocked in mitosis for several hours tend to disintegrate" (p. 590). Data collected during the calculation of this stathmokinetic index also indicate that approximately one white body cell in a thousand entered mitosis per hour under in vitro conditions. It was also noted that changes in the length of various mitotic phases were displayed by white body cells within the colchicine-free medium. At zero culture time, the freshly prepared white body suspension exhibited a large number of cells (approximately 55%) undergoing telophase. This

indicated to Necco and Martin that the duration of this mitotic phrase was extremely long in vivo. However, with increased culture time, the duration of telophase shortened and it was the length of metaphase that became progressively longer.

Values representing the proliferative activity of white body cells from I. illecebrosus and O. vulgaris may be evaluated upon their comparison with known indices for mammalian tissue. To this end, the mitotic indices recorded for mammalian bone marrow have been chosen as the standard by which the cephalopod values will be assessed. The selection of these particular mammalian indices was influenced by the hemocytogenic nature that characterizes the bone marrow. All bone marrow samples cited in the following discussion were obtained from one of four different species (Altman & Katz, 1976): (1) Homo sapiens, normal, 29-45 year old males; (2) Canis familiaris Linnaeus, 34-52 month old Beagles; (3) Mus musculus Linnaeus, CF₁ strain, 8-16 week old females; and (4) Rattus norvegicus (Berkenhout), Sprague-Dawley strain, 190-210 gram females.

The proliferative activity of human bone marrow is approximately 0.9%. By comparison, bone marrow samples from Beagle dogs exhibit 4.7% mitosis, while those from mice average 1.5%. With regard to the species tested, the greatest percentage of mitotic activity (7.8% mitosis) is that recorded for marrow samples from the Norway rat.

When comparing the proliferative activity of cells from the bone marrow of mammals with the activity of cells from the white bodies of cephalopods, one must be aware of certain discrepancies in the above references. First, the mitotic indices cited for mammalian bone marrow samples usually represent an average value calculated from data obtained over a 24-hour period. This procedure could not be maintained when sampling squid tissues due to the shortage of available specimens. Therefore, the mitotic indices of white body tissue from I. illecebrosus were calculated once during a 24-hour period. White body tissue from O. vulgaris was also collected a single time, however the sample was maintained in vitro such that the proliferative activity of its individual cells could be studied over a period of 20 hours. Second, age differences exist with regard to the animals tested. While I. illecebrosus, R. norvegicus, M. musculus, C. familiaris, and H. sapiens were all represented by adult members of the species, the O. vulgaris specimen was a juvenile. Thus it is recognized that a population of mitotic cells may vary in number not only during one day of an animal's life but also throughout its entire lifetime. As a result, it is not feasible to suggest that specific relationships exist between any of the indices cited above. However, certain generalizations are possible. ONE, the values recorded for each white body sample from I. illecebrosus and O. vulgaris are sufficiently high as to indicate that mitotic activity occurs frequently within

this tissue. Indeed, the magnitude of such activity is similar to that associated with a renewing cell population. TWO, this information lends support to the hypothesis that the white body tissue produces hemocytes. THREE, furthermore, the data provide sound arguments for the employment of labeling experiments involving tritiated thymidine (a discussion of these results to follow). FOUR, the twofold increase in mitotic activity observed within white body samples from O. vulgaris (in comparison to those from I. illecebrosus) may be dependent upon age; the white body cells of the juvenile octopod exhibiting greater proliferation than those white body cells of the adult squid. However, it should also be noted that those values for the squid tissue represent a conservative estimate. As stated earlier, the omission of telophase nuclei from the mitotic index calculations resulted from an inability to distinguish the latter from sectioned reniform nuclei. Necco and Martin (1963), working with a suspension of white body cells, did not have to contend with such ambiguity.

Cells within the white bodies of I. illecebrosus were studied with the aid of tritiated thymidine. This investigation was based upon the following general assumptions: (1) the white body cells represent a renewing cell population; (2) tritiated thymidine is incorporated into DNA when cells are within the synthesis stage of the cell cycle; (3) through the process of mitosis, the labeled chromatin is passed to the resulting daughter cells when cell division occurs;

(4) transferal of labeled chromatin from parent cell to daughter cell is repeated with each subsequent cell division; and (5) cells that contain the labeled chromatin can be identified by autoradiographic techniques which enable visualization of the radioisotope's presence.

More specifically, if hemocytes are produced by the white body, then the population of dividing cells (stem cells and/or precursor cells) should incorporate a radioactive label upon exposure to tritiated thymidine. Over time, the various developmental stages should exhibit label and, eventually, the mature circulating hemocytes will become labeled.

A successful conclusion to this investigation would not only elucidate the physiological nature of the white bodies but also further the understanding of the circulating hemocytes.

Results obtained during the labeling studies indicate that tritiated thymidine remains in the bloodstream of I. illecebrosus for only a short period of time. Pools of the radioisotope could be demonstrated within arterial and venous blood samples collected 30 minutes after injection of the label. However, this profuse quantity of label was substantially reduced within those arterial and venous blood samples obtained one hour after injection. Under no circumstances could label be detected within any blood samples collected after exposure times greater than one hour. These findings are interesting in light of those reported for

mammalian species. In man (Rubini, J., E. Cronkite, V. Bond, and T. Fliedner, 1960), the removal of tritiated thymidine from the bloodstream is initiated immediately upon the label's injection therein. One minute later, approximately 90% of this activity is lost from the blood. At one hour following injection, the label is readily identified within cell lineages or catabolized. The above authors further state that similar results have been recorded for mice. The North-Holland Research Monograph (Cleaver, 1967) that describes thymidine metabolism within a variety of biological systems indicates an identical fate for this labeled compound.

Thus, the overall clearance rate for intravascular injections of tritiated thymidine is relatively constant among those species studied, including I. illecebrosus. However, the elevated levels of radioisotope within blood samples collected from I. illecebrosus 30 minutes after injection are not consistent with the mammalian values cited previously. This delay in the immediate removal of tritiated thymidine may be the result of administrative procedures. Firstly, the recommended dosage (Feinendegen, 1967) for short-term labeling experiments involving a renewing cell population is 1.0 μ Ci of tritiated thymidine per gram weight of experimental animal. Due to the lack of pertinent teuthoid data, this author chose a conservative approach and reduced the suggested dosage by 25%; thereby injecting 0.75 μ Ci of tritiated thymidine per gram weight of squid.

Secondly, considerable apprehension was expressed with regard to the squid's ability to survive the manipulations associated with the injection of this labeled compound. Therefore, the single-injection method (a pulse label) was deemed more advantageous than a multiple-injection approach.

It is now apparent that even this reduced dosage, when administered as a pulse label, was excessive and that the direct result was a persistence of label (in the blood) at the 30 minute sampling interval. However, it is noteworthy that the squid were still able to substantially reduce this pool of tritiated thymidine before the one hour sampling interval; an accomplishment similar to that recorded for mammalian species. Speculation as to the fate of the label upon its removal from the bloodstream is offered within the statements that follow.

As noted in the results, the radioisotope was not incorporated into the DNA of white body cells. The high concentration of circulating label over an exposure period of 30 minutes could have been of sufficient magnitude to elicit an inhibitory response mediated via the process known as negative feedback or end-product inhibition. Elevated levels of tritiated thymidine within a biological system subsequently result in an accumulation of end-products at a particular point along the incorporation pathway. When such a condition arises, the further synthesis of these end-products is regulated by the elevated level of end-products through restrictions in the activity of initial

reactions of the pathway (Cleaver, 1967). It is suggested that a similar mechanism might be operating within the white body cells of I. illecebrosus.

Alternately, and possibly more likely, the lack of incorporation may have resulted from effects of temperature. Within mammals, the differences in temperature that characterize the various regions of the body are thought to be responsible for differences in the rate of DNA synthesis. Specifically, the DNA synthesis time for epithelium of the lower ileum (37°C) within male mice (6 to 8 weeks old; an inbred strain derived from the disease-free Walter Reed Hospital Swiss mice) is approximately 7 hours. This rate increases to 30 hours in duration for those dividing cells within the epidermis of the ear (35°C) (Sherman, F., H. Quastler, and D. Wimber, 1961). The fact that cellular metabolism and proliferation occur at much lower temperatures ($11-14^{\circ}\text{C}$) within I. illecebrosus would suggest a further prolongation of the synthetic process. At such a rate, the pulse labeling technique employed during this study would be ineffective.

The previous observations indicate that the fate of the injected tritiated thymidine is probably not one of incorporation (by cells of the white bodies or any other proliferative tissue within I. illecebrosus). Therefore, it may be hypothesized that the tritiated thymidine had been: (1) stored in the acid-soluble pool within the nuclei of these dividing cells; (2) transported to the intercellular

hemal spaces by means of the vasculature of the white body, and/or (3) catabolized. Rubini et al., 1960, have reported that, in man, a third of the injected tritiated thymidine is catabolized for subsequent excretion. If similar conditions exist within squid, then such a proportion of the labeled material (as observed within blood samples obtained from I. illecebrosus 30 minutes after injection) would represent a considerable volume for the teuthoid's excretory system to process. This is particularly true in light of the low rate of renal filtration attributed to cephalopods (Wells, 1962).

Studies were undertaken to investigate immunological relationships existing between I. illecebrosus white body tissue cells and the hemocytes of the blood. To this end, the author selected a New Zealand rabbit as the experimental animal for antibody production.

Through a series of injections, the rabbit was exposed to the squid's white body cells. When challenged by this foreign material, the rabbit's immune system was stimulated to produce antibodies. The serum which contained these antibodies (the antiserum) was then isolated from rabbit blood samples by centrifugation and tested by means of indirect immunofluorescence against a variety of selected I. illecebrosus tissues.

If hemocytes are indeed produced in the white body, then one would expect the hemocytes to be antigenically identical to the cells of the white body. A minor loss or

gain of antigens upon release from the white body is a possibility, however the majority of antigens would still be shared between the two tissues. Elevated levels of antibody binding to white body tissue and hemocytes (rather than to muscular or nervous tissue) would indicate that the white body tissue and the hemocytes share more antigenic determinants. Hence, a closer relationship would be demonstrated between white body tissue and hemocytes than between white body tissue and the other squid tissues tested.

Further evidence for this immunological relationship may also be obtained from absorption studies. Here, antiserum is exposed (individually by tissue) to ink sac, liver, mantle muscle, optic ganglion, ovary, or stomach homogenate. If, subsequent to this exposure of the antiserum to each of the above tissues, antibodies are still available for binding to white body cells and hemocytes, it may be inferred that a definite degree of immunological relationship has been demonstrated. Furthermore, this finding would support the hypothesis that the hemocytes are derived from the white body tissue due to common immunological characteristics.

The following observations were noted during the above immunological studies. These encompass basic information pertaining to the nature of the antigen (those white body cells injected into the rabbit) through specific references to the reactions that resulted upon the immunological testing of the unabsorbed and absorbed rabbit

antiserum. ONE, the rabbit antiserum was produced in response to surface antigens displayed by the injected white body cells. Figure 88 provides evidence for this statement by demonstrating that it is only the cellular membranes of the sectioned material which fluoresce. TWO, when a New Zealand rabbit is challenged with white body cells from I. illecebrosus, it produces an antiserum that reacts not only with white body cell suspensions and white body, liver, and muscle tissue sections from I. illecebrosus but also with the hemocytes of I. illecebrosus and O. pteropus. (These reactions are strongly positive, +++, when the antiserum is diluted 1:10 with phosphate-buffered saline.) Furthermore, antiserum absorbed with ink sac, liver, mantle muscle, optic ganglion, ovary, or stomach reacts positively (++) upon exposure to white body cell suspension smears from I. illecebrosus and, in most instances, strongly positively (+++) upon exposure to the hemocytes of O. pteropus. These findings suggest that antibodies with an intergeneric or general "squid" specificity constitute a portion of the antiserum. Conversely, the cells that comprise each of the tissues tested (from the two squids) must exhibit some intergeneric antigenic determinants on their surface membranes. THREE, the surface antigens displayed by hemocytes from the blood of O. pteropus are sensitive to ethanol. This inference was based on data gathered from fixed and unfixed blood smears. The antiserum reacted only with the latter. However, it is not

known whether these antigens were denatured or eluted by the alcohol. FOUR, the antiserum which had previously been absorbed with liver homogenate exhibited only a marginally positive reaction upon exposure to the hemocytes of I. illecebrosus. Initially, it would appear that a population of developing blood cells might be present within the liver homogenate. Antibody binding to these formative cells would leave a minimal quantity of antibodies available for subsequent binding with the hemocytes of the prepared blood smears; hence the marginally positive reaction. However, neither Bidder's (1950) paper on the digestive mechanism of squids nor Bradbury's (1970) thesis on the functional anatomy of I. illecebrosus record the presence of hemocytogenic foci within liver (the hepatic portion of the hepatopancreas) tissue. Aggregates of hemocytes were not even cited. Bradbury (1970, p. 16) did state, though, that the hepatic portion of the hepatopancreas receives a copious supply of blood from the cephalic aorta. Therefore, it becomes reasonable to suggest that hemocytes, which would comprise a substantial portion of the liver homogenate, were responsible for the removal of serum antibodies during the above absorption study. FIVE, antiserum absorbed with white body homogenate still displayed a positive (++) reaction upon exposure to hemocytes from the blood of I. illecebrosus. This reaction contrasts with those in which similar aliquots of absorbed antiserum were exposed to white body cell suspension smears (marginally positive, +, reaction; i.e.,

the antiserum had not been absorbed to completion) and white body tissue sections (marginally positive, +, reaction). The higher level of immunofluorescence demonstrated within the blood smears could be due to the availability of antibodies present within the absorbed antiserum. As illustrated by the blood smears presented in Figure 89, the number of hemocytes occurring within a random field of view is extremely few. As a result, there is a correspondingly higher quantity of antibodies available per hemocyte and this could account for the stronger display of immunofluorescence. White body cell suspension smears and prepared slides of white body tissue sections each represent dense concentrations of cells, in comparison. Under these circumstances, the ratio of antibodies to cells is relatively low. Therefore, one would expect a weaker display of immunofluorescence. Another possibility is that the antibodies remaining in the absorbed serum are specific for an antigenic determinant present in higher concentrations on the surface of hemocytes than on white body cells. SIX, data collected during the various studies involving absorbed antiserum indicate that more antigenic determinants are shared between white body cells and hemocytes than between white body cells and any of the other squid tissues tested. Antiserum absorbed with ink sac, liver (hepatic portion of the hepatopancreas), mantle (muscle), optic ganglion, ovary, stomach, or white body tissue was tested in the above experiments. Each absorbed serum was exposed to the

hemocytes of I. illecebrosus. If the cells of a particular tissue homogenate share many determinants with the hemocytes then one would expect a high level of antibodies to be removed from the antiserum upon the latter's exposure to the tissue homogenate. As a result, a very low level of antibodies would be available for binding when the absorbed antiserum was subsequently exposed to the squid's hemocytes. Conversely, if the cells of a particular tissue homogenate share few determinants with the hemocytes, then a low level of antibodies would be removed from the antiserum during absorption. In this instance, a high level of antibodies would be available for binding upon subsequent exposure to the hemocytes and, therefore, strong displays of immunofluorescence would be the observable result. In the majority of these absorption experiments (4 out of 7; antiserum absorbed with ink sac, optic ganglion, ovary, or stomach homogenate) the reaction was strongly positive (+++). Of the remaining three absorption tests, two (antiserum absorbed with liver and antiserum absorbed with white body) displayed reactions which have been interpreted by this author as corroborating the hypothesis that the white body produces the circulating hemocytes. A description of these results obtained from antiserum absorbed with liver or white body homogenate is recorded under points 4 and 5 of the present discussion. The antiserum absorbed with mantle (muscle) homogenate exhibited a positive (++) reaction upon exposure to the hemocytes. While this response was weaker

than those exhibited by the antiserum absorbed with ink sac, optic ganglion, ovary, or stomach homogenate, it does not necessarily establish a relationship between muscle cells and hemocytes, based on the arguments outlined above. Thus, the results obtained from 6 of the 7 absorption experiments support the existence of a close relationship between white body cells and the circulating hemocytes. This premise is further strengthened by evidence collected from immunological tests involving the blood cells of O. pteropus. SEVEN, unabsorbed antiserum in addition to antiserum absorbed with ink sac, liver, mantle (muscle), optic ganglion, ovary, stomach, or white body homogenate were individually exposed to the hemocytes of the squid, O. pteropus. It was observed that only the absorption with white body homogenate removed, completely, the antibodies binding with the circulating blood cells of O. pteropus. These results indicate the white body cells of I. illecebrosus and the circulating hemocytes of O. pteropus share antigens which are not present on those cells of the other squid tissues tested. One may conclude, therefore, that based upon immunological characteristics the possibility of hemocytes being derived from white body tissue is very high. EIGHT, results obtained from the absorption experiments may also elucidate the origin of the white bodies, themselves. (It should be noted that these experiments were not initiated with the question of white body origin in mind. However, as analysis of the data progressed, the need to report their significance

became apparent.) Currently, it is thought that the white bodies arise from the ectodermal germ layer. Raven (1966, p. 176) described their embryonic development as follows: "Behind and medially to them (the eyes) there is an extensive area of proliferation. It's medial part forms the cerebral ganglion, the lateral part, the optic ganglion, while the remainder produces the so-called 'white body'". If the white body tissue were derived from nervous tissue, then one would expect their cells to share many antigens. This relationship could be demonstrated immunologically by absorption experiments in which antiserum prepared against white body cells would be exposed to a nervous tissue homogenate. Antibodies should be removed, leaving low levels of antibodies (or none at all) available for binding upon subsequent exposure to white body and/or blood cell preparations. Such a procedure was undertaken by this author in the course of the absorption experiments outlined previously. Specifically, the antiserum which had been prepared against white body cells was absorbed with optic ganglion homogenate. The resulting absorbed antiserum was then exposed to hemocytes and white body cell suspension smears. However, the reaction proposed above did not occur. Rather, there were strong displays of immunofluorescence which indicated that few antigens are shared between nervous tissue (in this case, optic ganglion tissue) and the cells of the white body or blood. Such data appear to contradict an ectodermal origin until one considers such lymphoid

tissue as the thymus wherein an ectodermal framework surrounds and supports a cell population of mesodermal origin. The isolation methods employed in the preparation of the white body cell suspensions for rabbit injection and anti-serum/absorbed antiserum testing yielded a cell population comprised primarily of free white body cells. The latter would correspond to those cells of mesodermal origin within the thymus; thus an exodermal origin of the white body framework cannot be excluded.

The Variation 1 cell, illustrated in Figure 91 and elsewhere in this thesis, is considered to be the "stem cell" in the hemocytogenic cycle of I. illecebrosus. Stem cells representative of other phyla of invertebrates have been discovered, described, and discussed by a variety of authors including: Bergquist, 1978 (Porifera), Jordan and Reynolds, 1933 (Platyhelminthes, Trematoda), Kindred, 1929 (Annelida, Oligochaeta), Johnson, 1980 (Arthropoda, Crustacea), Gupta, 1979 and Hoffmann et al., 1979 (Arthropoda, Insecta), Hetzel, 1965 and Endean, 1966 (Echinodermata, Holothuroidea), Holland et al., 1965 (Echinodermata, Echinoidea), and Smith, 1970 (Urochordata, Tunicata).

It may be discerned that all cells recognized as "stem cells" exhibit certain basic properties regardless of the phylum which they represent. All stem cells are undifferentiated cells, morphologically similar to the hyaline "leucocytes" of the less advanced invertebrate species. Most

are derived from mesoderm, whether it be connective tissue or peritoneum. In the case of the lowest of the metazoans, stem cells are derived from mesoglea. Lastly, most are capable of differentiating into a variety of cell types.

A study of comparative hemocytogenesis reveals the existence of two mechanisms whereby hemocytes may be replenished, namely "expanding" as opposed to "renewing". Furthermore, each mechanism can be associated with a particular stage in the phylogenetic development of the hemocytogenic organs. The "expanding" cell population is replenished only when hemocytes are destroyed or lost from the system. Under this mechanism, cell life spans are relatively long and consequently few mitotic figures are observed among stem cells or precursor cells. Examples of expanding populations occur within the Porifera where stem cells and their descendents are found scattered throughout the mesoglea. The "renewing" cell population is replenished continually. Under this mechanism, cell life spans are relatively short and, therefore, mitotic figures are frequently observed among stem cells or precursor cells. The Crustacea, Insecta, and Cephalopoda represent such examples. Additionally, renewing cell populations are associated with highly organized hemocytogenic organs. All three invertebrate classes mentioned above possess hemocyte-producing tissue which is (1) distinguished from its surroundings by a layer of epithelial cells or connective tissue, (2) organized into cellular cords or loci that are supported by

a network of fibers, and (3) confluent with the fluid medium into which the mature cells are ultimately freed. The Oligochaeta differ slightly in that mitotic figures are few in number and mature cells enter the coelomic fluid before passing into the blood. The Trematoda and Echinodermata appear as intermediary groups. Although these groups demonstrate the persistence of an expanding hemocyte population, the hemocytogenic tissue exhibits progressive signs of developing into distinct loci. Descriptions of hemocytogenesis within the Gastropoda (Sminia, 1974) and Pelecypoda (Takatsuki, 1934) suggest that these two classes of molluscs belong to just such an intermediary group as well.

It is hoped that this investigation of the white bodies within I. illecebrosus will serve as a springboard or point of departure for future research. Such work should include: (1) additional immunological studies in which the antiserum would be absorbed with 2-3 times the volume of white body, liver, and muscle tissue homogenate that was employed in this study in order to completely absorb the antibodies, (2) additional immunological studies in which the antiserum would be absorbed with hemocytes, (3) an investigation into the possibility of identifying the white body cells immunologically, through the development of monoclonal antibodies, (4) an embryological study of the white bodies with regard to their gross and microscopic anatomy, and (5) autoradiographic studies in which modifications relating to dosage level and exposure intervals would be considered.

REFERENCES CITED

- ALDRICH, F.A. and C.C. LU, 1968, "A Reconsideration of Forms of Squid of the Genus Illex (Illicinae, Ommastrephidae) in Newfoundland Waters", Can. Jour. Zool., 46(5): 815-818.
- ALTMAN, P. and D. DITTMER (Eds.), 1973, Biology Data Book, 2nd. Edition, Volume II, Federation of American Societies for Experimental Biology, Bethesda, Maryland, xix, 607-1432 pp.
- and D. KATZ (Eds.), 1976, Cell Biology, Federation of American Societies for Experimental Biology, Bethesda, Maryland, xix, 454 pp.
- BAGINSKI, S., 1965, "Histophysiology of the Parabranchial Gland in Cephalopods of the Family Eledone", Folia Morphologica, 24(3):215-232.
- BERGQUIST, P., 1978, Sponges, Univ. of Calif. Press, Berkeley, 268 pp.
- BESSIS, M., 1973, Living Blood Cells and Their Ultra-structure (Translated by R. Weed), Springer-Verlag, New York, xxiii, 767 pp.
- BIDDER, A., 1950, "The Digestive Mechanism of the European Squids, Loligo vulgaris, Loligo forbesii, Alloteuthis media, and Alloteuthis subulata", Quart. Jour. Micros. Sci., 91(1):1-45.
- BOGOROCH, R., 1972, "Liquid Emulsion Autoradiography", Chapter 5 of Autoradiography for Biologists, P. Gahan (Ed.), Academic Press, London, xi, 124 pp.
- BOLOGNARI, A., 1949, "Morfologia, Struttura e Funzione del 'Corpo Bianco' dei Cefalopodi. I. Morfologia", Arch. Zool. Ital., 34:78-97.
- , 1950, "Sulla Genesi degli Elementi Figurati del Sangue dei Molluschi Cefalopodi", Boll. di Zool., 17:369-378.
- , 1951, "Morfologia, Struttura e Funzione del 'Corpo Bianco' dei Cefalopodi. II. Struttura e Funzione", Arch. Zool. Ital., 36:253-287.
- , S. FASULO, and A. LICATA, 1981, "Aspetti Comparati del Corpo Bianco dei Cefalopodi e del Midollo Osseo dei Mammiferi", Boll. Soc. It. Biol. Sper., 56:454-457.

- BRADBURY, H., 1970, "Observations on the Functional Anatomy of the Ommastephid, Illex illecebrosus (LeSueur, 1821) (Coleoidea:Cephalopoda), with Emphasis on Musculature and the Blood Vascular System". Doctor of Philosophy Thesis, Memorial University of Newfoundland, St. John's, Newfoundland, Canada, 410 pp.
- CARAZZI, D., 1901, "Studi sui Molluschi", Int. Monatsch. Anat. U. Physiol., 19:1-18.
- CAZAL, P. and D. BOGORAZE, 1943, "Recherches sur les Corps Blanc du Poulpe (Octopus vulgaris, Lam.). Leur Fonction Globuligène et Néphrocitaire", Bull. Inst. Oceanogr. Monaco, 40(842):1-12.
- CLEAVER, J.E., 1967, Thymidine Metabolism and Cell Kinetics, North-Holland Publishing Company, Amsterdam, 259 pp.
- COWDEN, R., 1972, "Some Cytological and Cytochemical Observations on the Leucopoietic Organs, the 'White Bodies', of Octopus vulgaris", Jour. Invert. Path., 19:113-119.
- and S. CURTIS, 1973, "Observations on Living Cells Dissociated from the Leukopoietic Organ of Octopus briareus", Exp. and Mole. Path., 19:178-185.
- and -----, 1974, "The Octopus White Body: An Ultrastructural Survey", Contemporary Topics in Immunobiology, E.L. Cooper (Ed.), 4:77-90, Plenum Press, New York, xvii, 299 pp.
- and -----, 1981, "Cephalopods", Invertebrate Blood Cells, Volume I, N. Ratcliffe and A. Rowley (Eds.), Academic Press, New York, xii, 323 pp.
- CUÉNOT, L., 1891, "Étude sur le Sang et les Glandes Lymphatiques dans la Série Animale. Invertébrés", Arch. Zool. Exp. et Gén., 9:13-90.
- , 1897, "Les Globules Sanguins et les Organes Lymphoïdes des Invertébrés", Arch. d'Anatomie Micro. et de Morph. Exp., 1:153-192.
- CUVIER, G., 1817, "Mémoires pour Servir a l'Histoire et a l'Anatomie des Mollusques", Mémoire sur les Cephalopodes et sur leur Anatomie. Du Poulpe, Deterville, Paris, pp. 6-43.
- DILLY, P. and J. MESSENGER, 1972, "The Branchial Gland: A Site of Haemocyanin Synthesis in Octopus", Z. Zellforsch., 132:193-201.

- ENDEAN, R., 1966, "The Coelomocytes and Coelomic Fluids" in *Physiology of Echinodermata*, R. Booloottian (Ed.), Interscience Publishers, New York, xviii, 822 pp.
- FAUSSEK, V., 1893, "Ueber den Sogenannten 'weissen Korper' sowie über die Embryonale Entwicklung desselben, der Cerebralganglien und des Knorpels bei Cephalopoden", *Mém. Acad. imp. Sc., St. Petersburg*, 41(9):27. (Quoted from NOEL, R. and A. JULLIEN, 1933).
- FEINENDEGEN, L., 1967, *Tritium-Labeled Molecules in Biology and Medicine*, Academic Press, New York, x, 430 pp.
- FÉRUSSE, M. and A. d'ORBIGNY, 1835-1848, "Histoire Naturelle Générale et Particulière des Céphalopodes Acétabulifères Vivants et Fossiles", Paris, ix, 361 pp.
- GUPTA, A., 1979, "Hemocyte Types: Their Structures, Synonymies, Interrelationships, and Taxonomic Significance" in *Insect Hemocytes: Development, Forms, Functions, and Techniques*, A. Gupta (Ed.), Cambridge Univ. Press, Cambridge, x, 614 pp.
- HARRISON, F. and A. MARTIN, 1965, "Excretion in the Cephalopod, Octopus dofleini", *Jour. Exp. Biol.*, 42(1):71-98.
- HAWKES, J. and C. STEHR, 1980, "Ultrastructural Studies of Marine Organisms: A Manual of Techniques and Applications", *Norelco Reporter*, 27(1):27-34.
- HENSEN, V., 1865, "Ueber das Auge einiger Cephalopoden", *Zeit. wiss. Zool.*, 15:155-242.
- HETZEL, H., 1965, "Studies on Holothurian Coelomocytes. II. The Origin of Coelomocytes and the Formation of Brown Bodies", *Biol. Bull.*, 128:102-111.
- HOFFMANN, J., D. ZACHARY, D. HOFFMANN, and M. BREHELIN, 1979, "Postembryonic Development and Differentiation: Hemopoietic Tissues and their Functions in Some Insects" in *Insect Hemocytes: Development, Forms, Functions, and Techniques*, A. Gupta (Ed.), Cambridge Univ. Press, Cambridge, x, 614 pp.
- HOLLAND, N., J. PHILLIPS, and A. GIESE, 1965, "An Autoradiographic Investigation of Coelomocyte Production in the Purple Sea Urchin (Strongylocentrotus purpuratus)", *Bio. Bull.*, 128:259-270.
- HUMASON, G., 1972, *Animal Tissue Techniques*, 3rd Edition, W.H. Freeman and Company, San Francisco, 641 pp.

- HYAM, P. 1981, "Same Day Electron Microscopy", Can. Jour. Med. Tech., 43: 255-260.
- JOHNSON, P., 1980, Histology of the Blue Crab, Callinectes sapidus: A Model for the Decapoda, Praeger Publishers, New York, xv, 440 pp.
- JORDAN, H.E. and B.D. REYNOLDS, 1933, "The Blood Cells of the Trematode Diplodiscus temperatus", Jour, Morph., 55:119-129.
- JOUBIN, L., 1885, "Structure et Développement de la Branchie de Quelques Céphalopodes des Côtes de France", Arch. de Zool. Exp. et Gen., 3:75-150.
- KINDRED, J.E., 1929, "The Leucocytes and Leucocytopoietic Organs of an Oligochaete, Pheretima indica (Horst)", Jour, Morph., 47:435-478.
- KOLLMANN, M., 1908, "Recherches sur les Leucocytes et le Tissu Lymphoïde des Invertébrés", Ann. des Sciences Natur. (Zool.), 8:1-238.
- , 1924, "Note sur l'Évolution de la Glande Lymphoïde et des Leucocytes des Céphalopodes", C.R. Soc. Biol., 91:1317.
- KRAUSE, W. and J. CUTTS, 1981, Concise Text of Histology, Williams and Wilkins, Baltimore, 429 pp.
- KRUSE, P. and M. PATTERSON, 1973, Tissue Culture; Methods and Applications, Academic Press, New York, 868 pp.
- LESUEUR, C.A., 1821, "Descriptions of Several New Species of Cuttlefish", Jour. Acad. Nat. Sci. Philadelphia, 2:86-101.
- LU, C.C., 1968, "Determination of Growth and Related Phenomena in Illex illecebrosus illecebrosus (Lesueur) (Decapoda: Cephalopoda) from Newfoundland", Master of Science Thesis, Memorial University of Newfoundland, St. John's, Newfoundland, Canada, 178 pp.
- MANGOLD, K., C.C. LU, and F.A. ALDRICH, 1969, "A Reconsideration of Forms of Squid of the Genus Illex (Illicinae, Ommastrephidae), II. Sexual Dimorphism", Can. Jour. Zool., 47(6):1153-1156.
- MESSINGER, J., E. MUZII, G. NARDI, and H. STEINBERG, 1974, "Haemocyanin Synthesis and the Branchial Gland of Octopus", Nature, 250:154-155.

- MUZII, E., 1981, "Intracellular Polymerized Haemocyanin in the Branchial Gland of a Cephalopod", *Cell and Tiss. Res.*, 220:435-438.
- NECCO, A. and R. MARTIN, 1963, "Behavior and Estimation of the Mitotic Activity of the White Body Cells in Octopus vulgaris, Cultured In Vitro", *Exp. Cell Res.*, 30:588-590.
- NIE, N.H., 1983, *SPSSx User's Guide*, McGraw-Hill Book Company, New York, xxvi, 806 pp.
- , C.H. HULL, J.G. JENKINS, K. STEINBRENNER, and D. BENT, 1975, *SPSS, Statistical Package for the Social Sciences*, 2nd. Edition, McGraw-Hill Book Company, New York, xxiv, 675 pp.
- NOEL, R. and A. JULLIEN, 1933, "Recherches Histologiques sur le Corps Blanc des Céphalopodes", *Arch. de Zool. Exp. et Gen.*, 75:485-499.
- POTTS, W., 1965, "Ammonia Excretion in Octopus dofleini", *Comp. Biochem. Physiol.* 14(2):339-355.
- , 1968, "Aspects of Excretion in the Molluscs", *Symp. Zool. Soc. London*, 22:187-192.
- RAVEN, C., 1966, *Morphogenesis: The Analysis of Molluscan Development*, Pergamon Press, New York, xiii, 365 pp.
- ROPER, C.F.E., R.E. YOUNG, and G.L. VOSS, 1969, "An illustrated Key to the Families of the Order Teuthoidea (Cephalopoda)", *Smithsonian Contrib. Zool.*, 13:1-32.
- RUBINI, J., E. CRONKITE, V. BOND, and T. FLIEDNER, 1960, "The Metabolism and Fate of Tritiated Thymidine in Man", *Jour. Clin. Invest.*, 39:909-918.
- SHEELER, P. and D. BIANCHI, 1980, *Cell Biology: Structure, Biochemistry, and Function*. John Wiley and Sons, New York, xvi, 578 pp.
- SHERMAN, F., H. QUASTLER, and D. WIMBER, 1961, "Cell Population Kinetics in the Ear Epidermis of Mice", *Exp. Cell Res.*, 25:114-119.
- SMINIA, T., 1974, "Haematopoiesis in the Freshwater Snail Lymnaea stagnalis Studied by Electron Microscopy and Autoradiography", *Cell and Tiss. Res.*, 150:443-454.
- SMITH, M., 1970, "The Blood Cells and Tunic of the Ascidian Halocynthia aurantium (Pallas) I. Hematology, Tunic Morphology, and Partition of Cells Between Blood and Tunic", *Biol. Bull.*, 138(3):354-378.

- TAKATSUKI, S., 1934, "On the Nature and Function of the Amoebocytes of Ostrea edulis", Quart. Journ. Micros. Sci., 76:379-431.
- THORE, S., 1936, "Cephalopodstudien. Beiträge zur Kenntniss der Sog. weissen Körper nebst Mitteilung über ein Neues Organ bei Octopus vulgaris", Kungl. Fysiografiska Sällskapet I. Lund Forhandlingar, 6(15):147-162.
- VERRILL, A.E., 1880, "Synopsis of the Cephalopoda of the Northeastern Coast of America", Amer. Jour. Sci., 19:284-295.
- VILLANUEVA, A.R., 1970, "A New Biological Stain for Peripheral Blood and Bone Marrow Smears", Henry Ford Hos. Med. Jour., 18(1):11-20.
- VOGT, C. and E. YUNG, 1888, "Traite d'Anatomie Comparee Pratique", Paris.
- WAY, F.E., 1975, "Cellular Elements Within the Blood of the Newfoundland Bait Squid Illex illecebrosus (LeSueur, 1821) (Cephalopoda:Coleoidea): A Study in Functional Morphology", Master of Science Thesis, Memorial University of Newfoundland, St. John's, Newfoundland, Canada, 112 pp.
- WELLS, M.J., 1962, Brain and Behavior in Cephalopods, Stanford Univ. Press, Stanford, California, 171 pp.
- WITMER, A. and A. MARTIN, 1973, "The Fine Structure of the Branchial Heart Appendage of the Cephalopod Octopus dofleini martini", Z. Zellforsch., 136:545-568.
- YOUNG, J.Z., 1971, The Anatomy of the Nervous System of Octopus vulgaris", Oxford Univ. Press, London, xxxi, 690 pp.

APPENDICES

APPENDIX 1: Descriptive statistics pertaining to the morphological variables ascertained in the course of the morphometric study of the white bodies of the squid Illex illecebrosus.

RPL1 Right Postganglionic Lobe Width (in centimeters)
 Mean 0.817 Std. Dev. 0.178
 Mode 0.800 Median 0.828
 Minimum 0.400 Maximum 1.300 Range 0.900
 Valid Cases 178 *Missing Cases 1

RPL2 Right Postganglionic Lobe Length (in centimeters)
 Mean 1.369 Std. Dev. 0.257
 Mode 1.400 Median 1.387
 Minimum 0.600 Maximum 2.000 Range 1.400
 Valid Cases 178 Missing Cases 1

LPL1 Left Postganglionic Lobe Width (in centimeters)
 Mean 0.826 Std. Dev. 0.178
 Mode 0.800 Median 0.828
 Minimum 0.300 Maximum 1.400 Range 1.100
 Valid Cases 175 Missing Cases 4

LPL2 Left Postganglionic Lobe Length (in centimeters)
 Mean 1.366 Std. Dev. 0.244
 Mode 1.500 Median 1.384
 Minimum 0.600 Maximum 2.000 Range 1.400
 Valid Cases 175 Missing Cases 4

RSP1 Right Subganglionic Process Width (in centimeters)
 Mean 0.252 Std. Dev. 0.068
 Mode 0.200 Median 0.252
 Minimum 0.050 Maximum 0.500 Range 0.450
 Valid Cases 178 Missing Cases 1

RSP2 Right Subganglionic Process Length (in centimeters)
 Mean 2.003 Std. Dev. 0.154
 Mode 2.000 Median 2.004
 Minimum 1.200 Maximum 2.500 Range 1.300
 Valid Cases 178 Missing Cases 1

LSP1 Left Subganglionic Process Width (in centimeters)
 Mean 0.254 Std. Dev. 0.069
 Mode 0.300 Median 0.256
 Minimum 0.100 Maximum 0.450 Range 0.350
 Valid Cases 175 Missing Cases 4

APPENDIX 1 (cont'd.)

| | | | | |
|-------------|--|---------------|-------|-------------|
| LSP2 | Left Subganglionic Process Length (in centimeters) | | | |
| Mean | 2.004 | Std. Dev. | 0.148 | |
| Mode | 2.000 | Median | 2.004 | |
| Minimum | 1.400 | Maximum | 2.400 | Range 1.000 |
| Valid Cases | 175 | Missing Cases | 4 | |
| RIPL1 | Right Inferior Preganglionic Lobe Width (in centimeters) | | | |
| Mean | 0.500 | Std. Dev. | 0.125 | |
| Mode | 0.500 | Median | 0.491 | |
| Minimum | 0.200 | Maximum | 0.900 | Range 0.700 |
| Valid Cases | 177 | Missing Cases | 2 | |
| RIPL2 | Right Inferior Preganglionic Lobe Length (in centimeters) | | | |
| Mean | 0.979 | Std. Dev. | 0.152 | |
| Mode | 1.000 | Median | 0.979 | |
| Minimum | 0.600 | Maximum | 1.500 | Range 0.900 |
| Valid Cases | 177 | Missing Cases | 2 | |
| LIPL1 | Left Inferior Preganglionic Lobe Width (in centimeters) | | | |
| Mean | 0.522 | Std. Dev. | 0.121 | |
| Mode | 0.500 | Median | 0.514 | |
| Minimum | 0.300 | Maximum | 0.900 | Range 0.600 |
| Valid Cases | 174 | Missing Cases | 5 | |
| LIPL2 | Left Inferior Preganglionic Lobe Length (in centimeters) | | | |
| Mean | 1.001 | Std. Dev. | 0.178 | |
| Mode | 1.100 | Median | 1.003 | |
| Minimum | 0.700 | Maximum | 1.900 | Range 1.200 |
| Valid Cases | 174 | Missing Cases | 5 | |
| RSPL1 | Right Superior Preganglionic Lobe Width (in centimeters) | | | |
| Mean | 0.323 | Std. Dev. | 0.090 | |
| Mode | 0.300 | Median | 0.312 | |
| Minimum | 0.200 | Maximum | 0.600 | Range 0.400 |
| Valid Cases | 177 | Missing Cases | 2 | |
| RSPL2 | Right Superior Preganglionic Lobe Length (in centimeters) | | | |
| Mean | 0.592 | Std. Dev. | 0.147 | |
| Mode | 0.500 | Median | 0.578 | |
| Minimum | 0.300 | Maximum | 1.100 | Range 0.800 |
| Valid Cases | 177 | Missing Cases | 2 | |

APPENDIX 1 (cont'd)

| | | | | |
|-------------|---|---------------|---------|---------------|
| LSPL1 | Left Superior Preganglionic Lobe Width (in centimeters) | | | |
| Mean | 0.336 | Std. Dev. | 0.083 | |
| Mode | 0.300 | Median | 0.330 | |
| Minimum | 0.200 | Maximum | 0.600 | Range 0.400 |
| Valid Cases | 173 | Missing Cases | 6 | |
| LSPL2 | Left Superior Preganglionic Lobe Length (in centimeters) | | | |
| Mean | 0.599 | Std. Dev. | 0.134 | |
| Mode | 0.500 | Median | 0.584 | |
| Minimum | 0.300 | Maximum | 1.000 | Range 0.700 |
| Valid Cases | 173 | Missing Cases | 6 | |
| RLENGTH | Total Length of Right White Body (in centimeters) | | | |
| Mean | 4.947 | Std. Dev. | 0.504 | |
| Mode | 5.000 | Median | 5.000 | |
| Minimum | 3.700 | Maximum | 6.400 | Range 2.700 |
| Valid Cases | 177 | Missing Cases | 2 | |
| LLength | Total Length of Left White Body (in centimeters) | | | |
| Mean | 4.976 | Std. Dev. | 0.488 | |
| Mode | 4.800 | Median | 5.000 | |
| Minimum | 4.000 | Maximum | 6.100 | Range 2.100 |
| Valid Cases | 173 | Missing Cases | 6 | |
| DML | Dorsal Mantle Length of Squid (in millimeters) | | | |
| Mean | 246.374 | Std. Dev. | 29.334 | |
| Mode | 260.000 | Median | 249.000 | |
| Minimum | 163.000 | Maximum | 307.000 | Range 144.000 |
| Valid Cases | 179 | Missing Cases | 0 | |
| WEIGHT | Weight of Squid (in grams) | | | |
| Mean | 308.449 | Std. Dev. | 115.808 | |
| Mode | 139.000 | Median | 318.500 | |
| Minimum | 55.000 | Maximum | 664.000 | Range 609.000 |
| Valid Cases | 178 | Missing Cases | 1 | |
| SEX | Sex of Squid | | | |
| Males | 41 | Per Cent | 23 | |
| Females | 138 | Per Cent | 77 | |
| Valid Cases | 179 | Missing Cases | 0 | |

*Missing cases arise when the squid's eye collapses, thereby making accurate measurement of the white bodies impossible.

Appendix 2. Raw data from morphometric study of the white bodies of the squid Illex illecebrosus.

| | |
|----------|--|
| Column A | Squid Specimen Number |
| Column B | Dorsal Mantle Length of Squid (mm) |
| Column C | Weight of Squid (gm) |
| Column D | Sex of Squid (1 = male; 2 = female) |
| Column E | Width of Right Postganglionic Lobe (cm) |
| Column F | Length of Right Postganglionic Lobe (cm) |
| Column G | Width of Right Subganglionic Process (cm) |
| Column H | Length of Right Subganglionic Process (cm) |
| Column I | Width of Right Inferior Preganglionic Lobe (cm) |
| Column J | Length of Right Inferior Preganglionic Lobe (cm) |
| Column K | Width of Right Superior Preganglionic Lobe (cm) |
| Column L | Length of Right Superior Preganglionic Lobe (cm) |
| Column M | Width of Left Postganglionic Lobe (cm) |
| Column N | Length of Left Postganglionic Lobe (cm) |
| Column O | Width of Left Subganglionic Process (cm) |
| Column P | Length of Left Subganglionic Process (cm) |
| Column Q | Width of Left Inferior Preganglionic Lobe (cm) |
| Column R | Length of Left Inferior Preganglionic Lobe (cm) |
| Column S | Width of Left Superior Preganglionic Lobe (cm) |
| Column T | Length of Left Superior Preganglionic Lobe (cm) |

| A | B | C | D | E | F | G | H | I | J | K | L | M | N | O | P | Q | R | S | T |
|-----|-----|-----|---|-----|-----|------|-----|-----|-----|-----|-----|-----|-----|------|-----|-----|-----|-----|-----|
| 001 | 195 | 122 | 1 | 0.6 | 1.0 | 0.20 | 1.8 | 0.3 | 0.7 | 0.2 | 0.5 | 0.7 | 1.2 | 0.20 | 1.7 | 0.4 | 0.7 | 0.2 | 0.4 |
| 002 | 200 | 139 | 1 | 0.5 | 1.1 | 0.20 | 1.8 | 0.5 | 0.9 | 0.3 | 0.6 | 0.6 | 1.0 | 0.15 | 1.8 | 0.5 | 0.7 | 0.3 | 0.5 |
| 003 | 220 | 202 | 1 | 0.6 | 1.1 | 0.20 | 1.8 | 0.4 | 0.8 | 0.2 | 0.5 | 0.7 | 1.2 | 0.20 | 1.8 | 0.4 | 0.8 | 0.2 | 0.7 |
| 004 | 211 | 183 | 1 | 0.6 | 1.0 | 0.15 | 2.0 | 0.5 | 0.8 | 0.3 | 0.7 | 0.6 | 1.1 | 0.15 | 2.1 | 0.3 | 0.8 | 0.3 | 0.9 |
| 005 | 220 | 187 | 2 | 0.7 | 1.1 | 0.20 | 2.0 | 0.6 | 0.9 | 0.3 | 0.5 | 0.6 | 1.2 | 0.20 | 1.9 | 0.3 | 0.8 | 0.3 | 0.7 |
| 006 | 211 | 174 | 1 | 0.4 | 1.0 | 0.20 | 1.9 | 0.5 | 0.8 | 0.4 | 0.7 | 0.4 | 1.0 | 0.20 | 2.0 | 0.3 | 0.8 | 0.3 | 0.5 |
| 007 | 221 | 198 | 1 | 0.6 | 0.9 | 0.15 | 2.0 | 0.4 | 0.7 | 0.3 | 0.6 | 0.6 | 1.0 | 0.15 | 2.0 | 0.5 | 0.8 | 0.4 | 0.6 |
| 008 | 214 | 175 | 1 | 0.6 | 1.0 | 0.15 | 2.0 | 0.5 | 0.8 | 0.3 | 0.7 | 0.6 | 1.0 | 0.15 | 1.9 | 0.5 | 0.9 | 0.3 | 0.6 |
| 009 | 245 | 252 | 2 | 0.7 | 1.2 | 0.20 | 2.0 | 0.4 | 0.7 | 0.2 | 0.5 | 0.8 | 1.2 | 0.20 | 2.0 | 0.5 | 0.9 | 0.3 | 0.5 |
| 010 | 211 | 182 | 1 | 0.6 | 1.0 | 0.20 | 1.5 | 0.5 | 0.8 | 0.2 | 0.6 | 0.7 | 1.0 | 0.20 | 1.5 | 0.5 | 0.9 | 0.3 | 0.6 |
| 011 | 228 | 224 | 2 | 0.7 | 1.1 | 0.20 | 2.0 | 0.6 | 0.8 | 0.3 | 0.7 | 0.7 | 1.2 | 0.20 | 2.0 | 0.6 | 1.0 | 0.4 | 0.6 |
| 012 | 240 | 270 | 2 | 0.6 | 1.2 | 0.20 | 2.0 | 0.4 | 1.0 | 0.3 | 0.4 | 0.7 | 1.3 | 0.20 | 2.0 | 0.5 | 1.1 | 0.4 | 0.5 |
| 013 | 240 | 336 | 2 | 1.0 | 1.9 | 0.25 | 2.5 | 0.9 | 1.0 | 0.6 | 1.0 | 0.9 | 1.7 | 0.25 | 2.4 | 0.5 | 1.0 | 0.4 | 0.7 |
| 014 | 220 | 206 | 2 | 0.7 | 1.1 | 0.20 | 1.8 | 0.6 | 0.7 | 0.4 | 0.7 | 0.7 | 1.3 | 0.20 | 1.8 | 0.6 | 0.8 | 0.3 | 0.7 |
| 015 | 242 | 273 | 2 | 0.7 | 1.3 | 0.20 | 1.9 | 0.4 | 0.9 | 0.3 | 0.6 | 0.7 | 1.1 | 0.20 | 1.9 | 0.6 | 0.9 | 0.3 | 0.5 |
| 016 | 237 | 256 | 2 | 0.8 | 1.4 | 0.20 | 1.2 | 0.6 | 0.9 | 0.4 | 0.8 | 0.8 | 1.2 | 0.25 | 1.7 | 0.6 | 0.9 | 0.4 | 0.7 |
| 017 | 232 | 276 | 2 | 0.7 | 1.4 | 0.25 | 2.2 | 0.6 | 1.0 | 0.4 | 0.8 | 0.8 | 1.4 | 0.25 | 1.8 | 0.6 | 1.1 | 0.4 | 0.7 |
| 018 | 234 | 266 | 1 | 0.8 | 1.1 | 0.30 | 2.0 | 0.7 | 1.0 | 0.5 | 0.8 | 0.6 | 1.3 | 0.30 | 2.0 | 0.8 | 1.2 | 0.4 | 0.8 |
| 019 | 250 | 335 | 2 | 0.8 | 1.3 | 0.30 | 2.2 | 0.5 | 1.0 | 0.4 | 0.6 | 0.9 | 1.5 | 0.30 | 2.2 | 0.5 | 1.0 | 0.3 | 0.6 |
| 020 | 256 | 323 | 2 | 0.7 | 1.4 | 0.30 | 1.9 | 0.5 | 1.0 | 0.4 | 0.7 | 0.7 | 1.9 | 0.30 | 1.9 | 0.7 | 1.3 | 0.6 | 0.6 |
| 021 | 265 | 408 | 2 | 0.7 | 1.3 | 0.20 | 1.9 | 0.5 | 1.0 | 0.2 | 0.5 | 0.7 | 1.3 | 0.20 | 2.0 | 0.5 | 0.9 | 0.4 | 0.8 |
| 022 | 257 | 332 | 2 | 0.7 | 1.1 | 0.20 | 1.9 | 0.5 | 1.1 | 0.3 | 0.5 | 0.9 | 1.2 | 0.20 | 1.9 | 0.6 | 1.1 | 0.4 | 0.8 |

| A | B | C | D | E | F | G | H | I | J | K | L | M | N | O | P | Q | R | S | T |
|-----|-----|-----|---|-----|-----|------|-----|-----|-----|-----|-----|-----|-----|------|-----|-----|-----|-----|-----|
| 023 | 247 | 332 | 2 | 0.6 | 1.1 | 0.20 | 2.4 | 0.7 | 1.0 | 0.3 | 0.7 | 0.7 | 1.1 | 0.20 | 2.4 | 0.6 | 1.0 | 0.3 | 0.7 |
| 024 | 262 | 453 | 2 | 1.1 | 2.0 | 0.45 | 1.9 | 0.6 | 1.5 | 0.4 | 1.0 | 1.2 | 2.0 | 0.45 | 2.0 | 0.8 | 1.4 | 0.4 | 0.7 |
| 025 | 265 | 340 | 2 | 0.7 | 1.3 | 0.20 | 2.2 | 0.5 | 1.0 | 0.3 | 0.8 | 0.6 | 1.3 | 0.15 | 2.2 | 0.5 | 1.0 | 0.3 | 0.7 |
| 026 | 275 | 345 | 2 | 0.9 | 1.5 | 0.20 | 2.4 | 0.7 | 1.0 | 0.4 | 1.0 | 0.8 | 1.5 | 0.25 | 2.4 | 0.8 | 1.0 | 0.5 | 0.9 |
| 027 | 274 | 476 | 2 | 0.9 | 1.2 | 0.25 | 1.9 | 0.8 | 1.2 | 0.4 | 1.1 | 1.1 | 1.5 | 0.20 | 1.9 | 0.9 | 1.3 | 0.3 | 0.8 |
| 028 | 250 | 277 | 2 | 0.6 | 1.1 | 0.20 | 1.9 | 0.4 | 1.0 | 0.2 | 0.4 | 0.9 | 1.3 | 0.25 | 1.9 | 0.6 | 1.1 | 0.4 | 0.6 |
| 029 | 260 | 366 | 2 | 0.9 | 1.3 | 0.25 | 1.9 | 0.6 | 1.0 | 0.4 | 0.8 | 0.8 | 1.2 | 0.25 | 1.9 | 0.5 | 1.0 | 0.4 | 0.8 |
| 030 | 254 | 300 | 1 | 0.8 | 1.3 | 0.20 | 1.5 | 0 | 0 | 0 | 0 | 0.8 | 1.1 | 0.20 | 1.5 | 0.4 | 1.0 | 0.2 | 0.5 |
| 031 | 242 | 280 | 2 | 0.8 | 1.4 | 0.20 | 2.2 | 0.5 | 1.1 | 0.3 | 0.6 | 0.9 | 1.3 | 0.20 | 2.0 | 0.4 | 1.0 | 0.3 | 0.6 |
| 032 | 258 | 348 | 2 | 0.9 | 1.4 | 0.25 | 2.0 | 0.5 | 1.1 | 0.3 | 0.5 | 0.9 | 1.5 | 0.30 | 2.0 | 0.6 | 1.2 | 0.5 | 0.6 |
| 033 | 227 | 331 | 2 | 0.9 | 1.4 | 0.25 | 1.7 | 0.4 | 1.1 | 0.3 | 0.5 | 1.0 | 1.4 | 0.25 | 1.7 | 0.5 | 1.1 | 0.3 | 0.5 |
| 034 | 260 | 327 | 2 | 1.0 | 1.6 | 0.25 | 1.8 | 0.5 | 1.1 | 0.3 | 0.7 | 1.0 | 1.5 | 0.25 | 1.7 | 0.7 | 1.2 | 0.5 | 0.7 |
| 035 | 242 | 270 | 2 | 0.8 | 1.4 | 0.20 | 1.4 | 0.5 | 1.1 | 0.3 | 0.6 | 0.9 | 1.4 | 0.20 | 1.5 | 0.5 | 1.0 | 0.4 | 0.6 |
| 036 | 245 | 349 | 1 | 0.9 | 1.5 | 0.25 | 2.2 | 0.6 | 1.1 | 0.4 | 0.5 | 0.9 | 1.3 | 0.25 | 2.3 | 0.6 | 1.1 | 0.4 | 0.6 |
| 037 | 223 | 250 | 1 | 0.8 | 1.3 | 0.20 | 2.0 | 0.4 | 0.9 | 0.2 | 0.6 | 0.7 | 1.2 | 0.20 | 2.0 | 0.4 | 1.1 | 0.2 | 0.4 |
| 038 | 270 | 356 | 2 | 0.9 | 1.3 | 0.20 | 2.0 | 0.5 | 1.1 | 0.3 | 0.6 | 0.9 | 1.3 | 0.15 | 2.0 | 0.5 | 1.0 | 0.4 | 0.6 |
| 039 | 230 | 243 | 2 | 0.9 | 1.4 | 0.15 | 1.7 | 0.5 | 0.9 | 0.3 | 0.4 | 0.8 | 1.4 | 0.20 | 1.4 | 0.5 | 0.7 | 0.3 | 0.7 |
| 040 | 228 | 209 | 1 | 0.8 | 1.2 | 0.20 | 2.1 | 0.4 | 0.9 | 0.2 | 0.4 | 0.8 | 1.2 | 0.20 | 2.1 | 0.4 | 0.9 | 0.3 | 0.5 |
| 041 | 265 | 362 | 2 | 1.1 | 1.7 | 0.30 | 2.0 | 0.5 | 1.2 | 0.5 | 0.8 | 0.9 | 1.6 | 0.30 | 2.0 | 0.6 | 1.3 | 0.4 | 1.0 |
| 042 | 265 | 362 | 2 | 0.9 | 1.4 | 0.30 | 2.2 | 0.4 | 0.9 | 0.3 | 0.6 | 0.9 | 1.4 | 0.30 | 2.3 | 0.5 | 1.0 | 0.4 | 0.7 |
| 043 | 260 | 355 | 2 | 1.0 | 1.4 | 0.25 | 2.2 | 0.5 | 1.0 | 0.3 | 0.6 | 1.0 | 1.5 | 0.30 | 2.1 | 0.5 | 1.1 | 0.3 | 0.6 |
| 044 | 270 | 365 | 2 | 1.1 | 1.6 | 0.25 | 2.0 | 0.4 | 1.1 | 0.3 | 0.5 | 1.0 | 1.5 | 0.25 | 2.0 | 0.5 | 1.2 | 0.4 | 0.5 |

| A | B | C | D | E | F | G | H | I | J | K | L | M | N | O | P | Q | R | S | T |
|-----|-----|-----|---|-----|-----|------|-----|-----|-----|-----|-----|-----|-----|------|-----|-----|-----|-----|-----|
| 067 | 246 | 291 | 2 | 1.0 | 1.4 | 0.30 | 2.0 | 0.5 | 0.9 | 0.3 | 0.8 | 1.2 | 1.5 | 0.30 | 2.0 | 0.4 | 0.8 | 0.3 | 0.7 |
| 068 | 243 | 271 | 2 | 0.8 | 1.4 | 0.25 | 2.0 | 0.3 | 0.8 | 0.2 | 0.5 | 0.8 | 1.4 | 0.20 | 2.0 | 0.4 | 0.9 | 0.2 | 0.5 |
| 069 | 258 | 324 | 2 | 0.9 | 1.5 | 0.30 | 2.0 | 0.5 | 0.9 | 0.3 | 0.5 | 0.9 | 1.4 | 0.30 | 2.0 | 0.4 | 0.9 | 0.3 | 0.4 |
| 070 | 244 | 318 | 2 | 0.7 | 1.5 | 0.20 | 2.0 | 0.4 | 0.9 | 0.3 | 0.5 | 0.7 | 1.3 | 0.25 | 2.0 | 0.4 | 0.8 | 0.3 | 0.5 |
| 071 | 268 | 352 | 2 | 0.9 | 1.4 | 0.30 | 2.0 | 0.6 | 0.9 | 0.3 | 0.6 | 1.0 | 1.4 | 0.30 | 2.0 | 0.6 | 1.0 | 0.4 | 0.5 |
| 072 | 246 | 279 | 1 | 0.8 | 1.3 | 0.20 | 2.0 | 0.4 | 0.9 | 0.2 | 0.5 | 0.8 | 1.2 | 0.20 | 2.0 | 0.4 | 0.7 | 0.4 | 0.6 |
| 073 | 247 | 260 | 2 | 0.6 | 1.2 | 0.20 | 2.0 | 0.4 | 0.8 | 0.3 | 0.5 | 0.6 | 1.3 | 0.25 | 2.0 | 0.4 | 0.8 | 0.2 | 0.5 |
| 074 | 260 | 330 | 2 | 0.9 | 1.3 | 0.30 | 2.0 | 0.5 | 1.1 | 0.4 | 0.8 | 0.9 | 1.3 | 0.30 | 2.0 | 0.6 | 1.0 | 0.3 | 0.5 |
| 075 | 265 | 373 | 2 | 1.0 | 1.4 | 0.30 | 1.6 | 0.5 | 1.1 | 0.4 | 0.6 | 0.9 | 1.4 | 0.35 | 1.6 | 0.6 | 1.1 | 0.3 | 0.5 |
| 076 | 257 | 356 | 2 | 0.9 | 1.4 | 0.35 | 1.9 | 0.5 | 1.0 | 0.3 | 0.6 | 0.9 | 1.3 | 0.30 | 1.9 | 0.6 | 1.0 | 0.3 | 0.5 |
| 077 | 281 | 430 | 2 | 1.0 | 1.5 | 0.35 | 1.6 | 0.5 | 1.0 | 0.4 | 0.6 | 1.1 | 1.4 | 0.30 | 1.6 | 0.5 | 1.1 | 0.4 | 0.6 |
| 078 | 238 | 248 | 2 | 0.7 | 1.3 | 0.35 | 2.2 | 0.4 | 0.9 | 0.3 | 0.5 | 0.6 | 1.2 | 0.30 | 2.1 | 0.5 | 0.8 | 0.3 | 0.5 |
| 079 | 245 | 290 | 1 | 0.9 | 1.3 | 0.25 | 2.3 | 0.4 | 1.0 | 0.2 | 0.4 | 0.8 | 1.4 | 0.30 | 2.1 | 0.4 | 0.9 | 0.3 | 0.4 |
| 080 | 285 | 473 | 2 | 1.0 | 1.8 | 0.25 | 1.8 | 0.5 | 1.0 | 0.4 | 0.7 | 1.0 | 1.8 | 0.30 | 1.7 | 0.6 | 1.2 | 0.3 | 0.7 |
| 081 | 277 | 418 | 2 | 1.0 | 1.7 | 0.30 | 2.2 | 0.5 | 1.1 | 0.4 | 0.8 | 1.0 | 1.6 | 0.30 | 2.1 | 0.5 | 1.0 | 0.4 | 0.8 |
| 082 | 238 | 302 | 1 | 0.9 | 1.5 | 0.30 | 2.1 | 0.5 | 0.9 | 0.3 | 0.5 | 0.8 | 1.5 | 0.25 | 2.0 | 0.4 | 1.0 | 0.3 | 0.6 |
| 083 | 254 | 303 | 2 | 0.8 | 1.4 | 0.30 | 2.0 | 0.5 | 0.8 | 0.2 | 0.5 | 0.9 | 1.4 | 0.30 | 2.0 | 0.5 | 0.8 | 0.4 | 0.7 |
| 084 | 265 | 444 | 2 | 0.9 | 1.5 | 0.30 | 2.0 | 0.5 | 1.1 | 0.4 | 0.6 | 1.0 | 1.5 | 0.30 | 2.1 | 0.5 | 1.0 | 0.2 | 0.5 |
| 085 | 297 | 362 | 2 | 1.1 | 1.7 | 0.30 | 2.2 | 0.6 | 1.2 | 0.4 | 0.7 | 1.0 | 1.8 | 0.35 | 2.3 | 0.5 | 1.1 | 0.3 | 0.5 |
| 086 | 275 | 379 | 2 | 0.7 | 1.4 | 0.30 | 1.9 | 0.5 | 1.0 | 0.2 | 0.5 | 0.8 | 1.6 | 0.30 | 2.0 | 0.5 | 1.1 | 0.2 | 0.6 |
| 087 | 247 | 280 | 2 | 0.8 | 1.3 | 0.30 | 2.1 | 0.4 | 1.0 | 0.2 | 0.5 | 0.7 | 1.3 | 0.25 | 2.2 | 0.3 | 0.7 | 0.3 | 0.5 |
| 088 | 270 | 398 | 2 | 0.9 | 1.5 | 0.30 | 2.0 | 0.6 | 1.0 | 0.3 | 0.7 | 0.9 | 1.5 | 0.30 | 2.0 | 0.6 | 1.2 | 0.4 | 0.7 |

| A | B | C | D | E | F | G | H | I | J | K | L | M | N | O | P | Q | R | S | T |
|-----|-----|-----|---|-----|-----|------|-----|-----|-----|-----|-----|-----|-----|------|-----|-----|-----|-----|-----|
| 089 | 268 | 313 | 2 | 0.9 | 1.7 | 0.30 | 2.3 | 0.4 | 1.2 | 0.3 | 0.5 | 0.8 | 1.5 | 0.35 | 2.1 | 0.5 | 1.1 | 0.3 | 0.6 |
| 090 | 278 | 515 | 2 | 1.2 | 2.0 | 0.50 | 2.2 | 0.7 | 1.2 | 0.4 | 0.6 | 1.2 | 2.0 | 0.40 | 2.3 | 0.6 | 0.9 | 0.5 | 0.9 |
| 091 | 307 | 664 | 2 | 1.0 | 1.7 | 0.35 | 2.0 | 0.5 | 1.0 | 0.3 | 0.6 | 1.0 | 1.7 | 0.40 | 2.0 | 0.5 | 1.1 | 0.3 | 0.6 |
| 092 | 279 | 459 | 2 | 0.9 | 1.5 | 0.40 | 2.0 | 0.8 | 1.0 | 0.5 | 0.8 | 0.9 | 1.4 | 0.40 | 2.0 | 0.7 | 1.3 | 0.5 | 0.8 |
| 093 | 267 | 452 | 1 | 0.9 | 1.5 | 0.30 | 2.0 | 0.5 | 1.2 | 0.3 | 0.5 | 1.0 | 1.6 | 0.30 | 2.0 | 0.5 | 1.1 | 0.4 | 0.5 |
| 094 | 292 | 454 | 2 | 1.1 | 1.8 | 0.40 | 2.2 | 0.5 | 1.0 | 0.4 | 0.6 | 1.1 | 1.8 | 0.40 | 2.2 | 0.5 | 1.0 | 0.4 | 0.7 |
| 095 | 252 | 325 | 2 | 1.0 | 1.4 | 0.30 | 2.2 | 0.7 | 1.2 | 0.4 | 0.7 | 0.9 | 1.4 | 0.35 | 2.2 | 0.5 | 1.2 | 0.4 | 0.8 |
| 096 | 235 | 268 | 2 | 0.8 | 1.4 | 0.20 | 2.0 | 0.4 | 0.9 | 0.3 | 0.7 | 0.8 | 1.1 | 0.25 | 2.0 | 0.4 | 0.8 | 0.2 | 0.5 |
| 097 | 236 | 305 | 1 | 0.9 | 1.5 | 0.30 | 2.0 | 0.5 | 0.8 | 0.3 | 0.5 | 0.8 | 1.5 | 0.30 | 2.0 | 0.5 | 1.0 | 0.3 | 0.5 |
| 098 | 286 | 511 | 2 | 1.0 | 1.8 | 0.30 | 2.0 | 0.4 | 1.0 | 0.3 | 0.6 | 1.1 | 1.6 | 0.30 | 2.0 | 0.4 | 0.9 | 0.2 | 0.5 |
| 099 | 235 | 304 | 1 | 0.8 | 1.2 | 0.20 | 2.0 | 0.5 | 0.8 | 0.3 | 0.6 | 0.7 | 1.3 | 0.20 | 2.0 | 0.4 | 0.8 | 0.3 | 0.4 |
| 100 | 263 | 365 | 2 | 0.8 | 1.5 | 0.35 | 2.0 | 0.5 | 1.1 | 0.3 | 0.5 | 0.8 | 1.4 | 0.25 | 2.0 | 0.5 | 0.9 | 0.3 | 0.6 |
| 101 | 263 | 367 | 2 | 0.9 | 1.3 | 0.30 | 2.0 | 0.6 | 1.0 | 0.5 | 0.8 | 0.9 | 1.6 | 0.30 | 2.0 | 0.6 | 1.1 | 0.5 | 0.8 |
| 102 | 232 | 231 | 2 | 0.7 | 1.2 | 0.20 | 2.0 | 0.4 | 0.8 | 0.4 | 0.4 | 0.7 | 1.2 | 0.20 | 2.0 | 0.5 | 1.0 | 0.3 | 0.5 |
| 103 | 241 | 287 | 2 | 0.8 | 1.2 | 0.20 | 2.0 | 0.6 | 1.0 | 0.3 | 0.6 | 0.7 | 1.3 | 0.25 | 2.0 | 0.6 | 1.0 | 0.4 | 0.6 |
| 104 | 281 | 405 | 2 | 0.8 | 1.5 | 0.30 | 2.0 | 0.4 | 0.8 | 0.3 | 0.5 | 0.8 | 1.5 | 0.25 | 2.0 | 0.6 | 1.1 | 0.4 | 0.6 |
| 105 | 249 | 317 | 1 | 0.8 | 1.5 | 0.30 | 2.0 | 0.4 | 0.7 | 0.3 | 0.6 | 0.9 | 1.7 | 0.30 | 2.0 | 0.5 | 0.7 | 0.4 | 0.6 |
| 106 | 261 | 352 | 2 | 0.9 | 1.4 | 0.30 | 2.0 | 0.5 | 1.0 | 0.2 | 0.6 | 0.9 | 1.5 | 0.30 | 2.0 | 0.8 | 1.2 | 0.4 | 0.6 |
| 107 | 271 | 403 | 2 | 0.9 | 1.1 | 0.30 | 2.0 | 0.6 | 1.1 | 0.3 | 0.5 | 0.9 | 1.5 | 0.35 | 2.0 | 0.7 | 1.0 | 0.3 | 0.5 |
| 108 | 281 | 415 | 2 | 0.8 | 1.5 | 0.25 | 2.0 | 0.6 | 1.2 | 0.4 | 0.8 | 0.8 | 1.4 | 0.20 | 2.0 | 0.5 | 1.1 | 0.3 | 0.6 |
| 109 | 237 | 242 | 1 | 0.7 | 1.3 | 0.20 | 2.0 | 0.5 | 0.9 | 0.3 | 0.5 | 0.8 | 1.3 | 0.20 | 2.0 | 0.5 | 1.0 | 0.2 | 0.5 |
| 110 | 258 | 445 | 1 | 1.0 | 1.7 | 0.30 | 2.0 | 0.6 | 1.0 | 0.4 | 0.7 | 0.9 | 1.8 | 0.30 | 2.0 | 0.7 | 1.1 | 0.4 | 0.8 |

| A | B | C | D | E | F | G | H | I | J | K | L | M | N | O | P | Q | R | S | T |
|-----|-----|-----|---|-----|-----|------|-----|-----|-----|-----|-----|-----|-----|------|-----|-----|-----|-----|-----|
| 111 | 299 | 498 | 2 | 1.0 | 1.7 | 0.30 | 2.0 | 0.7 | 1.1 | 0.4 | 0.7 | 0.9 | 1.5 | 0.35 | 2.0 | 0.8 | 1.3 | 0.3 | 0.7 |
| 112 | 289 | 458 | 2 | 1.0 | 1.7 | 0.30 | 2.0 | 0.7 | 1.0 | 0.4 | 0.7 | 1.0 | 1.8 | 0.30 | 2.0 | 0.7 | 1.5 | 0.4 | 0.6 |
| 113 | 269 | 373 | 2 | 1.0 | 1.7 | 0.30 | 2.1 | 0.5 | 0.9 | 0.3 | 0.5 | 0.9 | 1.5 | 0.30 | 2.2 | 0.5 | 1.1 | 0.5 | 0.7 |
| 114 | 241 | 244 | 2 | 0.8 | 1.2 | 0.30 | 2.1 | 0.5 | 0.9 | 0.2 | 0.5 | 0.9 | 1.5 | 0.25 | 2.2 | 0.5 | 0.9 | 0.4 | 0.4 |
| 115 | 255 | 304 | 2 | 0.8 | 1.4 | 0.25 | 2.1 | 0.6 | 1.0 | 0.4 | 0.7 | 0.7 | 1.4 | 0.25 | 2.1 | 0.6 | 1.2 | 0.3 | 0.5 |
| 116 | 261 | 320 | 2 | 0.9 | 1.4 | 0.30 | 2.2 | 0.6 | 1.1 | 0.3 | 0.6 | 0.8 | 1.5 | 0.25 | 2.0 | 0.5 | 1.0 | 0.3 | 0.6 |
| 117 | 254 | 312 | 2 | 0.8 | 1.4 | 0.25 | 2.0 | 0.5 | 0.9 | 0.3 | 0.5 | 0.8 | 1.4 | 0.30 | 2.0 | 0.5 | 1.1 | 0.3 | 0.5 |
| 118 | 252 | 383 | 1 | 0.8 | 1.6 | 0.30 | 2.0 | 0.6 | 1.0 | 0.4 | 0.7 | 0.8 | 1.5 | 0.25 | 2.1 | 0.7 | 1.1 | 0.5 | 0.8 |
| 119 | 259 | 333 | 2 | 0.7 | 1.2 | 0.25 | 1.9 | 0.5 | 1.0 | 0.2 | 0.4 | 0.7 | 1.4 | 0.20 | 2.0 | 0.5 | 1.1 | 0.5 | 0.9 |
| 120 | 250 | 325 | 1 | 0.7 | 1.4 | 0.20 | 2.0 | 0.5 | 1.0 | 0.2 | 0.5 | 0.8 | 1.4 | 0.25 | 2.0 | 0.5 | 0.8 | 0.3 | 0.6 |
| 121 | 295 | 485 | 2 | 1.0 | 1.7 | 0.30 | 2.0 | 0.5 | 1.0 | 0.3 | 0.5 | 1.0 | 1.6 | 0.30 | 2.0 | 0.6 | 1.1 | 0.4 | 0.6 |
| 122 | 246 | 292 | 2 | 0.8 | 1.4 | 0.30 | 2.0 | 0.5 | 1.0 | 0.3 | 0.6 | 0.8 | 1.4 | 0.30 | 2.0 | 0.6 | 1.1 | 0.3 | 0.5 |
| 123 | 277 | 477 | 2 | 1.0 | 1.5 | 0.35 | 2.3 | 0.6 | 1.3 | 0.5 | 0.7 | 0.9 | 1.8 | 0.40 | 2.0 | 0.7 | 1.5 | 0.3 | 0.6 |
| 124 | 242 | 338 | 1 | 0.8 | 1.4 | 0.20 | 2.0 | 0.5 | 1.1 | 0.2 | 0.6 | 0.8 | 1.4 | 0.20 | 2.1 | 0.6 | 1.1 | 0.4 | 0.9 |
| 125 | 270 | 422 | 2 | 0.8 | 1.4 | 0.20 | 2.1 | 0.4 | 1.0 | 0.3 | 0.5 | 0.9 | 1.5 | 0.25 | 2.2 | 0.5 | 1.1 | 0.3 | 0.5 |
| 126 | 257 | 348 | 2 | 0.8 | 1.2 | 0.30 | 2.2 | 0.6 | 1.0 | 0.5 | 0.7 | 0.8 | 1.6 | 0.30 | 2.1 | 0.7 | 1.1 | 0.3 | 0.7 |
| 127 | 255 | 361 | 2 | 0.8 | 1.4 | 0.20 | 2.0 | 0.6 | 1.2 | 0.3 | 0.6 | 0.8 | 1.1 | 0.30 | 2.0 | 0.7 | 1.1 | 0.5 | 0.8 |
| 128 | 266 | 396 | 2 | 0.9 | 1.5 | 0.35 | 2.1 | 0.7 | 1.3 | 0.3 | 0.7 | 0.9 | 1.5 | 0.35 | 2.0 | 0.6 | 1.9 | 0.3 | 0.6 |
| 129 | 268 | 390 | 2 | 0.9 | 1.5 | 0.40 | 2.2 | 0.6 | 1.4 | 0.3 | 0.6 | 0.8 | 1.4 | 0.40 | 2.2 | 0.6 | 1.1 | 0.4 | 0.5 |
| 130 | 234 | 268 | 2 | 0.7 | 1.5 | 0.30 | 2.1 | 0.6 | 0.9 | 0.3 | 0.5 | 0.7 | 1.5 | 0.30 | 2.2 | 0.6 | 1.0 | 0.3 | 0.7 |
| 131 | 244 | 334 | 2 | 0.8 | 1.6 | 0.30 | 2.1 | 0.7 | 1.1 | 0.3 | 0.6 | 0.9 | 1.4 | 0.20 | 2.1 | 0.7 | 1.1 | 0.4 | 0.6 |
| 132 | 255 | 287 | 2 | 0.9 | 1.5 | 0.30 | 2.2 | 0.7 | 0.9 | 0.5 | 1.0 | 1.0 | 1.6 | 0.20 | 2.2 | 0.6 | 0.9 | 0.4 | 0.9 |

| A | B | C | D | E | F | G | H | I | J | K | L | M | N | O | P | Q | R | S | T |
|-----|-----|-----|---|-----|-----|------|-----|-----|-----|-----|-----|-----|-----|------|-----|-----|-----|-----|-----|
| 133 | 267 | 414 | 2 | 0.9 | 1.5 | 0.30 | 2.1 | 0.5 | 1.0 | 0.3 | 0.5 | 0.9 | 1.4 | 0.30 | 2.2 | 0.5 | 1.3 | 0.3 | 0.4 |
| 134 | 260 | 320 | 2 | 0.9 | 1.4 | 0.30 | 2.0 | 0.4 | 0.9 | 0.3 | 0.6 | 0 | 0 | 0 | 0 | 0 | 0 | 0 | 0 |
| 135 | 250 | 333 | 2 | 0.8 | 1.1 | 0.20 | 2.0 | 0.4 | 1.1 | 0.3 | 0.4 | 0 | 0 | 0 | 0 | 0 | 0 | 0 | 0 |
| 136 | 261 | 348 | 2 | 0.8 | 1.6 | 0.20 | 1.9 | 0.7 | 0.9 | 0.4 | 0.8 | 0.9 | 1.3 | 0.20 | 2.0 | 0.7 | 1.1 | 0.3 | 0.5 |
| 137 | 254 | 364 | 2 | 1.0 | 1.4 | 0.30 | 2.0 | 0.7 | 1.1 | 0.5 | 0.7 | 0.9 | 1.4 | 0.30 | 2.0 | 0.7 | 1.0 | 0.4 | 0.8 |
| 138 | 164 | 074 | 2 | 0.4 | 0.8 | 0.10 | 2.0 | 0.4 | 1.0 | 0.2 | 0.5 | 0.4 | 0.8 | 0.10 | 2.0 | 0.4 | 0.7 | 0.3 | 0.5 |
| 139 | 185 | 116 | 1 | 0.5 | 0.8 | 0.05 | 2.0 | 0.5 | 0.8 | 0.3 | 0.4 | 0 | 0 | 0 | 0 | 0 | 0 | 0 | 0 |
| 140 | 213 | 196 | 1 | 0.5 | 1.0 | 0.15 | 2.0 | 0.3 | 0.8 | 0.3 | 0.6 | 0.6 | 0.9 | 0.20 | 2.0 | 0.3 | 0.9 | 0.3 | 0.6 |
| 141 | 192 | 127 | 2 | 0.4 | 0.9 | 0.20 | 2.0 | 0.4 | 0.8 | 0.3 | 0.3 | 0.6 | 1.0 | 0.15 | 2.0 | 0.3 | 0.8 | 0.2 | 0.4 |
| 142 | 219 | 177 | 2 | 0.6 | 1.1 | 0.20 | 2.0 | 0.3 | 0.9 | 0.3 | 0.6 | 0.8 | 1.4 | 0.20 | 2.0 | 0.5 | 0.9 | 0.4 | 0.6 |
| 143 | 202 | 150 | 1 | 0.5 | 0.9 | 0.20 | 2.0 | 0.3 | 0.6 | 0.2 | 0.6 | 0.6 | 1.0 | 0.20 | 2.0 | 0.3 | 0.7 | 0.2 | 0.5 |
| 144 | 197 | 123 | 1 | 0.5 | 1.0 | 0.10 | 1.8 | 0.2 | 0.6 | 0.2 | 0.4 | 0.6 | 1.0 | 0.10 | 1.9 | 0.3 | 0.8 | 0.2 | 0.4 |
| 145 | 204 | 151 | 2 | 0.5 | 1.2 | 0.20 | 2.0 | 0.4 | 0.8 | 0.3 | 0.6 | 0.6 | 1.1 | 0.20 | 2.0 | 0.4 | 0.7 | 0.2 | 0.5 |
| 146 | 208 | 139 | 1 | 0.6 | 1.0 | 0.20 | 2.0 | 0.5 | 0.9 | 0.2 | 0.3 | 0.6 | 1.1 | 0.20 | 2.0 | 0.5 | 1.0 | 0.3 | 0.3 |
| 147 | 206 | 144 | 2 | 0.6 | 1.2 | 0.20 | 2.1 | 0.5 | 0.9 | 0.3 | 0.5 | 0.8 | 1.2 | 0.20 | 2.0 | 0.5 | 0.8 | 0.3 | 0.5 |
| 148 | 193 | 143 | 1 | 0.6 | 1.1 | 0.20 | 2.0 | 0.5 | 1.1 | 0.3 | 0.5 | 0.6 | 1.1 | 0.20 | 2.0 | 0.6 | 0.8 | 0.3 | 0.5 |
| 149 | 188 | 115 | 1 | 0.5 | 0.7 | 0.20 | 2.0 | 0.4 | 1.0 | 0.3 | 0.4 | 0.4 | 0.9 | 0.15 | 2.0 | 0.3 | 0.8 | 0.2 | 0.3 |
| 150 | 228 | 205 | 2 | 0.6 | 1.1 | 0.20 | 2.0 | 0.4 | 0.9 | 0.3 | 0.3 | 0.6 | 1.2 | 0.20 | 2.0 | 0.5 | 0.9 | 0.2 | 0.6 |
| 151 | 214 | 165 | 2 | 0.5 | 1.1 | 0.20 | 2.0 | 0.3 | 0.9 | 0.3 | 0.4 | 0.6 | 0.9 | 0.15 | 2.0 | 0.4 | 0.7 | 0.2 | 0.4 |
| 152 | 220 | 203 | 2 | 0.7 | 1.2 | 0.20 | 2.0 | 0.5 | 0.9 | 0.3 | 0.5 | 0.8 | 1.2 | 0.20 | 2.0 | 0.5 | 1.0 | 0.4 | 0.5 |
| 153 | 188 | 106 | 1 | 0.5 | 1.0 | 0.20 | 2.0 | 0.4 | 0.9 | 0.2 | 0.3 | 0.5 | 0.9 | 0.15 | 2.0 | 0.3 | 0.7 | 0.2 | 0.4 |
| 154 | 196 | 119 | 2 | 0.6 | 0.9 | 0.20 | 2.0 | 0.5 | 0.9 | 0.3 | 0.3 | 0.5 | 0.9 | 0.20 | 2.0 | 0.4 | 0.9 | 0.3 | 0.4 |
| 155 | 186 | 099 | 2 | 0.5 | 1.0 | 0.10 | 1.9 | 0.3 | 0.8 | 0.2 | 0.4 | 0.6 | 1.0 | 0.10 | 2.0 | 0.3 | 0.9 | 0 | 0 |
| 156 | 232 | 255 | 2 | 0 | 0 | 0 | 0 | 0 | 0 | 0 | 0 | 0.7 | 1.3 | 0.20 | 2.0 | 0.5 | 0.9 | 0.3 | 0.6 |

| A | B | C | D | E | F | G | H | I | J | K | L | M | N | O | P | Q | R | S | T |
|-----|-----|-----|---|-----|-----|------|-----|-----|-----|-----|-----|-----|-----|------|-----|-----|-----|-----|-----|
| 157 | 214 | 164 | 1 | 0.7 | 1.3 | 0.10 | 1.9 | 0.4 | 1.0 | 0.3 | 0.6 | 0.7 | 1.3 | 0.15 | 2.0 | 0.5 | 0.9 | 0.4 | 0.4 |
| 158 | 211 | 137 | 2 | 0.6 | 1.1 | 0.20 | 2.0 | 0.4 | 0.9 | 0.2 | 0.4 | 0.7 | 1.1 | 0.25 | 2.0 | 0.4 | 0.9 | 0.3 | 0.5 |
| 159 | 212 | 139 | 2 | 0.7 | 1.0 | 0.20 | 2.0 | 0.4 | 0.7 | 0.3 | 0.5 | 0.7 | 0.9 | 0.15 | 2.0 | 0.4 | 0.8 | 0.3 | 0.6 |
| 160 | 227 | 174 | 2 | 0.6 | 1.2 | 0.20 | 2.0 | 0.6 | 0.9 | 0.3 | 0.8 | 0.6 | 1.2 | 0.20 | 2.0 | 0.6 | 1.0 | 0.3 | 0.6 |
| 161 | 200 | 140 | 1 | 0.5 | 1.1 | 0.20 | 2.0 | 0.5 | 0.8 | 0.3 | 0.6 | 0.6 | 1.1 | 0.15 | 2.0 | 0.4 | 0.7 | 0.3 | 0.6 |
| 162 | 230 | 198 | 2 | 0.7 | 1.0 | 0.20 | 1.9 | 0.4 | 0.8 | 0.2 | 0.4 | 0.6 | 1.1 | 0.20 | 2.0 | 0.4 | 0.8 | 0.2 | 0.5 |
| 163 | 201 | 118 | 1 | 0.8 | 1.3 | 0.10 | 2.0 | 0.3 | 0.8 | 0.2 | 0.5 | 0.6 | 1.1 | 0.15 | 2.0 | 0.4 | 0.8 | 0.2 | 0.6 |
| 164 | 212 | 201 | 1 | 0.8 | 1.4 | 0.20 | 2.0 | 0.5 | 1.0 | 0.3 | 0.5 | 0.8 | 1.3 | 0.20 | 2.0 | 0.5 | 1.0 | 0.4 | 0.5 |
| 165 | 203 | 168 | 1 | 0.8 | 1.3 | 0.20 | 2.0 | 0.3 | 0.8 | 0.3 | 0.4 | 0.7 | 1.1 | 0.10 | 2.0 | 0.5 | 0.8 | 0.3 | 0.6 |
| 166 | 206 | 173 | 2 | 0.9 | 1.5 | 0.25 | 2.0 | 0.5 | 1.0 | 0.3 | 0.5 | 0.9 | 1.5 | 0.30 | 2.0 | 0.6 | 0.9 | 0.4 | 0.6 |
| 167 | 212 | 190 | 1 | 0.9 | 1.5 | 0.25 | 2.1 | 0.5 | 0.8 | 0.4 | 0.6 | 0.8 | 1.5 | 0.30 | 2.0 | 0.6 | 1.1 | 0.3 | 0.6 |
| 168 | 204 | 0 | 2 | 0.9 | 1.5 | 0.30 | 2.0 | 0.4 | 1.0 | 0.3 | 0.5 | 0.8 | 1.5 | 0.30 | 2.0 | 0.5 | 1.1 | 0.2 | 0.5 |
| 169 | 218 | 231 | 2 | 1.0 | 1.6 | 0.30 | 2.0 | 0.4 | 1.4 | 0.3 | 0.7 | 0.9 | 1.7 | 0.30 | 2.0 | 0.7 | 1.1 | 0.4 | 0.6 |
| 170 | 234 | 222 | 2 | 0.8 | 1.6 | 0.20 | 2.0 | 0.3 | 1.0 | 0.2 | 0.5 | 0.8 | 1.4 | 0.20 | 2.0 | 0.3 | 0.9 | 0.2 | 0.6 |
| 171 | 163 | 055 | 1 | 0.4 | 0.6 | 0.10 | 2.0 | 0.2 | 0.7 | 0.2 | 0.4 | 0.3 | 0.6 | 0.10 | 2.0 | 0 | 0 | 0 | 0 |
| 172 | 306 | 561 | 2 | 1.1 | 1.8 | 0.30 | 2.0 | 0.9 | 1.2 | 0.5 | 0.8 | 1.4 | 1.8 | 0.40 | 2.0 | 0.8 | 1.4 | 0.3 | 0.7 |
| 173 | 300 | 591 | 2 | 0.9 | 1.7 | 0.30 | 2.0 | 0.7 | 1.2 | 0.4 | 0.6 | 1.1 | 1.7 | 0.30 | 2.0 | 0.5 | 1.1 | 0.4 | 0.7 |
| 174 | 300 | 623 | 2 | 1.0 | 1.6 | 0.30 | 1.9 | 0.4 | 1.0 | 0.6 | 0.8 | 1.0 | 1.5 | 0.30 | 2.0 | 0.5 | 1.1 | 0.3 | 0.6 |
| 175 | 295 | 564 | 2 | 1.3 | 1.9 | 0.35 | 2.1 | 0.6 | 1.2 | 0.4 | 0.7 | 1.1 | 1.8 | 0.40 | 2.0 | 0.7 | 1.1 | 0.4 | 0.7 |
| 176 | 295 | 524 | 2 | 1.2 | 1.9 | 0.30 | 2.2 | 0.6 | 0.9 | 0.6 | 0.9 | 1.3 | 2.0 | 0.30 | 2.0 | 0.7 | 1.2 | 0.5 | 0.9 |
| 177 | 291 | 528 | 2 | 1.0 | 1.7 | 0.40 | 2.0 | 0.9 | 1.1 | 0.4 | 0.7 | 1.1 | 1.5 | 0.40 | 2.0 | 0.6 | 1.0 | 0.4 | 0.8 |
| 178 | 236 | 267 | 2 | 0.9 | 1.8 | 0.35 | 2.0 | 0.8 | 1.3 | 0.4 | 0.6 | 0 | 0 | 0 | 0 | 0 | 0 | 0 | 0 |
| 179 | 239 | 324 | 2 | 1.2 | 1.9 | 0.30 | 2.0 | 0.6 | 1.3 | 0.6 | 0.8 | 1.2 | 1.8 | 0.30 | 2.0 | 0.6 | 1.3 | 0.5 | 0.8 |

B. Right Subganglionic Process

| Stage in Proposed Cell Lineage | Diameters (μm) | | | | | | | | | | | | | | | | | | | | Mean | Standard Deviation | | | | | |
|--------------------------------|-----------------------------|----|----|----|----|----|----|----|----|----|----|----|----|----|----|----|----|----|----|----|------|--------------------|----|----|-------|-------|------|
| | 20 | 18 | 18 | 17 | 20 | 20 | 21 | 20 | 20 | 17 | 20 | 19 | 22 | 19 | 22 | 19 | 23 | 19 | 19 | 22 | | | 21 | 20 | 20 | 19.68 | 1.46 |
| Variation 1 | 20 | 18 | 19 | 18 | 18 | 17 | 20 | 20 | 21 | 21 | 20 | 20 | 17 | 20 | 19 | 22 | 19 | 22 | 19 | 19 | 22 | 21 | 20 | 20 | 19.68 | 1.46 | |
| Variation 2 | 12 | 14 | 15 | 11 | 13 | 13 | 12 | 13 | 15 | 15 | 13 | 15 | 13 | 13 | 12 | 13 | 12 | 13 | 12 | 11 | 12 | 13 | 13 | 12 | 12.92 | 1.26 | |
| Variation 3 | 11 | 13 | 12 | 12 | 10 | 11 | 9 | 11 | 12 | 9 | 11 | 12 | 10 | 11 | 12 | 11 | 10 | 13 | 13 | 10 | 11 | 11 | 10 | 11 | 10.64 | 2.26 | |
| Variation 4 | 7 | 7 | 9 | 8 | 8 | 9 | 7 | 8 | 7 | 7 | 9 | 8 | 10 | 8 | 10 | 8 | 10 | 9 | 8 | 8 | 10 | 10 | 9 | 8 | 9 | 08.40 | 0.98 |
| Circulating Hemocytes | 9 | 10 | 10 | 9 | 9 | 11 | 8 | 10 | 7 | 10 | 8 | 9 | 10 | 10 | 10 | 9 | 9 | 8 | 9 | 11 | 9 | 9 | 10 | 9 | 09.28 | 0.92 | |

C. Right Inferior Preganglionic Lobe

| Stage in Proposed Cell Lineage | Diameters (μm) | | | | | | | | | | | | | | | | | | | | | | | | | | | | Mean | Standard Deviation |
|---|-----------------------------|----|----|----|----|----|----|----|----|----|----|----|----|----|----|----|----|----|----|----|----|----|----|----|----|-------|-------|------|------|-----------------------|
| | 25 | 20 | 17 | 19 | 23 | 20 | 20 | 21 | 20 | 23 | 20 | 23 | 19 | 23 | 25 | 19 | 21 | 20 | 17 | 17 | 23 | 21 | 18 | 18 | 15 | 20.28 | 2.52 | | | |
| Variation 1 | 25 | 20 | 17 | 19 | 23 | 20 | 20 | 21 | 20 | 23 | 20 | 23 | 19 | 23 | 25 | 19 | 21 | 20 | 17 | 17 | 23 | 21 | 18 | 18 | 15 | 20.28 | 2.52 | | | |
| Variation 2 | 14 | 15 | 15 | 13 | 14 | 14 | 13 | 12 | 14 | 13 | 13 | 14 | 13 | 14 | 14 | 14 | 12 | 13 | 14 | 13 | 14 | 13 | 13 | 11 | 14 | 13.48 | 0.94 | | | |
| Variation 3 | 10 | 10 | 11 | 10 | 10 | 11 | 12 | 12 | 11 | 11 | 11 | 12 | 11 | 12 | 11 | 12 | 11 | 11 | 10 | 12 | 10 | 11 | 10 | 12 | 12 | 11.00 | 0.80 | | | |
| Variation 4 | 7 | 9 | 7 | 8 | 7 | 8 | 8 | 8 | 9 | 8 | 8 | 8 | 8 | 8 | 8 | 8 | 9 | 8 | 8 | 9 | 9 | 8 | 8 | 7 | 7 | 08.00 | 0.63 | | | |
| Circulating Hemocytes | 10 | 10 | 9 | 10 | 10 | 10 | 8 | 9 | 10 | 7 | 9 | 8 | 9 | 10 | 10 | 10 | 9 | 8 | 10 | 8 | 10 | 10 | 10 | 10 | 11 | 9 | 09.32 | 0.93 | | |

Mean diameters were calculated for each type of cell measured.
 Standard deviations for circulating hemocytes were calculated for hemocytes
 with diameters less than 10 μm . Hemocytes with diameters of 10 μm or greater
 were excluded from the calculation.

D. Right Superior Preganglionic Lobe

| Stage in Proposed Cell Lineage | Diameters (μ m) | | | | | | | | | | | | | | | | | | | | Mean | Standard Deviation | | | | | |
|---|-----------------------|----|----|----|----|----|----|----|----|----|----|----|----|----|----|----|----|----|----|----|------|-----------------------|----|----|----|-------|------|
| | 17 | 15 | 24 | 18 | 17 | 19 | 18 | 22 | 19 | 17 | 23 | 24 | 22 | 16 | 21 | 18 | 18 | 20 | 22 | 21 | | | 21 | 18 | 16 | 18 | 21 |
| Variation 1 | 17 | 15 | 24 | 18 | 17 | 19 | 18 | 22 | 19 | 17 | 23 | 24 | 22 | 16 | 21 | 18 | 18 | 20 | 22 | 21 | 21 | 18 | 16 | 18 | 21 | 19.40 | 2.51 |
| Variation 2 | 15 | 12 | 13 | 13 | 15 | 13 | 15 | 15 | 17 | 13 | 14 | 17 | 15 | 16 | 14 | 15 | 13 | 15 | 13 | 13 | 15 | 14 | 12 | 12 | 15 | 14.16 | 1.41 |
| Variation 3 | 9 | 9 | 9 | 10 | 9 | 10 | 8 | 10 | 9 | 10 | 9 | 11 | 10 | 12 | 11 | 12 | 9 | 12 | 11 | 8 | 10 | 9 | 10 | 10 | 12 | 09.96 | 1.18 |
| Variation 4 | 7 | 7 | 8 | 7 | 8 | 8 | 8 | 7 | 8 | 8 | 8 | 8 | 7 | 7 | 9 | 7 | 8 | 8 | 8 | 7 | 7 | 8 | 8 | 8 | 8 | 07.68 | 0.55 |
| Circulating* Hemocytes | 10 | 10 | 9 | 8 | 11 | 10 | 10 | 10 | 9 | 10 | 9 | 10 | 9 | 10 | 9 | 10 | 10 | 11 | 10 | 10 | 10 | 9 | 8 | 10 | 8 | 09.56 | 0.80 |

*Twenty-five samples were included for each type of cell measured.

*Measurements for circulating hemocytes were included for comparison.

Values recorded for cellular diameter were rounded off to the nearest whole number.

